

Seismic Fragility Assessment of Pre- and Post-Retrofit 1980s Concentrically  
Braced Frame Office Buildings in Moderate Seismic Zones

Ming Zheng Wang

A Thesis

in

The Department

of

Building, Civil and Environmental Engineering

Presented in Partial Fulfillment of the Requirements  
for the Degree of Master of Applied Science (Civil Engineering) at

Concordia University

Montreal, Quebec, Canada

September 2014

© Ming Zheng Wang, 2014

**CONCORDIA UNIVERSITY**

**School of Graduate Studies**

This is to certify that the thesis prepared

By: Ming Zheng Wang

Entitled: Seismic Fragility Assessment of Pre- and Post-Retrofit 1980s Concentrically  
Braced Frame Office Buildings in Moderate Seismic Zones

and submitted in partial fulfillment of the requirements for the degree of

**Master of Applied Science (Civil Engineering)**

complies with the regulations of the University and meets the accepted standards with respect  
to originality and quality.

Signed by the final Examining Committee:

Ashutosh Bagchi Chair

*Chair's name*

Lan Lin Examiner

*Examiner's name*

Ramin Sedaghati Examiner

*Examiner's name*

Lucia Tirca Supervisor

*Supervisor's name*

Approved by Fariborz Haghighat

Chair of Department or Graduate Program Director

Sep. 15 2014

Amir Asif

Dean of Faculty

## ABSTRACT

### Seismic Fragility Assessment of Pre- and Post-Retrofit 1980s Concentrically Braced Frame Office Buildings in Moderate Seismic Zones

Ming Zheng Wang

In the past decades, concentrically braced frames (CBFs) have been frequently employed as earthquake resistant systems due to their high stiffness and straightforward design. Over a time line ended in 2000, the existing office building stock designed in the interval 1980-1989 in Quebec is about 25% of non-residential buildings. Among these buildings, more than 50% are low- and middle-rise steel structures with a CBF system. Since 1980, both the National Building code of Canada (NBCC) and Steel design standard (CSA/S16) have continually evolved, while lower interest was allocated in the development of guidelines for seismic assessment and retrofit of existing buildings located in seismic zones.

This study focuses on the seismic fragility assessment of pre- and post-retrofit fictitious low-rise (3-storey) and middle-rise (6-storey) CBFs office buildings located in Montreal (Qc.) and designed according to the NBCC 1980 and CSA/S16.1-78 standard provisions. Using the performance based design approach and incremental dynamic analysis (IDA), the IDA curves computed as pairs of earthquake intensity measure parameter (e.g.  $S(T_a)g$ ) versus the engineering demand parameter (e.g. peak interstorey drift) were obtained. The analytical fragility curves of studied buildings have a lognormal distribution and are defined as a function of spectral acceleration ( $S_a$ ). Both aleatoric and epistemic uncertainties were considered.

The seismic force resisting system of the studied fictitious office buildings consists of four chevron CBFs in the E-W direction and two times two adjacent CBFs with diagonal tension/compression braces in the N-S direction. Each brace-to-frame connection consists of a gusset plate welded to the slotted end part of the HSS brace. First, the seismic assessment of these buildings was conducted through equivalent static force procedure, as well as linear

dynamic analysis and it was concluded that the ratio between the demanded factored base shear  $V_{f-10}$  (NBCC 2010) and  $V_{f-80}$  (NBCC 1980) is 2.2 for the low-rise buildings and 1.5 for the middle-rise buildings. In addition, it was found that several brace-to-frame connections, several beams and especially the middle column of CBFs with tension/compression diagonal braces do not possess sufficient strength and the retrofit action is required.

According to ASCE/SEI 41-13 the *Rehabilitation objective* is a combination of a *Target building performance* level, an *Earthquake hazard* level and an assigned *Objective rehabilitation class* which is *Basic Safety (BSO)* for office buildings, while the target building performance levels (PL) are *Life Safety* and *Collapse Prevention*. To reach the *BSO*, a conventional retrofit strategy implying the replacement of brace-to-frame connections, strengthening of CBFs beams and column cross-sections especially at lower floors was applied. In this light, three building performance levels: *Immediate Occupancy*, *Life Safety* and *Collapse Prevention*, with the associated earthquake intensity level (50%/50 yrs., 10%/50 yrs. and 2%/50 yrs) and three damage states (*Light*, *Moderate*, and *Severe*) were considered. The aforementioned performance levels were defined on each IDA curve resulted from nonlinear time-history analysis using OpenSees. The recorded engineering demand parameters were the interstorey drift and the residual interstorey drift, while the intensity measure parameter was  $S_a(T_1)g$ . In this study, the light damage is associated with the elastic response of the building, the moderate damage with the attainment of  $0.5\%h_s$  residual interstorey drift and severe damage when the building reaches a maximum interstorey drift of  $2\%h_s$ .

Because the existing building structures are non-ductile and brittle failure of brace-to-frame connections is expected due to shearing of welds, there is no a gradual transition between damage states. In this regard, the Severe damage state occurs suddenly after the structure response exceeds the elastic limit characterized by Light damage. For the post-retrofit buildings, the probabilities for Light damage are relatively larger compared with those for Moderate and Severe damage. In addition, the probability for all retrofitted buildings (E-W) to sustain Severe damage is 20% for the 3-storey and 30% for the 6-storey. A similar probability of Severe damage was obtained for the CBF with diagonal braces located in the N-S direction.

## ACKNOWLEDGEMENTS

The completion of this research project at Concordia University is a dream that became reality because of the great help and continuous support of many people throughout the past two years.

First of all, I want to express my sincere and deepest gratitude to my supervisor Professor Lucia Tirca for her patience, continued encouragement and expert guidance. Her strong background and rich expertise in the field of structural engineering was not only of a great help to overcome difficulties during my research, but also made her the role model that inspired me to strive for the best.

I would like to express my deepest appreciation to my colleague Ovidiu Serban for his support specially in the research of fragility assessment, and Yan Jiang from École Polytechnique for his assistance in the development of the numerical model of the concentrically braced frames and all the other university colleagues Liang Chen, Suliman Abdalla, Nenghui Lin, Qianli Xu and Masaaki Ohira for the moments shared during our studies.

I also would like to thank Professor Ashutosh Bagchi and Lan Lin whose feedback and evaluation of this Master Thesis proved to be nothing but constructive guidance.

Funding from the Natural Science and Engineering Research Council (NSERC) of Canada is acknowledged.

Last but not the least, I would like to thank my parents for their unconditional love, support and trust. I love you.

## TABLE OF CONTENTS

<b>ABSTRACT.....</b>	<b>III</b>
<b>TABLE OF CONTENTS.....</b>	<b>VI</b>
<b>LIST OF FIGURES .....</b>	<b>IX</b>
<b>LIST OF TABLES.....</b>	<b>XIV</b>
<b>CHAPTER 1. INTRODUCTION.....</b>	<b>1</b>
<i>1.1 Background .....</i>	<i>1</i>
<i>1.2 Objectives.....</i>	<i>3</i>
<i>1.3 Methodology.....</i>	<i>4</i>
<i>1.4 Thesis organization .....</i>	<i>6</i>
<b>CHAPTER 2. LITERATURE REVIEW.....</b>	<b>8</b>
<i>2.1 Introduction .....</i>	<i>8</i>
<i>2.2 Evolution of Seismic Design According to NBCC.....</i>	<i>8</i>
<i>2.2.1 Seismic design requirements according to NBCC 1980.....</i>	<i>11</i>
<i>2.2.2 Seismic design requirements according to NBCC 2010.....</i>	<i>14</i>
<i>2.3 Evolution of Seismic Provisions according to CSA S16 .....</i>	<i>16</i>
<i>2.3.1 Seismic provisions for CBFs according to CSA S16.1-M78.....</i>	<i>17</i>
<i>2.3.2 Seismic provisions for concentrically braced frame (CBF) according to CSA S16.1-09 .....</i>	<i>19</i>
<i>2.4 Seismic Assessment of Existing Buildings .....</i>	<i>22</i>
<i>2.4.1 FEMA P695(2009) and AISC/SEI 41-13 requirements .....</i>	<i>22</i>
<i>2.4.2 Incremental dynamic analysis .....</i>	<i>28</i>
<i>2.4.3 Fragility Analysis .....</i>	<i>30</i>

2.4.3	<i>Retrofitting for Existing Concentrically Braced Frame (CBF) Steel Buildings</i> .....	32
2.5	<i>OpenSees Modelling of Concentrically Braced Frame (CBF) Steel Building</i>	35
2.5.1	<i>Steel bracing member modelling</i> .....	35
2.5.2	<i>Brace connection modelling</i> .....	37
<b>CHAPTER 3. DESIGN OF CBF BUILDINGS ACCORDING TO NBCC 1980 AND CSA S16.1-M 78</b> .....		<b>39</b>
3.1	<i>Introduction</i> .....	39
3.2	<i>Building Description</i> .....	39
3.3	<i>Preliminary Design of Concentrically Braced Frame (CBF)</i> .....	40
3.4	<i>Design of Concentrically Braced Frame (CBF)</i> .....	53
3.4.1	<i>Brace design</i> .....	53
3.4.2	<i>Beam and column design</i> .....	55
3.4.3	<i>Brace connection design</i> .....	58
<b>CHAPTER 4. SEISMIC ASSESSMENT OF STUDIED BUILDINGS ACCORDING TO CURRENT CODE DEMAND</b> .....		<b>66</b>
4.1	<i>Results from Static Equivalent Method (NBCC 2010)</i> .....	66
4.2	<i>Results from Modal Response Spectrum Method</i> .....	67
4.3	<i>Results from Non-Linear Dynamic Analysis</i> .....	84
4.3.1	<i>OpenSees modelling</i> .....	84
4.3.2	<i>Ground motion selection</i> .....	88
4.3.3	<i>Results from OpenSees</i> .....	90
4.3.4	<i>Incremental dynamic analysis using OpenSees</i> .....	91
4.3.5	<i>Time-history seismic response of CBF structures</i> .....	95

4.4	<i>Seismic Assessment Conclusion</i> .....	101
<b>CHAPTER 5. FRAGILITY ASSESSMENT OF PRE- AND POST- RETROFIT BUILDING.....</b>		<b>103</b>
5.1	<i>Numerical Analysis of Post-Retrofit Buildings</i> .....	103
5.1.1	<i>Selection of Retrofit Scheme</i> .....	103
5.1.2	<i>Retrofitting of studied CBFs</i> .....	103
5.2	<i>Seismic Assessment of Retrofitted Buildings</i> .....	114
5.2.1	<i>Incremental dynamic analysis of retrofitted buildings</i> .....	115
5.2.2	<i>Detailed analysis example upon collapse of the retrofitted</i> .....	119
5.3	<i>Seismic Fragility Analysis</i> .....	125
5.3.1	<i>Damage State and Performance Limit State</i> .....	125
5.3.2	<i>Calculation of Fragility</i> .....	131
<b>CHAPTER 6. CONCLUSIONS AND RECOMMENDATIONS .....</b>		<b>137</b>
6.1	<i>Conclusions</i> .....	137
6.2	<i>Recommendations for Future Studies</i> .....	139
<b>REFERENCE.....</b>		<b>141</b>

## LIST OF FIGURES

Figure 1.1: Distribution of dwelling units built between 1948 and 1973 (Tirca et al., 2012).	2
Figure 1.2: Methodology for seismic fragility assessment of building structure .....	5
Figure 2.1: Significant earthquake in Eastern Canada (1600 – 2006) .....	10
Figure 2.2: Seismic zone map (NBCC 1980 supplement) (Montreal Zone 2) .....	12
Figure 2.3: Evolution of design spectrum for Montreal, site class C from 1970 to 2010.....	16
Figure 2.4: Bi-linear approximation used for $U$ , in CSA S16-14, for all slotted HSS welded connections with single concentric gusset plates (Packer, 2014) .....	22
Figure 2.5: Process for quantitatively establishing and documenting seismic performance of building structure (FEMA P695, 2009) .....	23
Figure 2.6: Rehabilitation objectives matrix (ASCE/SEI 41-13) .....	25
Figure 2.7: Damage control and building performance levels (ASCE/SEI, 2013).....	26
Figure 2.8: Target building performance levels and ranges (ASCE/SEI 41-13).....	27
Figure 2.9: Structural performance levels and damage for CBF structure (ASCE/SEI 41-13) .....	27
Figure 2.10: Target building performance levels and ranges including non-structural components (ASCE/SEI 41-13).....	28
Figure 2.11: IDA curves of a $T_l = 1.8$ s, 5-stoey steel braced frame subjected to four different records. (Vamvatsikos and Cornell, 2002).....	29
Figure 2.12: Seismic fragilities for Frames A and B. (Ellingwood et al., 2007).....	32
Figure 2.13: Traditional reinforcing of existing W shapes to increase their flexural strength (Schwinger, 2007).....	34
Figure 2.14: Traditional reinforcing of exiting W shapes to increase their compressive strength (Schwinger, 2007).....	34

Figure 2.15: Brace model and fiber cross-section discretization (Chen and Tirca, 2013)....	36
Figure 2.16: Gusset plate connection model for brace-to-frame (Hsiao et al., 2012).....	38
Figure 3.1: Building plan and elevation.....	40
Figure 3.2: Factored load on braces without consideration of torsional and P- $\Delta$ effects: (a) E-W direction, $V_{f,80} = 315$ kN; (b) N-S direction, $V_{f,80} = 630$ kN.....	42
Figure 3.3: Factored load on braces without consideration of torsional and P- $\Delta$ effects: (a) E-W direction, $V_{f,80} = 614$ kN; (b) N-S direction, $V_{f,80} = 1034$ kN.....	43
Figure 3.4: Factored load ( $1.5Q$ ) in braces of 3-storey CBF including torsion and P- $\Delta$ effect but without the tributary gravity load: (a) E-W; (b) N-S.....	45
Figure 3.5: Factored load ( $1.5Q$ ) in braces of 3-storey CBF including torsion and P- $\Delta$ effect but without the tributary gravity load: (a) E-W; (b) N-S.....	45
Figure 3.6: Factored load in members of 3-storey CBFs including the gravity component, torsion and P- $\Delta$ effects.....	50
Figure 3.7: Factored load in members of 6-storey CBF including the gravity component, torsion and P- $\Delta$ effects.....	52
Figure 3.8: Brace-to-frame gusset plate connection (CBF E-W direction).....	59
Figure 3.9: Brace-to-frame gusset plate connection (CBF N-S direction).....	59
Figure 3.10: Middle brace connection.....	62
Figure 4.1: ETABS model of the 3-st. building: a) 3-D view, b) elevation E-W; c) elevation N-S.....	68
Figure 4.2: ETABS model of the 6-st. building: a) 3-D view, b) elevation E-W; c) elevation N-S.....	69
Figure 4.3: Demand to capacity ratio of storey shear $V_{dyn,10}/V_{f,80}$ .....	71
Figure 4.4a: Structural members' resistance, 3-Storey.....	72
Figure 4.4b: Structural members' resistance, 6-Storey.....	72

Figure 4.5: Seismic assessment of bracing members of the CBF systems .....	74
Figure 4.6: Seismic assessment of beams of the CBF systems.....	76
Figure 4.7: Seismic assessment of columns of the CBF systems .....	76
Figure 4.8: Corner brace to frame connection (E-W direction, 2010).....	77
Figure 4.9: Corner brace to frame connection (N-S direction, 2010).....	77
Figure 4.10: Slotted-end HSS welded connection .....	79
Figure 4.11: Middle brace to frame connection (2010 design).....	80
Figure 4.12: OpenSees model of the 3- and 6-storey CBF together with their tributary leaning columns a) E-W direction and b) N-S direction .....	85
Figure 4.13: Model of one bay and one storey chevron braced frame .....	85
Figure 4.14: Fiber cross-section discretization a) HSS and b) W-shape.....	86
Figure 4.15: Brace to frame connection model (Hsiao et al., 2012).....	87
Figure 4.16: Response spectrum of scaled ground motions .....	90
Figure 4.17: IDA curves: a) 3-Storey, W-E direction; b) 6-Storey, W-E direction.....	92
Figure 4.18: IDA curves: a) 3-Storey, N-S direction; b) 6-Storey, N-S direction.....	93
Figure 4.19: Seismic response of CBFs: a) 3-storey building (E-W) under recorder M6C1-10.7; b) 3-storey building (E-W) under recorder M6C1-10.7; c) 6-storey building under recorder S8EN1; d) 6-storey building under recorder S8EN1 .....	94
Figure 4.20: The 6-st. (E-W) response under the record S8EN1: a) ground motion accelerogram; b) interstorey drift at the 5 <sup>th</sup> floor.....	96
Figure 4.21: 2D view of deformed braced frame under S8EN1 record: a) first brace buckling ( $t = 4.6s$ ); b) first gusset plate failure because beam hinging ( $t = 11.72s$ ).....	97
Figure 4.22a: Hysteresis loop of braces at each floor (4 <sup>th</sup> Floor ~ 6 <sup>th</sup> Floor).....	99
Figure 4.22b: Hysteresis loop of braces at each floor (1 <sup>st</sup> Floor~3 <sup>rd</sup> Floor).....	100

Figure 4.23: Axial load-bending moment interaction diagram of column of 6-st CBF (E-W) under the S8EN1 record.....	101
Figure 5.1: Detail of corner brace connection as per the current standard demand.....	105
Figure 5.2: Detail of middle brace connection according to model recommended by Hsiao et al. (2012).....	105
Figure 5.3: Cross-section view of HSS brace connection with added cover plates.....	109
Figure 5.4: Retrofitted column cross-section.....	112
Figure 5.5: Retrofitted beam cross-section.....	113
Figure 5.6: IDA curves of studied buildings: a) 3-st. (E-W); b) 6-st. (E-W).....	115
Figure 5.7: IDA curves of studied buildings: a) 3-st. (N-S); b) 6-st. (N-S).....	116
Figure 5.8: IDA curve of 6-storey CBF (E-W) subjected to ground motion M6C1-16.6.....	120
Figure 5.9: Seismic response of retrofitted 6-Storey chevron braced frame (E-W) under ground motion M6C1-16.6. (Point 5, Point 9 and Point 12 on the IDA curve; ● buckling of structural member, ★ failure of structural member) .....	121
Figure 5.10: Hysteresis loop of braces located at 5th floor under the ground motion intensity corresponding to <i>Point 12</i> of Figure 5.9 .....	122
Figure 5.11: Time history response: (a) Interstorey Drift; (b) Interstorey Drift Ratio; (c) Floor acceleration .....	123
Figure 5.12: Mapping damage control against building performance levels according to ASCE/SEI 41. (Tirca et al., 2014) .....	127
Figure 5.13: The 50 and 84 percentile peak interstorey drift of each floor: (a) 3-st CBF (E-W); (b) 6-st CBF (E-W).....	128
Figure 5.14: The 50 and 84 percentile residual interstorey drift of each floor: (a) 3-st CBF (E-W); (b) 6-st CBF (E-W).....	129

Figure 5.15: The 50 and 84 percentile floor acceleration of each floor: (a) 3-st CBF (E-W); (b) 6-st CBF (E-W).....	129
Figure 5.16: The 50 and 84 percentile peak interstorey drift of each floor: (a) 3-st CBF (N-S); (b) 6-st CBF (N-S) .....	130
Figure 5.17: The 50 and 84 percentile residual interstorey drift of each floor: (a) 3-st CBF (N-S); (b) 6-st CBF (N-S).....	130
Figure 5.18: The 50 and 84 percentile floor acceleration of each floor: (a) 3-st CBF (N-S); (b) 6-st CBF (N-S).....	131
Figure 5.19: Seismic response of each performance level: (a) 3-st E-W; (b) 6-st E-W; (c) 3-st N-S; (d) 6-st N-S.....	133
Figure 5.20a: Fragility curves of studied buildings: a) 3-st CBF (E-W); b) 6-st CBF (E-W) .....	134
Figure 5.20b: Fragility curves of studied buildings: a) 3-st CBF (N-S); b) 6-st CBF (N-S)...	135

## LIST OF TABLES

Table 2.1: Evolution of seismic hazard and the manner of determining the seismic design forces in the NBCC editions according to Heidebrecht (2005).....	9
Table 3.1: Minimum specified gravity loads .....	41
Table 3.2: Summary of seismic coefficients .....	41
Table 3.3a: Calculation of total unfactored storey shear (3-st E-W direction) .....	43
Table 3.3b: Calculation of total unfactored storey shear (3-st N-S direction).....	44
Table 3.4a: Calculation of total unfactored storey shear (6-st E-W direction) .....	44
Table 3.4b: Calculation of total unfactored storey shear (6-st N-S direction).....	44
Table 3.5: Gravity load component triggered in braces of the 3-st chevron CBF (E-W) .....	47
Table 3.6: Gravity load component triggered in braces of the 6-st chevron CBF (E-W) .....	48
Table 3.7a: Gravity load in the CBF column of the 3-st building (E-W) associated with each load combination.....	48
Table 3.7b: Gravity load in the CBF column of the 3-st building (N-S) associated with each load combination.....	48
Table 3.8a: Gravity load in the CBF column of the 6-st building (E-W) associated with each load combination.....	49
Table 3.8b: Gravity load in the CBF column of the 6-st building (N-S) associated with each load combination.....	49
Table 3.9a: Factored axial load and bending moment in beam (3-St E-W).....	50
Table 3.9b: Factored axial load and bending moment in beam (3-St N-S).....	51
Table 3.10a: Factored axial load and bending moment in beam (6-St E-W).....	52
Table 3.10b: Factored axial load and bending moment in beam (6-St N-S).....	53
Table 3.11a: Brace cross-sections of the 3-st CBF (E-W) as per 1980 design .....	54

Table 3.11b: Brace cross-sections of the 6-st CBF (E-W) as per 1980 design.....	54
Table 3.12a: Brace cross-sections of the 3-st CBF (N-S) as per 1980 design .....	54
Table 3.12b: Brace cross-sections of the 6-st CBF (N-S) as per 1980 design.....	54
Table 3.13a: Beam cross-sections of the 3-st CBF (E-W) as per 1980 design .....	55
Table 3.13b: Beam cross-sections of the 6-st CBF (E-W) as per 1980 design.....	56
Table 3.14a: Beam cross-sections of the 3-st CBF (N-S) as per 1980 design .....	56
Table 3.14b: Beam cross-sections of the 6-st CBF (N-S) as per 1980 design.....	56
Table 3.15a: Column cross-sections of the 3-st CBF (E-W) as per the 1980 design.....	57
Table 3.15b: Column cross-sections of the 6-st CBF (E-W) as per the 1980 design.....	58
Table 3.16a: Middle column cross-sections of the 3-st CBF (N-S) as per the 1980 design ...	57
Table 3.16b: Middle column cross-sections of the 6-st CBF (N-S) as per the 1980 design.....	57
Table 3.17a: Side column cross-sections of the 3-st CBF (N-S) as per the 1980 design.....	57
Table 3.17b: Side column cross-sections of the 6-st CBF (N-S) as per the 1980 design.....	58
Table 3.18a: Brace-to-frame connections design (3-st E-W) (unit: mm) .....	62
Table 3.18b: Brace-to-frame connections design (6-st E-W) (unit: mm).....	63
Table 3.19a: Brace-to-frame connections design (3-st N-S) (unit: mm).....	63
Table 3.19b: Brace-to-frame connections design (6-st N-S) (unit: mm).....	63
Table 3.20a: Brace-to-frame connection capacity based on 1980 design (3-st E-W).....	64
Table 3.20b: Brace-to-frame connection capacity based on 1980 design (6-st E-W).....	64
Table 3.21a: Brace-to-frame connection capacity based on 1980 design (3-st N-S).....	64

Table 3.21b: Brace-to-frame connection capacity based on 1980 design (6-st N-S).....	65
Table 4.1: Seismic load calculation based on static design method.....	67
Table 4.2: Base shear comparisons. (Unit: s, kN).....	70
Table 4.3a: Demand to capacity ratio of brace (3-st E-W) .....	73
Table 4.3b: Demand to capacity ratio of brace (6-st E-W).....	73
Table 4.4a: Demand to capacity ratio of brace (3-st N-S) .....	74
Table 4.4b: Demand to capacity ratio of brace (6-st N-S).....	74
Table 4.5a: Seismic assessment of brace connection (3-st, W-E) (unit: kN) .....	82
Table 4.5b: Seismic assessment of brace connection (6-st, W-E) (unit: kN).....	82
Table 4.6a: Seismic assessment of brace connection (3-st, N-S) (unit: kN).....	83
Table 4.6b: Seismic assessment of brace connection (6-st, N-S) (unit: kN).....	83
Table 4.7: Seismic ground motions.....	89
Table 4.8: Dynamic properties of buildings.....	90
Table 4.9: Seismic demand on each hazard level.....	93
Table 4.12: Collapse margin ratio .....	95
Table 4.13: Detailed record of building collapse .....	98
Table 5.1a: Re-designed brace connection (3-st, E-W), (unit: mm) .....	106
Table 5.1b: Re-designed brace connection (6-st, E-W), (unit: mm).....	106
Table 5.2a: Re-designed brace connection (3-st, N-S), (unit: mm) .....	106
Table 5.2b: Re-designed brace connection (6-st, N-S), (unit: mm).....	106
Table 5.3a: Resistance of brace connections (3-st, E-W), (unit: kN).....	107
Table 5.3b: Resistance of brace connections (6-st, E-W), (unit: kN).....	107
Table 5.4a: Resistance of brace connections (3-st, N-S), (unit: kN).....	108

Table 5.4b: Resistance of brace connections (6-st, N-S), (unit: kN).....	108
Table 5.5a: Design of braces cover plate (3-st E-W), (unit: mm; kN).....	110
Table 5.5b: Design of braces cover plate (6-st E-W), (unit: mm; kN).....	111
Table 5.6a: Design of braces cover plate (3-st N-S), (unit: mm; kN).....	111
Table 5.6b: Design of braces cover plate (6-st N-S), (unit: mm; kN).....	111
Table 5.7: Retrofitting of columns (6-st E-W), (unit: mm).....	112
Table 5.8a: Retrofitting of columns (3-st N-S), (unit: mm).....	112
Table 5.8b: Retrofitting of columns (6-st N-S), (unit: mm).....	113
Table 5.9a: Retrofitting of beams (3-st E-W), (unit: mm).....	113
Table 5.9b: Retrofitting of beams (6-st E-W), (unit: mm).....	114
Table 5.10a: Retrofitting of beams (3-st N-S), (unit: mm).....	114
Table 5.10b: Retrofitting of beams (6-st N-S), (unit: mm).....	114
Table 5.11: Dynamic properties of retrofitted buildings and pre-retrofit buildings.....	115
Table 5.12a: Summary of results from the IDA curves of post-retrofit 3-st CBF (E-W).....	117
Table 5.12b: Summary of results from the IDA curves of post-retrofit 6-st CBF (E-W).....	117
Table 5.13a: Summary of results from the IDA curves of post-retrofit 3-st CBF (N-S).....	118
Table 5.13b: Summary of results from the IDA curves of post-retrofit 6-st CBF (N-S).....	128
Table 5.14: Collapse margin ratio of retrofitted building for various performance levels ....	119
Table 5.15a: CBF components subjected to retrofit (3-st E-W).....	124
Table 5.15b: CBF components subjected to retrofit (6-st E-W).....	124
Table 5.16a: CBF components subjected to retrofit (3-st N-S).....	124
Table 5.16b: CBF components subjected to retrofit (6-st N-S).....	125
Table 5.17: Seismic hazard considered in this study.....	126

Table 5.18: Median peak interstorey drift, residual interstorey drift and floor acceleration of studied CBF buildings.....	127
Table 5.19: Seismic demand statistics of investigated steel structures.....	132
Table 5.20: Fragility of studied buildings for different hazard level (E-W).....	136
Table 5.21: Fragility of studied buildings for different hazard level (N-S).....	136

## CHAPTER 1. INTRODUCTION

### *1.1 Background*

Natural disasters caused by earthquakes are more likely to damage the existing building stock and in consequence to generate important economic losses (Coburn, 2002). To mitigate losses and to preserve buildings safe under earthquake loading, the National Building Code of Canada (NBCC) was constantly revised and improved. From the first introduction of seismic design provisions in NBCC 1941 to the current 2010 edition, the seismic design methodology was changed significantly, the ductility approach and capacity design method were introduced and the seismic hazard has evolved from 50%/50 years probability of exceedance to 2%/50 years probability of exceedance. Thus, the first probabilistic seismic hazard map based on the 50% probability of exceedance in 50 years (100 years return period) was introduced in the 1970 edition of NBCC. Further on, in the 1985 edition of NBCC, the seismic zones given in the previous map were revised and the hazard was raised to 10% probability of exceedance in 50 years. The 1990 edition of NBCC introduced the ductility-related force modification factor,  $R$ , and the capacity design method. In this respect, the 1990 edition of NBCC and the CSA/S16-89 standard linked the seismic design to structure ductility and special seismic detailing. Since then, the NBCC and CSA/S16 standard have been continually updated based on new research findings and lessons learned from past earthquakes (Tremblay, 2011). An important change was made in the 2005 edition of NBCC when the probability of earthquake exceedance was raised to 2%/50 years and the site specific Uniform Hazard Spectra was developed and introduced. In the same time, beside the ductility-related force modification factor, noted  $R_d$ , the overstrength-related force modification factor,  $R_o$ , was introduced (Mitchel et al, 2003).

In the event of an earthquake in Montreal, the high density building stock that was designed and built prior to 1990, is prone to considerable damage. Although the first probabilistic seismic hazard map was released in 1970, the 1970 NBCC edition was approved by the Administration council of the City of Montreal three years later. Therefore, buildings designed prior to 1973 were proportioned to withstand gravity loads in addition to wind loads. It is mentioned that the Limit States Design Method and the metric system was introduced in the 1978 edition of CSA/S16.1 standard labeled CSA/S16.1-M78 (where M means metric

system).

According to Statistics Canada, the percentage of dwelling units built in different provinces between 1948 and 1973 is given in Figure 1. Thus, the largest percentage of dwelling units was built in Eastern Canada and more specifically in areas characterized by medium to high seismic risk such as: Montreal (about 20%), Ottawa (about 12%) and Quebec City (6%). The percentage of existing office buildings is similar. Thus, the pre-1980 building stock is much larger than that of post-1980, which means that several existing buildings have lack of ductility and are more likely to show weakness in their seismic force resisting system. As illustrated, the existing building stock in Montreal area is vulnerable to earthquake.

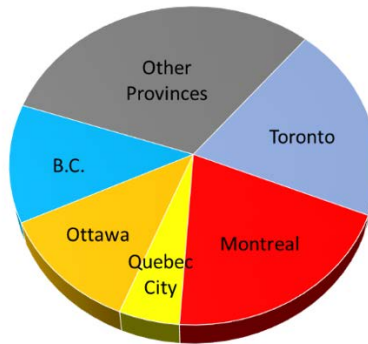


Figure 1.1: Distribution of dwelling units built between 1948 and 1973 (Tirca et al., 2012)

Steel structures, especially steel concentrically braced frames CBFs, were widely used for low-rise (2-3 storey) and middle-rise buildings with maximum 5 or 6 stories in height. The CBFs are characterised by high stiffness and moderate ductility. However, after braces reach buckling, the stiffness of the system diminishes. Meanwhile, braces were designed either to carry only axial tension forces or axial tension/compression forces. To summarize, the steel braced frame system is very popular especially in Eastern Canada.

Failure of brace connections designed without the consideration of ductility and seismic detailing is the most critical deficiency. Thus, the existing CBFs structures located in Montreal should be retrofitted before possible damage may happen. However, there is not a standardized methodology or guidelines to assess these buildings. In this regard, the performance based design method employed in the ASCE/SEI 41-13 standard was used

together with the NBCC 2010 and CSA/S16-09 standard requirements. According to ASCE/SEI 41-13 standard, the basic safety rehabilitation objective class is recommended for office buildings and the target performance levels are Life Safety and Collapse Prevention. In addition, the following retrofit strategies are promoted in ASCE/SEI 41-13 provisions: strengthening of structural components, global stiffening, mass reduction, base isolation or supplement energy dissipation (Constantinou et al., 1998). Thus, the first two retrofit technologies such as replacement of connections, enlarging section area, changing load path and adding steel cover plates are simple interventions aiming to strengthen the structure. Conversely, other retrofit technologies require increasing the damping amount by employing energy dissipation devices such as friction damper, viscous damper or base isolation. In order to select a proper retrofit strategy, a comprehensive consideration has to be taken into place, different retrofit strategies must be established and compared to evaluate costs, retrofitting time, and the post-retrofit seismic performance. In this study only the conventional retrofit strategy was applied to CBFs with hollow structural section (HSS) braces. Then, fragility assessment of pre- and post-retrofit buildings was conducted in order to emphasise the probability of damage for each considered damage state and to prevent the potential economic losses before they happen.

Since 2005 the OpenSees software was extensively used (Aguero et al., 2006; Uriz, 2004; Uriz and Mahin, 2008; Tremblay et al., 2009; Castonguay, 2009; Chen and Tirca, 2013 and others) and it was employed in this study. Moreover, to simulate the buckling and yielding of CBF braces, as well as the brace fracture due to low-cycle fatigue, an accurate OpenSees model was developed. In addition, in the OpenSees model, it is required to consider other deterioration models associated with plastic hinging of the CBF members like beams and columns. At the critical floor where braces or their connections reached failure, the columns at that floor buckle and lead to storey mechanism (Lignos and Karamanci, 2012). In addition, beams of the chevron CBF reach hinging at the location where braces are connected.

## ***1.2 Objectives***

The motivation of this project was to identify the seismic deficiencies of the 1980s low- and

middle-rise CBF office buildings located in Montreal (eastern Canada) and to find a cost-efficient seismic upgrading strategy. To achieve this goal, a 3- and 6-storey fictitious steel CBF buildings located in Montreal on firm soil (site class C) were designed according to NBCC 1980 and CSA.S16.1-M78 standard. Braces of CBFs were made of HSS cross-section and were designed to behave in tension and compression. The brace to frame connections consisted of a gusset plate welded to the slotted end part of HSS brace. The gusset plate was initially designed to respond to factored load combination that was transferred from the brace to the frame. The pre- and post-retrofit buildings were assessed using the equivalent static force procedure and the nonlinear time-history procedure by means of OpenSees. In addition, using the performance based design method, three performance levels such as: Immediate Occupancy, Life Safety and Collapse Prevention were considered and defined on each IDA curve. In this study, for one building, two times ten IDA curves were built for both directions of seismic loading (East-West and North-South). Each IDA curve gives the response of the building under a given ground motion. Further on, the fragility analysis comprising both epistemic and aleatoric uncertainties was conducted and the fragility curves were developed based on data collected from the IDA curves.

The proposed objectives are:

- To develop a seismic assessment procedure for existing low- and middle-rise CBF office buildings located in Montreal (Qc.) in order to evaluate the seismic deficiencies of their members and brace to frame connections.
- To derive the seismic fragility curves of pre- and post-retrofit fictitious low-rise (3-storey) and middle-rise (6-storey) CBF office buildings located in Montreal (Qc.) and designed according to the NBCC 1980 and CSA/S16.1-78 standard provisions in order to assess the probable potential losses before they happen.

### ***1.3 Methodology***

To achieve the above objectives, this study is divided into three main parts: i) the assessment of the 1980s CBF members and brace-to-frame connections in order to establish the failure

hierarchy, ii) the selection of the retrofit strategy based on the level of seismic deficiencies and performance based design procedure and iii) the incremental dynamic analysis and fragility assessment of pre- and post-retrofit buildings in order to assess the level of exceeding a given damage state.

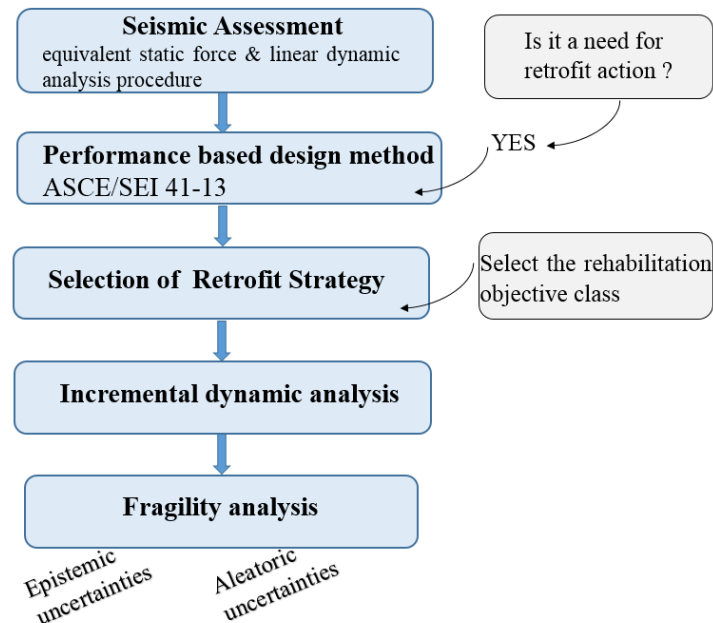


Figure 1.2: Methodology for seismic fragility assessment of building structure

The proposed methodology is illustrated in Figure 1.2. In this light, the first task is to investigate the response of existing building to the current code demand. The response of each CBF component is given in term of demand to capacity ratio. To accomplish this task the equivalent static force procedure and linear dynamic analysis by modal response spectrum method was performed. Then, the performance based design method considered in the ASCE/SEI 41-13 standard was employed in order to select the required rehabilitation objective class, the target performance level objectives and the suitable retrofit strategy. In order to obtain the IDA curves of the post-retrofit building, the incremental dynamic analysis by means of nonlinear time-history analysis conducted in the OpenSees environment was performed. By using data from the IDA curves, the damage levels were defined and the system's fragility was calculated by means of fragility curves. These curves emphasize the probability of exceedance of a damage state when both epistemic and aleatoric uncertainties were considered. It is noted

that each IDA curve is related to a ground motion.

#### ***1.4 Thesis organization***

This thesis includes six chapters:

- Chapter 1 covers the introduction, motivation, objectives and methodology.
- Chapter 2 contains detailed explanations of NBCC 1980 and CSA/S16.1-M78 standard requirements against those provided in the current code NBCC 2010 and CSA/S16-09 standard. In addition, the requirements addressed by ASCE/SEI 41-13 standard referring to the targeted performance levels and types of retrofit strategies are given. In addition, by using data from literature, a methodology for deriving analytical fragility curves based on data collected from the IDA curves is presented.
- Chapter 3 shows the design procedure of fictitious 3- and 6- storey CBFs office buildings according to the NBCC 1980 and CSA/S16.1-M78 standard. Additionally, detailed calculations of brace-to-frame connections are presented in order to identify the failure hierarchy.
- Chapter 4 consists in the application of seismic assessment procedure for the studied CBFs buildings that were evaluated against the current code demand (NBCC 2010) and CSA/S16-09 standard. The demand to capacity ratio is given for braces, beams, columns and brace to frame connections. The calculation was carried out based on the equivalent static force procedure, linear dynamic analysis by the modal response spectrum method (ETABS) and nonlinear time-history analysis (OpenSees) in order to detect seismic deficiencies in each structural member and connections.
- Chapter 5 covers the selection of retrofit strategy, the seismic assessment of post-retrofit buildings using non-linear time history analysis as explained in Chapter 4. Then, the IDA curves of the post-retrofit buildings are developed with the aim to

derive the analytical fragility curves.

- Chapter 6 concludes the research results and provides recommendations for further work.

## **CHAPTER 2. LITERATURE REVIEW**

### ***2.1 Introduction***

Concentrically braced frames (CBFs) are widely used in seismic zones in Canada due to their large stiffness. During the last decades, considerable research including experimental testing was carried out in order to assess the performance of the CBF system. In addition, the NBCC as well as the CSA/S16 standard have been continually updated as new research work was released. In this light, Sections 2.2 and 2.3 emphasise the evolution of seismic design procedure included in the NBCC and CSA S16 editions, respectively. The seismic design requirements given in the 1980 and 2010 editions of NBCC and the 1978 and 2009 editions of CSA/S16 standard are presented in detail.

Further, in Section 2.4, the seismic assessment recommendations provided in FEMA P695 and ASCE/SEI 41-13 standard are reviewed. Previous modelling approaches involved in the development of OpenSees models for CBFs with HSS braces and their connections are discussed in Section 2.5. These models are used as references in this research.

### ***2.2 Evolution of Seismic Design According to NBCC***

Since 1953, there are four generations of seismic hazard map that were released in NBCC editions. The first generation of seismic hazard map was released in the 1953 NBCC edition. It consisted of four seismic zones delimited based on the qualitative assessment of historical earthquakes. According to this seismic map, Montreal and Quebec City, as well as Vancouver were in Zone 3, which corresponds to the largest base shear coefficient. The second generation of seismic hazard map was released in the 1970 NBCC edition. This was the first probabilistic seismic hazard map computed for a return period of 100 years and a probability of exceedance of 50%/50 years. The distribution of seismic intensity on four zones was maintained. However, Montreal was moved in Zone 2, while Quebec City and Vancouver remained in the same Zone 3. The third generation of seismic hazard map was released in 1985 and was based on a probability of exceedance of 10%/50 years or 500 years return period. The 1985 map contains seven acceleration- and velocity-related zones (0 to 6). The base shear coefficient computed

for Montreal and that computed for Quebec City is comparable and is about half than that computed for Vancouver where the seismic demand has largely increased. Lastly, the fourth generation of the seismic hazard map is based on a probability of exceedance of 2%/50 years or 2500 years return period and was released in the 2005 edition of NBCC. Site-specific spectral acceleration ordinates corresponding to a period of 0.2, 0.5, 1.0 and 2.0s were provided for more than 600 locations. A brief summary referring to the evolution of seismic hazard information according to Heidebrecht (Heidebrecht, 2005) and the manner in which this information was used to determine the seismic hazard forces is given in Table 2.1.

Table 2.1: Evolution of seismic hazard and the manner of determining the seismic design forces in the NBCC editions according to Heidebrecht (2005)

NBC Edition	Nature of Hazard Information	Manner in which Hazard Information is Used to Determine Seismic Design Forces
1953 through 1965	Four zones (0, 1, 2, 3) based on the qualitative assessment of historical earthquake activity	Base shear coefficients are prescribed for the design of buildings in zone 1; these are doubled for zone 2 and multiplied by 4 for zone 3
1970	Four zones (0, 1, 2, 3) with boundaries based on peak acceleration at 0.01 annual probability of exceedance or 50% in 50 years (100 years return period)	Base shear coefficient includes a non-dimensional multiplier (0 for zone 0, 1 for zone 1, 2 for zone 2, and 4 for zone 3)
1975 through 1980		Base shear coefficient includes factor A, which is numerically equal to the zonal peak acceleration (0 for zone 0, 0.02 for zone 1, 0.04 for zone 2 and 0.08 for zone 3); value of seismic response factor is adjusted so that base shear is approximately 20% below that in the NBC 1970)
1985	Seven (0 to 6) acceleration- and velocity-related zones with boundaries based on 10% probability of exceedance in 50 years (500 years return period)	Base shear coefficient includes zonal velocity, $v$ , which is numerically equal to peak ground velocity in m/s (values are 0, 0.05, 0.10, 0.15, 0.20, 0.30 and 0.40); value of seismic response factor is adjusted by calibration process so that seismic forces are equivalent, on average across the country, to those in the NBC 1980
1990 and 1995		Elastic force coefficient includes zonal velocity, $v$ , (as above) with total seismic force $V$ calculated as elastic force divided by force reduction factor and then multiplied by a calibration factor of 0.6; the seismic response factor is modified to maintain the same design force for highly ductile systems as in the NBC 1985
2005 and 2010	Site-specific spectral acceleration ordinates determined at 2% probability of exceedance in 50 years (2500 years return period)	Dynamic analysis or static elastic force coefficient, both using spectral acceleration ordinates as input; site coefficients and higher mode factor also dependent upon spectral acceleration ordinates

As shown in Table 2.1, the seismic load calculation given in the 1965 edition of NBCC was based on empirical research and historical earthquakes, while no ductility design factors were considered. Similarly, in the 1970, 1975 and 1980 edition of NBCC, the considerations of ductility in the seismic load calculation was limited. It is noted that although the seismic hazard map is the same, due to the adjustment of seismic response factor in the 1980 edition, the base shear is approximately 20% lower than that in the 1970 edition. In addition, the ductility factor for each type of seismic force resisting system was released in the 1990 edition of NBCC. Important changes referring to seismic hazard and design procedure were made in the 2005 edition of NBCC when the level of seismic hazard increased to 2% probability of exceedance in 50 years. Referring to seismic design, the empirical equation for the estimation of fundamental period of braced frame structure was changed, a new equation for base shear calculation was provided and contains the period-dependent site factors, higher mode effects and the delineation of effects of overstrength and ductility in terms of the overstrength-related force modification factor,  $R_o$ , and ductility-related force modification factor,  $R_d$ . There are slight changes in the NBCC 2010 edition versus the 2005 edition.

Because this study focuses on the seismic response of existing CBF buildings located in Montreal, a brief presentation of historical earthquakes that occurred in Eastern Canada is provided. From data collected by Lamontagne et al. (2008), ten historical earthquakes with magnitudes between 5 and 7 that occurred in Eastern Canada during the interval 1600-2006 were selected (Tirca et al., 2013). Among them, nine earthquakes were recorded in the province of Quebec and one in Cornwall, Ontario. (Figure 2.1)

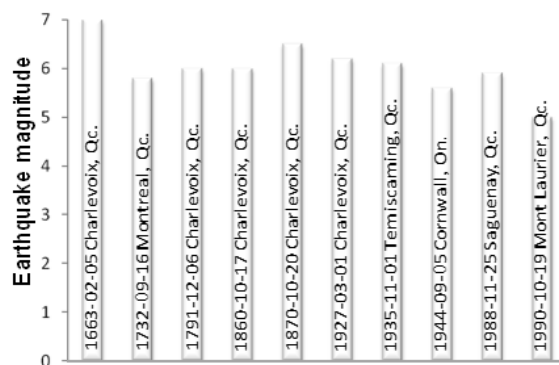


Figure 2.1: Significant earthquake in Eastern Canada (1600 – 2006)

### 2.2.1 Seismic design requirements according to NBCC 1980

In the 1980 edition of NBCC it is required to design the seismic force resisting system of each building structure (SFRS) to the combination of earthquake load and gravity load including dead load ( $D$ ), live load ( $L$ ), and snow load ( $S$ ). It is noted that 25% of the snow load is included in the calculation of seismic weight. The expression for snow load calculation is given below:

$$s = C_s \times g \quad (2.1)$$

where  $C_s$  is the basic snow load coefficient and  $g$  is the ground snow load given for different locations in the climate data table of supplement of NBCC 1980.

It is important to mention that the limit state design approach was introduced in the 1980 edition of NBCC and there was no difference between wind and earthquake load,  $Q$ , in the design combinations.

According to NBCC 1980 the following load combinations are considered:

$$a) 1.25 DL + 1.5 Q \quad (2.2(a))$$

$$b) 1.25 DL + 1.5 LL \quad (2.2(b))$$

$$c) 1.25 DL + 0.7(1.5 LL + 1.5 Q) \quad (2.2(c))$$

As explained above, the seismic map used in the 1980's, is shown in Figure 2.2, it contains four zones (0, 1, 2, 3) with boundaries based on peak acceleration at 0.01 annual probability (50%/50 years).

The lateral seismic force,  $V$ , assumed to act non-concurrently in any direction, depends on the horizontal ground acceleration ratio ( $A$ ), the seismic response factor ( $S$ ), the type of construction factor ( $K$ ), the importance factor ( $I$ ), the soil condition factor ( $F$ ), and the structure seismic weight ( $W$ ). The lateral seismic force  $V$  is given below:

$$V = A \times S \times K \times I \times F \times W \quad (2.3)$$

The horizontal design ground acceleration ratio ( $A$ ), which is numerically equal to the zonal peak acceleration, is: 0 for zone 0; 0.02 for zone 1; 0.04 for zone 2; and 0.08 for zone 3.

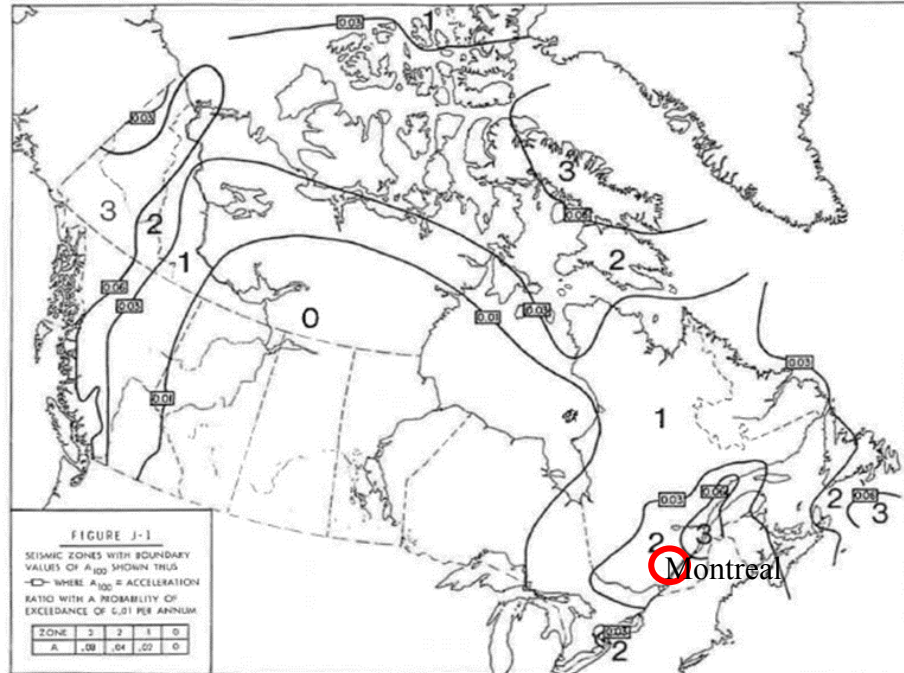


Figure 2.2: Seismic zone map (NBCC 1980 supplement) (Montreal Zone 2)

The seismic response factor ( $S$ ) is given by the following equation:

$$S = \frac{0.5}{\sqrt{T}} \leq 1.0 \quad (2.4)$$

where  $T$  is the fundamental period of the structure. In lieu of more accurate estimates, the following empirical formulas can be used for the determination of the fundamental period  $T$  for buildings:

$$T = \frac{0.09h_n}{\sqrt{D_n}} \quad (2.5)$$

where  $h_n$  is the total building height and  $D_n$  is the dimension of the building in a direction parallel to the direction of applied seismic force.

The distribution of base shear over the building height is computed according to Equation (2.6) in which an additional force  $F_t = 0.004V (h_n/D_n)^2$  is concentrated at the top level of the structure to account for the higher mode effects. It is noted that, for  $(h_n/D_n) < 3$  the value of  $F_t$  is zero and for  $(h_n/D_n) \geq 3$  the maximum value of  $F_t$  is limited to  $0.15V$  or  $F_t \leq 0.15V$ .

$$F_x = (V - Ft) \frac{W_x h_x}{\sum_{i=1}^n W_i h_i} \quad (2.6)$$

where  $F_x$  is the storey force,  $W_x$  is the storey weight and  $h_x$  is the vertical height from the frame base to the level of calculation.

The total shear force per floor including torsional effects and  $P-\Delta$  effects was transferred to SFRSs in proportion to their rigidities. According to NBCC 1980, the torsional moment in the horizontal plan of the building  $M_{tx}$  is given in Equation (2.7) and is computed by multiplying the storey shear force  $(V - \sum_{i=1}^x F_i)$  with the design eccentricity  $e_x$  computed at the level of calculation.

$$M_{tx} = (V - \sum_{i=1}^x F_i) e_x \quad (2.7)$$

The design eccentricity is computed by one of the following Equations, whichever provides the greater effect.

$$\begin{aligned} e_x &= 1.5e + 0.05D_n \\ &= 0.5e - 0.05D_n \end{aligned} \quad (2.8)$$

where  $e$  is calculated from Equation (2.9).

$$e = \frac{\sum_{i=x}^N F_i e_{ix}}{\sum_{i=x}^N F_i} \quad (2.9)$$

In Equation (2.9)  $F_i$  is the lateral force applied at level  $i$  and  $e_{ix}$  is the distance between the center of mass and center of rigidity. When the maximum design eccentricity exceeds  $0.25D_n$ , a dynamic analysis is required or  $M_{tx}$  calculated according to Equation (2.7) should be doubled.

There are three methods for  $P-\Delta$  calculation such as: iterative method, one-step maximum deflection method and modified iterative method that were introduced in CSA S16.1-1987. Regardless of which of the above  $P-\Delta$  method is used, the term  $\Sigma Pi$  in Equation (2.10) should be taken as the sum of the column loads causing the  $P-\Delta$  shear ( $V_i'$ ) which is carried by the lateral load system under consideration. Herein,  $\Delta_i$  and  $\Delta_{i-1}$  are the storey lateral deformation of floor  $i$  and the lower floor.  $P-\Delta$  force ( $H_i'$ ) is the difference of  $P-\Delta$  shear ( $V_i'$ ) of the upper and lower floor as is shown in Equation (2.11).

$$V'_i = \frac{\sum P_i}{h_i} (\Delta_i - \Delta_{i-1}) \quad (2.10)$$

$$H'_i = V'_i - V'_{i-1} \quad (2.11)$$

### 2.2.2 Seismic design requirements according to NBCC 2010

In NBCC 2010, snow load is calculated with Equation (2.12) where  $I_a$  is the importance factor,  $S_s$  is the ground snow load,  $C_b$  is the basic roof snow load factor,  $C_w$  is the wind exposure factor,  $C_s$  is the slope factor,  $C_a$  is the shape factor and  $S_r$  is the associated rain load.

$$S = I_a[S_s(C_b C_w C_s C_a) + S_r] \quad (2.12)$$

Thus, in comparison with NBCC 1980, the expression for snow load differs.

Regarding the seismic load calculation, the changing of the fundamental period equation greatly affects the base shear of the building. The expression used to calculate the fundamental period ( $T_a$ ) of the building has an empirical base and is given below for braced frames. Based on this equation, which depends on the total building height ( $h_n$ ),  $T_a$  results the same for both directions of consideration.

$$T_a = 0.025h_n \quad (2.13)$$

The lateral seismic force,  $V$ , is calculated based on the 5% damped spectrum response acceleration ( $S(T_a)$ ) values multiplied by the higher mode factor ( $M_v$ ), importance factor ( $I_E$ ) and the building weight ( $W$ ). The spectrum response acceleration ( $S(T_a)$ ) depends on the fundamental period ( $T_a$ ) and the site amplification factors  $F_a$  and  $F_v$  which are equal to unity for site class C. However, the resulted base shear is reduced by the ductility-related force modification factor ( $R_d$ ) and the overstrength-related force modification factor ( $R_o$ ).

$$V = S(T_a)M_v I_E W / (R_d R_o) \quad (2.14)$$

Another major difference is at the level of load combinations, which will affect the factored design load. The five load combinations given in NBCC 2010 are:

$$\text{Combo 1: } 1.4DL \quad (2.15(a))$$

$$\text{Combo 2: } 1.25DL + 1.5LL \quad (2.15(b))$$

$$\text{Combo 3: } 1.25DL + 1.5S \quad (2.15(c))$$

$$\text{Combo 4: } 1.25DL + 1.4W \quad (2.15(d))$$

$$\text{Combo 5: } 1.0DL + 1.0E \quad (2.15(e))$$

where  $S$  is the snow load and  $E$  is the earthquake load.

The distribution of earthquake load over the building height is given in Equation (2.16). For buildings with the fundamental period larger than 0.7s, the concentrated load applied at building top is  $F_t = 0.7TaV \leq 0.25V$ .

$$F_x = (V - F_t)W_x h_x / (\sum_{i=1}^n W_i h_i) \quad (2.16)$$

The torsional effect is considered and is calculated by one of the following Equations, whichever provides the greater effect.

$$\begin{aligned} T_x &= F_x(e_x + 0.10D_{nx}) \\ &= F_x(e_x - 0.10D_{nx}) \end{aligned} \quad (2.17)$$

where  $D_{nx}$  is the dimension of the building in a direction perpendicular to the direction of applied seismic force and  $e_x$  is the distance between the center of mass and center of rigidity

The  $P-\Delta$  effect is considered as the amplification of storey shear by a stability factor ( $\theta$ ) which is calculated with Eq. (2.18)

$$\theta_x = \frac{\sum_{i=x}^n W_i \Delta_{mx}}{R_o \sum_{i=x}^n F_i h_s} \quad (2.18)$$

where  $\sum_{i=x}^n F_i$  is the seismic design shear force at the level under consideration,  $\sum_{i=x}^n W_i$  is that portion of the factored dead plus live load above the storey under consideration,  $\Delta_{mx}$  is the maximum inelastic interstorey deflection,  $h_s$  is the storey height, while  $R_o$  is the overstrength-related force modification factor. Thus, the amplification of the seismic shear force according to  $P-\Delta$  effects is given by:  $\sum_{i=x}^n F_i^* = R_o \sum_{i=x}^n F_i (1 + \theta_x)$

The changes introduced in the 1970, 1975, 1980, 1985, 1995, 2005 and 2010 NBCC

editions with respect to the design spectrum for Montreal corresponding to site class C soil are illustrated in Figure 2.3.

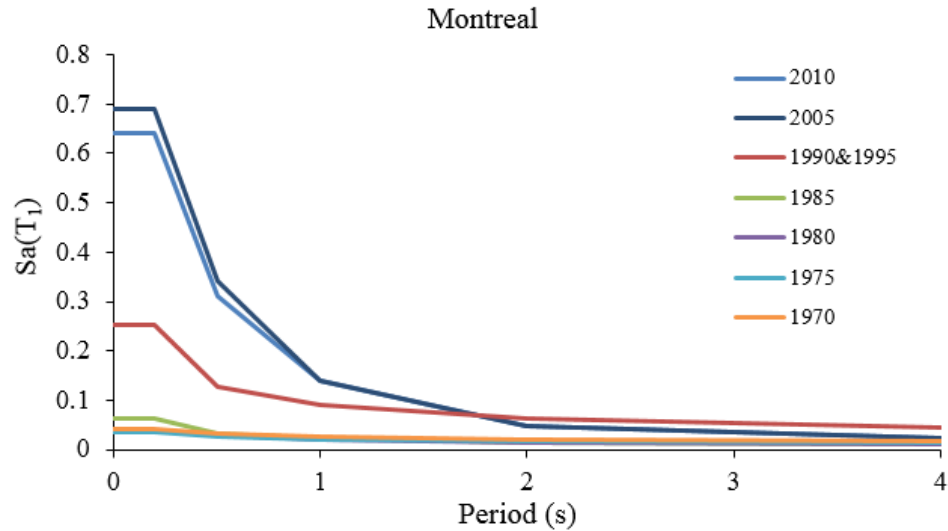


Figure 2.3: Evolution of design spectrum for Montreal, site class C from 1970 to 2010

From the above figure it can be seen that the seismic demand has significantly increased from 1980 to 1990 and from 1990 to 2005 especially for buildings characterized by a short to medium fundamental period.

### ***2.3 Evolution of Seismic Provisions according to CSA S16***

The evolution of the seismic design provisions can be emphasized by reviewing the 14 editions of CSA S16 standard that have been published so far. Among them, the first seven editions were based on the working stress design method and the last seven editions (1974, 1978, 1984, 1989, 1994, 2001 and 2009) were based on limit states design principle. The 1969 edition of CSA/S16 standard was the last edition based on working stress design. It is noted that the CSA S16-09 edition supersedes all the previous limit states editions published before.

Special design and detailing requirements implemented to achieve ductile seismic response were introduced for the first time in the 1989 edition of the CSA/S16 standard. It means that all structural members and their connections designed before 1990 were proportioned to carry the factored load and not the tensile and compression capacity of braces.

In addition, the failure hierarchy was not investigated and some undesirable (brittle) failure modes are more likely to occur (e.g. shearing of welding fillet, tension rupture on net section, buckling of gusset plates, etc.).

After the capacity design method was introduced (CSA/S16-89), braces of CBFs were designed to yield and buckle, their connections were designed to sustain the nonlinear response of braces and all the remaining CBF members were proportioned to behave elastically. The seismic detailing required in CSA/S16-09 standard is an evolved version of those required in the CSA/S16-89 standard. Thus, all CBF members such as brace connections, columns, beams, and other connections along the seismic load path, must be designed to resist the probable resistance of braces in addition to the tributary factored dead, live and snow loads. In addition, torsion and  $P-\Delta$  effect is considered.

### 2.3.1 Seismic provisions for CBFs according to CSA S16.1-M78

According to CSA/S16.1-M78 standard, compression members shall be designed on the basis of their effective length ( $KL$ ), where  $K$  is the effective length factor, and  $L$  is the unbraced length. The nominal yield strength used for W-shape members is  $F_y = 300 \text{ MPa}$  ( $F_u = 450 \text{ MPa}$ ), for hollow structural section (HSS) members  $F_y = 345 \text{ MPa}$  where ( $F_u = 448 \text{ MPa}$ ) whereas for gusset plates and splices  $F_y = 300 \text{ MPa}$  ( $F_u = 450 \text{ MPa}$ ).

Based on the slenderness ratio,  $\lambda$ , computed as:  $\lambda = \frac{KL}{r} \sqrt{\frac{F_y}{\pi^2 E}}$  the expression of factored compression resistance of a member is given below:

$$\begin{aligned}
 \text{(a) } 0 \leq \lambda \leq 0.15 & \quad C_r = \Phi A F_y \\
 \text{(b) } 0.15 \leq \lambda \leq 1.0 & \quad C_r = \Phi A F_y (1.035 - 0.202\lambda - 0.222\lambda^2) \\
 \text{(c) } 1.0 \leq \lambda \leq 2.0 & \quad C_r = \Phi A F_y (-0.111 + 0.636\lambda^{-1} + 0.087\lambda^{-2}) \quad (2.19) \\
 \text{(d) } 2.0 \leq \lambda \leq 3.6 & \quad C_r = \Phi A F_y (0.009 + 0.877\lambda^{-2}) \\
 \text{(e) } 3.6 < \lambda & \quad C_r = \Phi A F_y \lambda^{-2} = \Phi A \left[ \frac{1970000}{KL/r^2} \right]
 \end{aligned}$$

where  $A$  represents the gross cross-section area of the member,  $F_y$  is the yield strength of the steel,  $r$  is the radius of gyration and  $\Phi$  is the factor resistance taken as 0.9 unless otherwise specified, while  $E$  is the elastic modulus of steel.

For element subjected to axial tension, the factored tensile resistance,  $T_r$ , of a member can be calculated by Equation (2.20), as shown below:

$$\begin{aligned}
 (i) \quad T_r &= \Phi A_n F_y \quad \text{When } A_n/A_g \geq F_y/F_u \\
 &= \Phi \left( F_u \frac{A_n}{A_g} \right) A_n \quad \text{When } A_n/A_g < F_y/F_u \\
 (ii) \quad T_r &= 0.85 \Phi A_n F_y \quad (2.20)
 \end{aligned}$$

Where  $F_u$  is the ultimate yield strength,  $A_n$  and  $A_g$  is the net cross-section area and gross cross-section area, respectively.

Members subjected to a combine effect of bending moment and compression force should be checked by using the interaction Equation (2.21). The bending effect coefficient ( $\omega$ ) was taken as 1.0. Because beams of CBFs are laterally supported by the composite steel deck, the flexural resistance  $M_{rx}$ , can be calculated as  $\Phi Z_x F_y$  for Class 1 sections. Members subjected to tension force and bending moment should be proportioned to respond to the interaction equation (2.22).

$$\frac{C_f}{C_{rx}} + \frac{\omega_x M_{fx}}{M_{rx} \left( 1 - \frac{C_f}{C_{ex}} \right)} \leq 1.0 \quad (2.21)$$

$$\frac{T_f}{T_r} + \frac{M_f}{M_r} \leq 1.0 \quad (2.22)$$

The column failure mode can be either the cross-sectional strength or the overall member strength. The lateral-torsional buckling failure mode was introduced later on. In general, the the cross-sectional strength is the limiting strength of the short columns. For uniaxial bending about strong axis the equation proposed by Pillai (1974) was considered. According to his research, the interaction equation for wide flange beam-columns section (W shape) bending about the strong axis, is:

$$M_x \leq M_{px}, \text{ for } 0 \leq \frac{P}{P_y} \leq 0.15 \text{ and,}$$

$$M_x \leq 1.18 \left(1 - \frac{P}{P_y}\right) M_{px}, \text{ for } 0.15 \leq \frac{P}{P_y} \leq 1.0 \quad (2.23)$$

where  $M_{px}$  is the plastic moment,  $P$  is the factored compression force and  $P_y$  is the compression strength. However this equation is conservative.

Regarding the connection design, possible failure modes like yielding and buckling strength of gusset plate, net rupture of gusset plate or brace, and welding shear resistance were checked. The latter, is calculated as the minimum value between the factored resistance of base metal and weld metal as per Equation (2.24) and the other failure modes are discussed in Chapter 3.

$$V_r = \min(0.66\Phi A_m F_y ; 0.50\Phi A_w X_u) \quad (2.24)$$

In the above equation,  $A_m$  is the shear area of effective fusion face and  $A_w$  is the area off effective weld throat, plug or slot,  $X_u$  is the electrode ultimate strength.  $\Phi = 0.9$ .

### **2.3.2 Seismic provisions for concentrically braced frame (CBF) according to CSA S16.1-09**

As per the capacity design method, the probable compression resistance ( $C_u$ ) and probable tensile resistance ( $T_u$ ) of brace members are calculated in order to design brace connections, as well as the beams and columns of CBFs.

The tensile resistance,  $T_r$  and probable tensile resistance,  $T_u$  of HSS brace is:

$$T_r = 0.9A_g F_y \quad (2.25)$$

$$T_u = A_g R_y F_y \quad (2.26)$$

The class of sections calculated based on the CSA S16.1-M78 standard remain almost the same, while the equation for compression resistance calculation is:

$$C_r = \Phi A F_y (1 + \lambda^{2n})^{-\frac{1}{n}}, \lambda = \sqrt{\frac{F_y}{F_E}}, F_E = \frac{\pi^2 E}{\left(\frac{KL}{r}\right)^2} \quad (2.27)$$

where  $\lambda$  is the slenderness and  $KL/r$  is the slenderness ratio which is limited to 200 for compression members.

The probable compression resistance ( $C_u$ ) of brace member is given below:

$$C_u = \min(R_y F_y A_g, 1.2 R_y C_r / \Phi) \quad (2.28)$$

After buckling of brace occurs, the load transferred to other structural element reduces because the brace member possesses only the compressive strength corresponding to post buckling compression resistance ( $C_u'$ ) which can be calculated by the formula below:

$$C_u' = \min(0.2 R_y F_y A_g, R_y C_r / \Phi) \quad (2.29)$$

For W-shape class 1 and 2 members subjected to compression and bending the interaction equation is:

$$\frac{C_f}{C_r} + \frac{0.85 U_1 M_{fx}}{M_{rx}} \leq 1.0, U_1 = \left[ \frac{\omega_1}{1 - \frac{C_f}{C_e}} \right] \quad (2.30)$$

where the coefficient  $\omega_1$  is taken as 1.0 for members subjected to distributed loads or a series of point loads between supports and 0.85 for members subjected to a concentrated load or moment between supports.

As noted above, four mode of failure including local buckling, strength of the cross-section, overall member strength and lateral-torsional buckling strength as given in Clause 13.8 have to be checked for members subjected to axial compression and bending.

Members required to resist both bending moments and an axial tensile force shall be proportioned so that:

$$\frac{T_f}{T_r} + \frac{M_f}{M_r} \leq 1.0 \quad (2.31)$$

Regarding the brace-to-frame gusset plate connections the following verifications are required:

The welding shear resistance is calculated by the same Equation as Equation (2.24), but the coefficient was slightly modified:

$$V_r = \min(0.67\Phi_w A_m F_u ; 0.67\Phi_w A_w X_u) \quad (2.32)$$

where  $\Phi_w = 0.67$ .

Block shear failure of connection was introduced in the CSA S16.1-94 and modified in CSA S16-09 based on the assumption that the ultimate tensile strength and the ultimate shear strength are reached simultaneously along both failure planes. According to the current code the following equation is used to calculate block shear resistance:

$$T_r = \Phi_u [U_t A_n F_u + 0.6 A_{gv} \frac{(F_y + F_u)}{2}] \quad (2.33)$$

where  $A_n$  is the net area in tension and  $A_{gv}$  is the gross area in shear for block failure,  $U_t = 1.0$  for gusset plates and the factor  $\Phi_u = 0.75$ .

Shear lag effect is also required to be considered for net rupture of brace welded connections with single concentric gusset plate. The net area is reduced by the introduction of cross-sectional efficiency,  $U$ , as  $A_e = A_n U$  and therefor the effective capacity for tensile rupture in the net section is  $T_e = T_{r-net} U$ , where  $T_{r-net}$  is the net rupture resistance.

The cross-sectional efficiency ( $U$ ) is calculated by the following equation according to the new release edition of CSA/S16-14:

$$U = 1.1 - (\bar{x}'/L_w) \quad (2.34)$$

where  $\bar{x}'$  is the vertical distance between the upper face of gusset plate to the center of gravity of top half slotted-end HSS weld connection. If the ratio  $\bar{x}'/L_w \leq 0.1$  the shear lag effect can be neglected ( $U=1.0$ ). For the ratio  $\bar{x}'/L_w > 0.3$ , the block shear (tear-out) governs. For  $0.1 < \bar{x}'/L_w \leq 0.3$ , the shear lag effect has to be considered and the cross-sectional efficiency ( $U$ ) has to be larger than 0.8. The variation of  $U$  value versus the ratio  $\bar{x}'/L_w$  is given in Figure 2.4 according to CSA/S16-14.

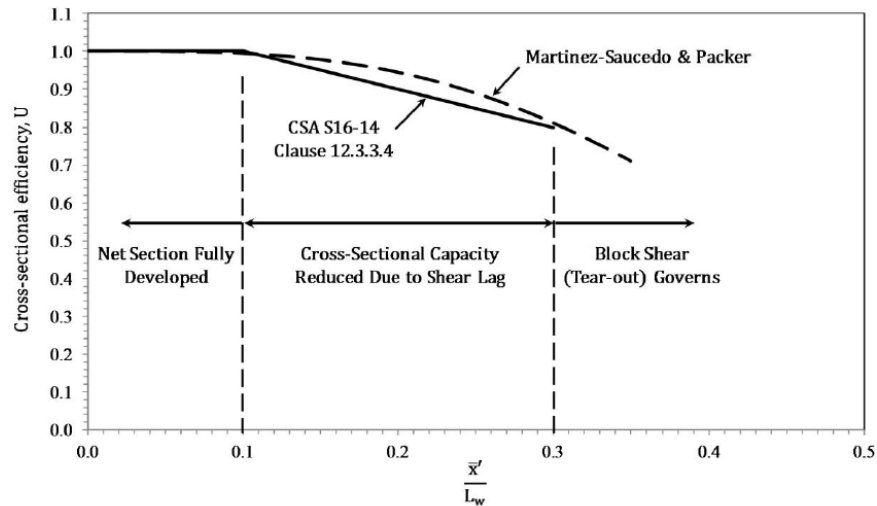


Figure 2.4: Bi-linear approximation used for  $U$ , in CSA S16-14, for all slotted HSS welded connections with single concentric gusset plates (Packer, 2014)

## 2.4 Seismic Assessment of Existing Buildings

### 2.4.1 FEMA P695(2009) and AISC/SEI 41-13 requirements

Seismic assessment is a required procedure with the aim to evaluate the strength of existing buildings to resist the seismic loads prescribed by the current code provisions in order to propose retrofit actions. However, there is no Canadian standard that can be used for seismic assessment of existing buildings and nor schemes of retrofit strategies. Due to this drawback and the large existing building stock, investigations based on case studies are required. There are some methodologies introduced in FEMA P695 (2009) and AISC/SEI 41-13 standard that are presented below.

The methodology introduced in FEMA P695 (2009) provides a quantitative basis for determining the building system performance. The methodology is illustrated in Figure 2.5 and requires several steps. However, this methodology was developed to assess the performance of building structures designed based on the current code and standard requirements.

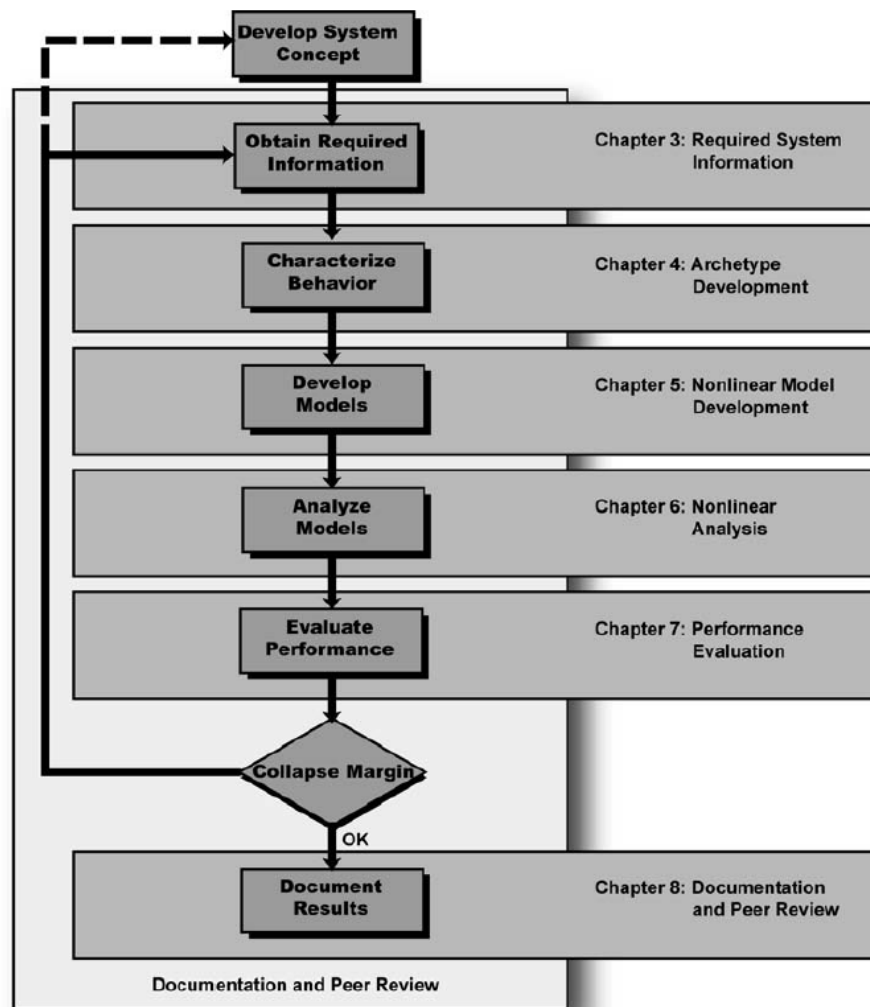


Figure 2.5: Process for quantitatively establishing and documenting seismic performance of building structure (FEMA P695, 2009)

The performance of the building structure is assessed based on the collapse margin ratio which is defined as the ratio of the intensity measure parameter at failure (e.g.  $S(TI)$ ) over the corresponding design spectrum ordinate. When the ratio is less than 1 the system fails before it can sustain the current code demand. Acceptable performance is achieved when the adjusted collapse margin ratios,  $ACMR$ , meet the following two criteria:

a) the average value of adjusted collapse margin ratio for each performance level exceeds  $ACMR_{10\%}$  or  $ACMR_i \geq ACMR_{10\%}$ ;

b) individual values of adjusted collapse margin ratio for each index archetype within a performance exceeds  $ACMR_{20\%}$  or  $ACMR_i \geq ACMR_{20\%}$ .

It is noted that the  $ACMR$  ratio resulted from the  $CMR$  ratio while including the uncertainties effect. If the building does not satisfies the aforementioned conditions the building design should be revised.

For existing and retrofitted building structures the requirements given in FEMA 356 (FEMA, 2000) and further included in ASCE/SEI 41-13 standard are discussed. The performance based approach was introduced in the ASCE/SEI 41-13 standard. Thus, depending on the building occupancy type three rehabilitation objective classes were proposed: Basic safety objective ( $BSO$ ), Enhanced objectives ( $EO$ ) and Limited objectives ( $LO$ ). For example, a typical Rehabilitation Objective class for office buildings and residential buildings is *Basic Safety*, for critical or essential structures (e.g. Hospitals, Fire stations, Police stations) the rehabilitation objective class is *Enhanced Rehabilitation*, while for other less critical structures is the *Limited Rehabilitation Objective*. In the aforementioned standard, four target building performance levels: Operational Performance ( $OP$ ), Immediate Occupancy ( $IO$ ), Life Safety ( $LS$ ), and Collapse Prevention ( $CP$ ) are defined and combined with different hazard levels. In this light, Figure 2.6 presents the matrix of Rehabilitation Objectives related to the extent of damage (Performance Level) and the earthquake hazard level. As illustrated in the figure, the Basic Safety Objective ( $BSO$ ) is the rehabilitation objective that achieves the dual rehabilitation goals of  $LS$  for the Basic Service Earthquake 1 (BSE-1) and  $CP$  for BSE-2. In other words, buildings meeting the  $BSO$  are expected to experience little damage from frequent, moderate earthquakes (10% in 50 years probability of exceedance) while for more severe rare events (2% in 50 years probability of exceedance) significantly damage and potential economic losses are expected.

Structural and nonstructural damage associated with each performance level are introduced. Thus, in Table C1-2 of ASCE/SEI 41-13 standard, which is reproduced in Figure 2.7, there are defined four damage control levels namely: very light ( $VLD$ ), light ( $LD$ ), moderate ( $MD$ ) and severe damage ( $SD$ ). In addition to the aforementioned four building performance levels, two performance ranges: Damage control range and Limited safety range

are also defined. The expected post-earthquake state represented on the performance axes is given in Figure 2.8. Thus, high building performance corresponds to reduced losses and low building performance with significant losses.

**Table C1-1. Rehabilitation Objectives**

		Target Building Performance Levels			
		Operational Performance Level (1-A)	Immediate Occupancy Performance Level (1-B)	Life Safety Performance Level (3-C)	Collapse Prevention Performance Level (5-E)
Earthquake Hazard Level	50%/50 year	a	b	c	d
	20%/50 year	e	f	g	h
	BSE-1 (~ 10%/50 year)	i	j	k	l
	BSE-2 (~ 2%/50 year)	m	n	o	p

<sup>1</sup>Each cell in the above matrix represents a discrete Rehabilitation Objective.

<sup>2</sup>The Rehabilitation Objectives in the matrix above may be used to represent the three specific Rehabilitation Objectives defined in Sections 1.4.1, 1.4.2, and 1.4.3, as follows:

Basic Safety Objective (BSO)	k and p
Enhanced Objectives	k and m, n, or o p and i or j k and p and a, b, c, or f m, n, or o alone
Limited Objectives	k alone p alone c, d, g, h, or l alone

Figure 2.6: Rehabilitation objectives matrix (ASCE/SEI 41-13)

As given above, the Rehabilitation objective is a combination of a Target building performance level, an Earthquake hazard level and an assigned Objective rehabilitation class. It is a common practice to investigate the building performance based on the maximum interstorey drift parameter. However, in order to have a more detailed analysis, a second response parameter namely the maximum residual interstorey drift should be introduced. In the case of CBF building structure, the description of damage associated to each performance level, as well as the suggested interstorey drift values are provided in Figure 2.9 according to ASCE/SEI 41-13 standard.

**Table C1-2. Damage Control and Building Performance Levels**

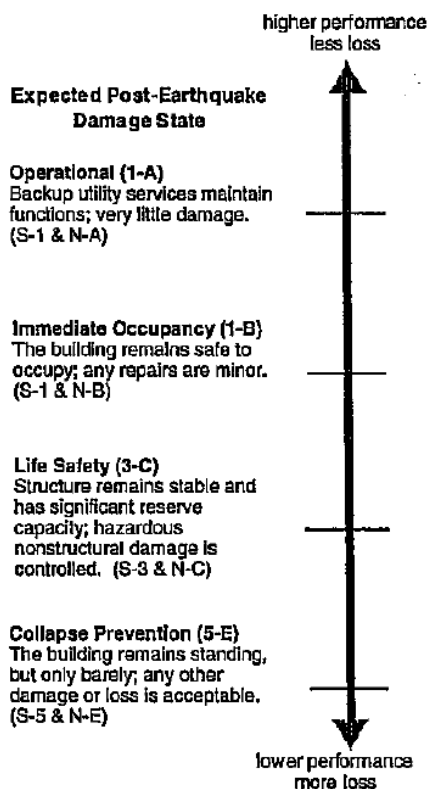
	Target Building Performance Levels			
	Collapse Prevention Level (5-E)	Life Safety Level (3-C)	Immediate Occupancy Level (1-B)	Operational Level (1-A)
Overall Damage	Severe	Moderate	Light	Very Light
General	Little residual stiffness and strength, but load-bearing columns and walls function. Large permanent drifts. Some exits blocked. Infills and unbraced parapets failed or at incipient failure. Building is near collapse.	Some residual strength and stiffness left in all stories. Gravity-load-bearing elements function. No out-of-plane failure of walls or tipping of parapets. Some permanent drift. Damage to partitions. Building may be beyond economical repair.	No permanent drift. Structure substantially retains original strength and stiffness. Minor cracking of facades, partitions, and ceilings as well as structural elements. Elevators can be restarted. Fire protection operable.	No permanent drift. Structure substantially retains original strength and stiffness. Minor cracking of facades, partitions, and ceilings as well as structural elements. All systems important to normal operation are functional.
Nonstructural components	Extensive damage.	Falling hazards mitigated but many architectural, mechanical, and electrical systems are damaged.	Equipment and contents are generally secure, but may not operate due to mechanical failure or lack of utilities.	Negligible damage occurs. Power and other utilities are available, possibly from standby sources.
Comparison with performance intended for buildings designed under the NEHRP Provisions, for the Design Earthquake	Significantly more damage and greater risk.	Somewhat more damage and slightly higher risk.	Less damage and lower risk.	Much less damage and lower risk.

Figure 2.7: Damage control and building performance levels (ASCE/SEI, 2013)

The building performance axis depicted in Figure 2.8 is given as a function of structural members' performance, as well as non-structural components performance. Non-structural components are drift-sensitive (ceiling, cladding etc.) and acceleration-sensitive (HVAC units, mechanical system, etc.). Thus, the target building performance and ranges incorporating the performance of non-structural components according to ASCE/SEI 41-13 is given in Figure 2.10.

Therefore, in order to assess the performance up to failure of a pre- and post-retrofit building, an analysis framework and a nonlinear model are required. The retrofit strategies proposed in ASCE/SEI 41-13 standard are: strengthening of structural components, global stiffening, mass reduction, base isolation or supplement energy dissipation. To identify the collapse point, FEMA P695 recommends using the incremental dynamic analysis (*IDA*)

method presented below.



**FIGURE C1-2. Target Building Performance Levels and Ranges.**

Figure 2.8: Target building performance levels and ranges (ASCE/SEI 41-13)

**Table C1-3. Structural Performance Levels and Damage<sup>1,2,3</sup>—Vertical Elements**

Elements	Type	Structural Performance Levels		
		Collapse Prevention (S-5)	Life Safety (S-3)	Immediate Occupancy (S-1)
Braced Steel Frames	Primary	Extensive yielding and buckling of braces. Many braces and their connections may fail.	Many braces yield or buckle but do not totally fail. Many connections may fail.	Minor yielding or buckling of braces.
	Secondary	Same as primary.	Same as primary.	Same as primary.
	Drift	2% transient or permanent.	1.5% transient; 0.5% permanent.	0.5% transient; negligible permanent.

Figure 2.9: Structural performance levels and damage for CBF structure (ASCE/SEI 41-13)

**Table C1-8. Target Building Performance Levels and Ranges**

Nonstructural Performance Levels	Structural Performance Levels and Ranges					
	Immediate Occupancy (S-1)	Damage Control Range (S-2)	Life Safety (S-3)	Limited Safety Range (S-4)	Collapse Prevention (S-5)	Not Considered (S-6)
Operational (N-A)	Operational 1-A	2-A	Not recommended	Not recommended	Not recommended	Not recommended
Immediate Occupancy (N-B)	Immediate Occupancy 1-B	2-B	3-B	Not recommended	Not recommended	Not recommended
Life Safety (N-C)	1-C	2-C	Life Safety 3-C	4-C	5-C	6-C
Hazards Reduced (N-D)	Not recommended	2-D	3-D	4-D	5-D	6-D
Not Considered (N-E)	Not recommended	Not recommended	Not recommended	4-E	Collapse Prevention 5-E	Not rehabilitation

Figure 2.10: Target building performance levels and ranges including non-structural components (ASCE/SEI 41-13)

#### 2.4.2 Incremental dynamic analysis

The concept of incremental dynamic analysis was first proposed by Bertero (1977). Since then, Vamvatsikos and Cornell (2002, 2004) proposed a detailed methodology that was applied for several researchers (e.g. Tirca and Tremblay, 2009, etc.). In addition, the U.S. Federal Emergency Management Agency (FEMA) also included guidelines that recommend using IDA to determine the global collapse capacity of steel moment resisting frames. (FEMA 350, 2000)

However, the methodology developed by Vamvatsikos and Cornell (2002) is widely used and employed in this study. The proposed methodology is based on constructing an IDA curve that is obtained by joining points defined by two coordinates: an intensity measure parameter (*IM*) and an engineering demand parameter (*ED*) where the *IM* is incremented gradually. For *IM*, one of the following parameter can be selected: Peak ground acceleration (*PGA*), Peak ground velocity, the 5% damped spectral acceleration at the structure's first-mode period ( $S_a(T_1, 5\%)$ ), etc. and the *ED* parameter can be: maximum base shear, node rotations, peak storey ductility, peak roof drift, peak interstorey drift or any observable response quantity. Based on Vamvatsikos and Cornell's research, the IDA curves of any structural model with

initially linearly elastic elements will exhibit a distinct elastic linear region, which terminates when the first non-linearity comes into play, i.e. when any element reaches the end of its plasticity. The studied IDA curves by Vamvatsikos and Cornell are shown on Figure 2.11. It can be seen that the IDA curves could be “softened” after the initial buckling and accelerates towards large drifts and eventual collapse, Figure 2.11(a). On the other hand, twisting patterns can be seen due to successive segments of “softening” and “hardening” and display a non-monotonic function of the  $IM$ , Figure 2.11(d). A final softening segment occurs when the structure accumulates  $DM$  at increasing higher rates, signaling the onset of dynamic instability. The curves then flattens out in a plateau of the maximum value in  $IM$  as it reaches the flat line and  $DM$  moves towards ‘infinity’ (Figure 2.11(a) and Figure 2.11(b)) (Vamvatsikos and Cornell, 2002)

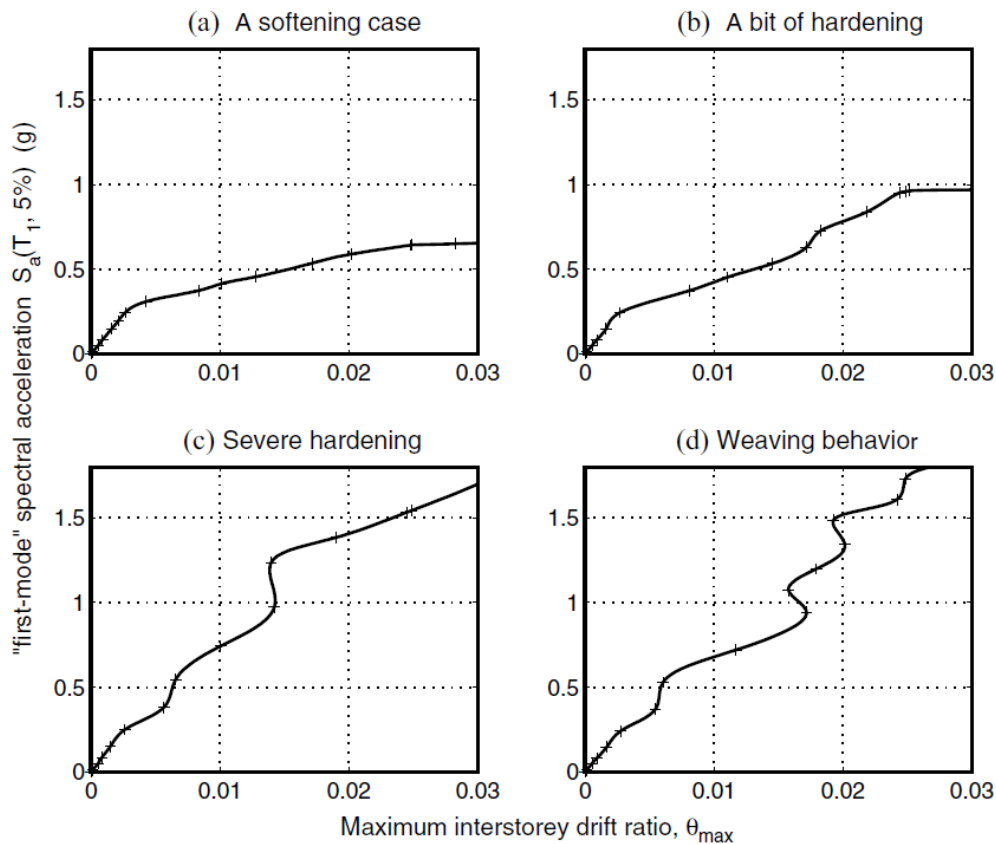


Figure 2.11: IDA curves of a  $T_l = 1.8$  s, 5-stoey steel braced frame subjected to four different records. (Vamvatsikos and Cornell, 2002)

When subjected to different ground motion excitations a CBF model will respond in a different manner due to the frequency content of applied records. In this light, the shape of IDA curve is difficult to be predicted in order to capture the full range of responses a sufficient number of records need to be employed. Further, in the case studied the 5% damped spectral acceleration at the structure's first-mode period,  $S_a(T_1, 5\%)$  was retained as the IM parameter and the peak interstorey drift as a *ED* parameter able to measure the structural damage. By using the target performance objectives explained above in Figure 2.6-Figure 2.8, the structure performance can be defined on each IDA curve. In this light, *IO* performance can be defined when the first brace reaches buckling, *CP* when for a very small increase in *IM* a large interstorey drift occurs and the plot (IDA curve) is characterised by a flat line. However, the *LS* performance is difficult to be identified on the IDA curve. Tirca et al. (2014) proposed to consider the *LS* performance of CBF structure when the maximum residual interstorey drift is  $0.5\%h_s$  that complies with ASCE/SEI 41-13 recommendations.

### 2.4.3 Fragility Analysis

Fragility analysis quantifies the probability of structural collapse or the probability of exceeding some limit states of interest that are required to assess the structural performance when subjected to the associated ground motion intensity measure, *IM*, in dynamic structural analysis. A variety of approaches have been introduced by different researchers to calculate fragility of structure, like field observations of damage (Kennedy and Ravindra, 1984), static structural analyses (Masanobu et al., 2000) and analytical fragility function (Baker and Cornell, 2005). Among all these approaches, the latter is presented in detail because it is employed further to develop fragility of studied buildings.

Thus, Baker and Cornell (2005) considered lognormal distribution to estimate fragility of structure. By considering the results from the IDA curves, the lognormal cumulative distribution function used to define the fragility function is:

$$P(C|IM = x) = \Phi\left(\frac{\ln(x / \theta)}{\beta}\right) \quad (2.35)$$

where  $P(C | IM = x)$  is the probability that a ground motion with  $IM = x$  will cause the structure to collapse,  $\Phi(\cdot)$  is the standard normal cumulative distribution function (CDF),  $\theta$  is the median of the fragility function (the  $IM$  level with 50% probability of collapse) and  $\beta$  is the standard deviation of  $\ln IM$ .

In addition, Ellingwood et al. (2007) considered the same fragility as above but include both epistemic and aleatoric uncertainties. The fragility is described by

$$F_R(x) = \Phi[\ln(x/m_R)/\beta_R] \quad (2.36)$$

in which  $m_R$  is the median capacity of the considered damage level (expressed in units that are dimensionally consistent with the control variable used to define the seismic hazard, e.g. spectral acceleration),  $\beta_R$  is the logarithmic standard deviation, and  $\Phi(\cdot)$  is the standard normal cumulative distribution function. Parameters  $m_R$  and  $\beta_R$  measure aleatoric inherent uncertainty in the structural seismic capacity. An overall estimate of fragility for review, assessment, and decision purposes that reflects both aleatoric and epistemic uncertainty is then provided by replacing  $\beta_R$  in Equation (2.36) with the following expression

$$\beta_R = \sqrt{\beta_{RR}^2 + \beta_{RU}^2} \quad (2.37)$$

where  $\beta_{RR}$  is the aleatoric component of uncertainty and  $\beta_{RU}$  is the modelling (epistemic) uncertainty. With the consideration of different performance level ( $PL$ ), the relationship used to define  $\beta_{RR}$  is:

$$\beta_{RR} = \sqrt{\beta_{D|Sa}^2 + \beta_c^2} \quad (2.38)$$

where  $\beta_{D|Sa}$  is the seismic demand uncertainty,  $\beta_c$  is the uncertainty in capacity and depends on the considered  $PL$ . To assess  $\beta_{D|Sa}$ , a nonlinear regression analysis of the power-law form was used, as shown in equation given below:

$$\theta_{max} = a \cdot S_a^b \cdot \varepsilon \quad (2.39)$$

where  $a$  and  $b$  are constants,  $\varepsilon$  is a lognormal random variable with median 1.0 and the

parameters  $a$  and  $b$  were determined by regression of  $\ln\theta_{max}$  versus  $\ln S_a$ . The “best” fitted linear regression line is the one that passes through the data points with the least total error which can be obtained by minimizing the sum of the squared errors,  $s^2$ . The  $s^2$  parameter is also known as the standard error and  $s$  is the conditional standard deviation. The expression of seismic demand uncertainty is  $\beta_{D|S_a} = \text{sqrt}(\ln(1+s^2))$ . According to this research, three performance level were considered: Immediate Occupancy ( $IO$ ), Significant Structural Damage ( $SD$ ) rather than Life Safety and Collapse Prevention ( $CP$ ). The fragility curves were built for two steel moment-resisting frame (Frame A and B) that was designed based on the current standard and the 1980 standards respectively. Non-linear time-history analysis was conducted for each of the studied frame, and fragility curves were built with consideration of uncertainties, as shown in Figure 2.12.

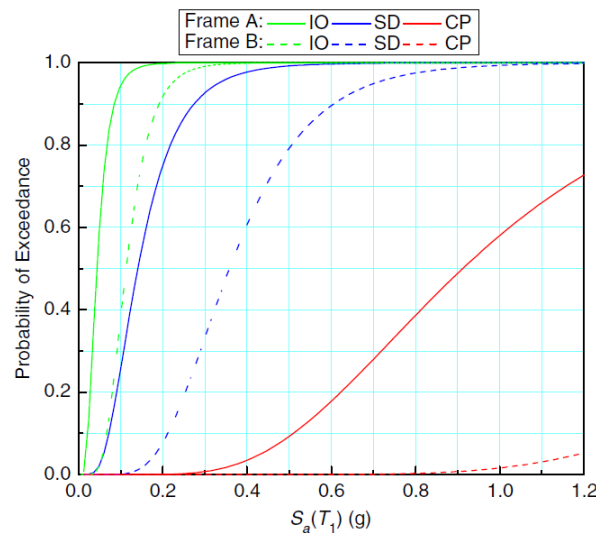


Figure 2.12: Seismic fragilities for Frames A and B. (Ellingwood et al., 2007)

#### 2.4.3 Retrofitting for Existing Centrally Braced Frame (CBF) Steel Buildings

Seismic retrofitting strategy selection for an existing building is a rather complex procedure. It requires both technical and economical consideration. Di Sarno and Elnashai (2002) defined two groups of seismic retrofit strategies: traditional and nonconventional. Both of them are aimed at modifying structural strength, stiffness and damping to improve the

seismic performance of building.

For CBF buildings, a traditional seismic retrofit strategy consists in strengthening of existing members and their connections. When a strengthened CBF cannot sustain the demanded earthquake forces a supplemental CBF is required. Nonconventional seismic retrofit strategies consist of adding damping to the structural system by means of viscous dampers or others such as hysteretic devices (BRB, friction dampers, dissipative connections, etc.). The purpose of this retrofit strategy is to diminish the seismic energy transferred into the structure members that were designed to respond elastically. More precisely, addition of friction dampers to the structural system was reported by Pall and Marsh (1982); Soong et al. (1998); Ramirez and Tirca (2012) and others. In addition, replacement of deficient gusset plate connections with dissipative pin connections while preserving all structural members to behave elastically could be a solution (Plumier et al., 2004; Tirca et al., 2012). Adding base isolation strategy is a nonconventional strategy as well (Anoop et al., 1996; Vasant and R.S. Jangid, 2008).

Brace connections of an existing CBF system are the most critical components prone to failure. Brace connections can be retrofitted by welding additional plates in order to trigger braces to yield in their gross section, or introducing slotted holes in the gusset plate between the brace ends and the surrounding beams while controlling the force level in the braced frame (Jiang, 2013). In addition, brittle failure of brace connections due to gusset fracture, welds fracture, or bolts shearing should be avoided.

Beams and columns made of W-shape can also be retrofitted in a traditional way as shown in Figure 2.13 and Figure 2.14. Beams are pinned connected to the CBF system, while columns could be continuous over two storeys or pin connected at each floor level. The most common failure mode of beams is hinging at their mid-span where chevron braces are attached. The most common failure mode of columns is buckling due to compression and bending. It is noted that buckling of column under axial compression force is a stability problem. However, under compression force and bending moment applied on the strong axis, the column fails when it reaches its in-plane moment capacity, reduced for the presence of axial load. For columns subjected to compression and bending due to lateral loading, at the end where bending is developed due to column continuity over 2 floors, the cross-section may be reinforced at that

specific location. In order to increase the flexural strength of existing W-shape members, some conventional retrofit recommendations are provided by Schwinger (2007) and are illustrated in Figure 2.13. For increasing the compression strength of W-shape members Schwinger (2007) has provided conventional retrofit scheme illustrated in Figure 2.14.

According to ASCE/SEI 41-13 the following retrofit strategies are defined: i) local modification of components, ii) global structural stiffening and strengthening, iii) mass reduction, and iv) seismic isolation or supplemental energy dissipation. Regardless of the retrofit strategy, the selection depends on the type of structural deficiencies, building occupancy, the target rehabilitation performance objectives and their associated cost.

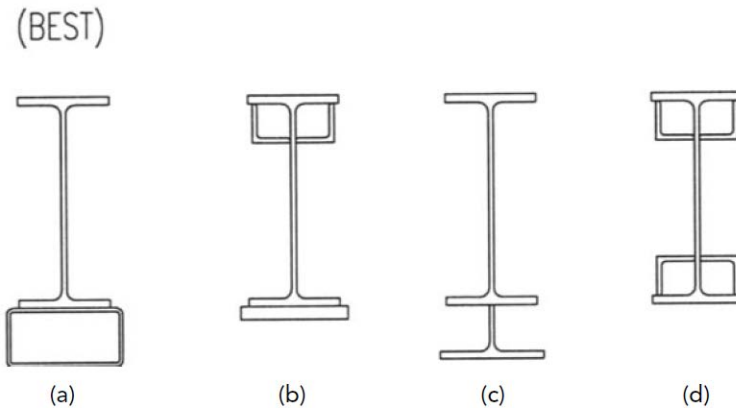


Figure 2.13: Traditional reinforcing of existing W shapes to increase their flexural strength (Schwinger, 2007)

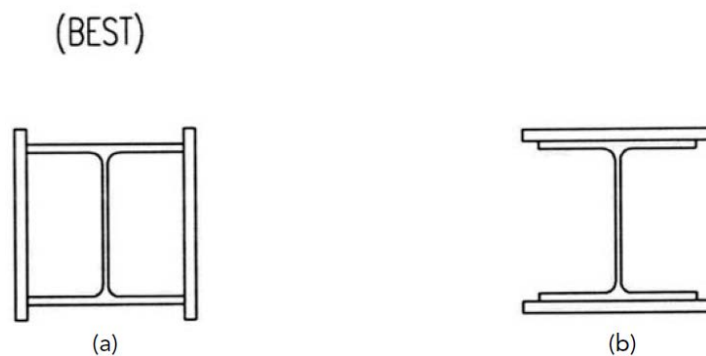


Figure 2.14: Traditional reinforcing of existing W shapes to increase their compressive strength (Schwinger, 2007)

## ***2.5 OpenSees Modelling of Concentrically Braced Frame (CBF) Steel Building***

OpenSees software framework is developed for modeling and computational simulates the response of structure under earthquake excitation. This software is object-oriented and opens source (McKenna and Fenves, 2004) and it has been widely used in structural engineering (Uriz, 2004, Uriz and Mahin, 2008, etc.).

Modelling of concentrically braced steel frame consists in capturing the hysteresis response of braces upon fracture, modelling of connections and the remaining structural members like beams and columns. However, different modeling approaches can be applied.

### ***2.5.1 Steel bracing member modelling***

The first fiber-type finite element model for brace response simulation was developed by Uriz and Mahin (2004) and Gunnarsson (2004), having the purpose of provide reasonable accuracy versus acceptable computational cost compared with the phenomenological method (Nilforoushan, 1973) and conventional finite element (*FE*) method (Ikeda et al, 1986; Soroushian et al., 1988). In Gunnarsson's brace model, force-based nonlinear beam-column elements with distributed plasticity and fiber cross-section formulation were assigned to braces. Steel 02 material and an initial imperfection of  $L/500$  ( $L$  is the effective length of brace) was applied and the brace member was discretized into 10 elements. This model was adopted as the basis of OpenSees brace modelling until now. Chen and Tirca (2013) proposed a similar hollow structural section brace modeling approach recently. In this OpenSees brace model, the hollow structural section brace model consists of nonlinear beam-column elements with distributed plasticity using Gauss-Lobatto integration rule and fiber cross-section formulation. The Giuffre-Menegotto-pinto material was assigned to all brace members and the parameters that define the transition from the elastic to plastic response were the same as those used by Aguero et al. For considering the isotropic hardening, the parameters are:  $R_0 = 25$ ,  $cR_1 = 0.925$ ,  $cR_2 = 0.15$ ;  $a_1 = 0.00001$ ,  $a_2 = a_4 = 0.00002$ , while the kinematic hardening parameter,  $b$ , was set to 0.01. For an accurate representation of a linear curvature distribution along the element, 4 integration points were assigned. A schematic representation of the brace model with end gusset plates and the assigned fiber discretization technique is illustrated in Figure 2.15.

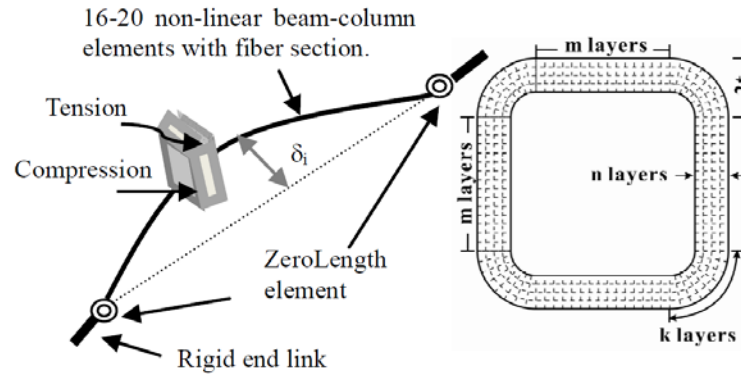


Figure 2.15: Brace model and fiber cross-section discretization (Chen and Tirca, 2013)

There are several models to simulate brace fracture due to low-cycle fatigue. The first model developed in OpenSees for HSS braces is the fatigue material proposed by Uriz and Mahin (2005). Fatigue material was developed in OpenSees to be assigned to parental material of brace (Steel02) to simulate brace fracture. For rectangular HSS braces, the value of strain at which one cycle will cause failure ( $\epsilon_o$ ) was considered equal to 0.9, and the slope of Coffin-Manson curve in log-log space ( $m$ ) were calculated based on the predictive equation ( $m = -0.5$ ).

Further, Lignos and Karamaci (2013) and Tirca and Chen (2014) propose empirical equations based on regression analysis where the strain at which one cycle cause failure  $\epsilon_o$  is computed as a function of slenderness ratio, width-to-thickness ratio and properties of steel material. To developed equation for  $\epsilon_o$  calculation, several experimental tests were performed. The  $\epsilon_o$  value and the slope of Coffin-Manson curve in log-log space ( $m$ ) are required as input parameters in the definition of fatigue material in OpenSees.

The expression for  $\epsilon_o$  calculation proposed by Lignos and Karamaci (2013) is given below.

$$\epsilon_o = 0.291 \left( \frac{KL}{r} \right)^{-0.484} \left( \frac{w}{t} \right)^{-0.613} \left( \frac{E}{F_y} \right)^{0.3} \quad (2.40)$$

This equation is obtained for the following range of predictive parameters:

- $27 \leq KL/r \leq 85$
- $4.20 \leq w/t \leq 30.40$
- $223 \leq F_y \leq 532 \text{ Mpa}$

In the fatigue model, the proposed slope of Coffin-Manson curve in log-log space ( $m$ ) was -0.3.

For a wide range of slenderness ratios of square HSS brace cross-sections,  $50 < KL/r < 150$ , Tirca and Chen proposed a similar empirical equation to estimate the parameters that control fracture. In addition, the slope of Coffin-Manson curve in log-log space ( $m$ ) was assumed as -0.5, the same as that proposed by Uriz and Mahin (2005).

$$\varepsilon_{o,pred.} = 0.006 \left(\frac{KL}{r}\right)^{-0.859} \left(\frac{b_0}{t}\right)^{-0.6} \left(\frac{E}{F_y}\right)^{0.1} \quad (2.41)$$

where  $b_0/t$  is the width-to-thickness ratio. According to CSA/S16 standard,  $b_0 = b - 4t$ , where  $b$  is the HSS width/depth and  $t$  is the thickness.

For accuracy, Uriz and Mahin proposed the use of 20 nonlinear beam-column elements with distributed plasticity for simulating accurately the hysteretic response of HSS brace upon failure. However, to reduce the computational cost, Hsiao et al. (2012) concluded that minimum 16 nonlinear beam-column elements with distributed plasticity are sufficient.

### 2.5.2 *Brace connection modelling*

Brace connection modelling is very complex as large plastic deformation is expected. There are two models for gusset plates simulation: the first model proposed by Uriz and Mahin (2008) employed concentrated springs with fiber cross-section elastic beam-column elements and that proposed by Hsiao et al. (2012) who added two rotational and one torsional spring to simulate the gusset plate response when HSS brace buckles out-of-plane. The former approach simplified the modelling by considering the connection pinned or rigid joint. However, the gusset plate connections do not act perfectly as pinned or rigid joint in real structures. The gusset plate model for brace-toframe connection proposed by Hsiao et. al. (2012), is depicted

in Figure 2.16.

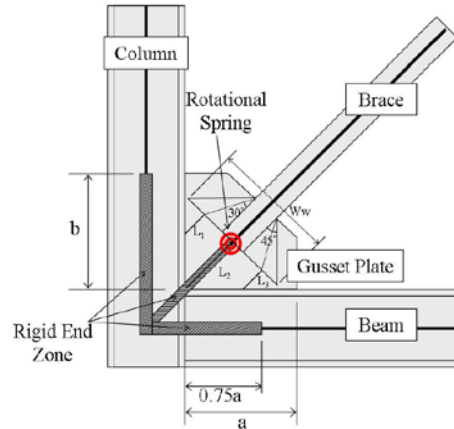


Figure 2.16: Gusset plate connection model for brace-to-frame (Hsiao et al., 2012)

In this model, two rotational springs and one torsional spring were assigned in a zero-length element located at the end of brace. The first rotational spring replicate the out-of-plan bending while the stiffness was computed using the Whitmore width ( $W_w$ ) cross-section (see Equation (2.42)). The second rotational spring was added to capture the in-plan bending, thus its stiffness is larger than the HSS brace stiffness. The torsional spring was used to capture the torsional effect with an elastic material. Steel02 material was assigned to both rotational and torsional spring. Thus, these springs were located at the physical end of the brace and the rest of the gusset plate was assumed as rigid link. Therefore the stiffness of this rotational spring was based upon the geometry and properties of the gusset plate. Those rigid links were simulated by using elastic beam-column elements with extremely large stiffness in OpenSees program. (Hsiao, 2012)

$$K_{cal}^{rotational} = \frac{E}{L_{ave.}} \left( \frac{W_w t_p^2}{12} \right) \quad (2.42)$$

where  $L_{ave.}$  is the average value of  $L_1$ ,  $L_2$  and  $L_3$ , and  $t_p$  is the thickness of gusset plate.

## **CHAPTER 3. DESIGN OF CBF BUILDINGS ACCORDING TO NBCC 1980 AND CSA S16.1-M 78**

### ***3.1 Introduction***

In this chapter, selection and seismic design of the prototype buildings are described. This study aiming to simulate the behaviour of low- and middle-rise buildings designed and built during the 1980 in Montreal. Calculation of gravity load and lateral load, design of gravity columns, beams and girders and design of the seismic force resisting system are according to NBCC 1980 and CSA S16.1-M78. Members were preliminary design based on the equivalent static force procedure. Then, linear dynamic analysis was performed using ETABS software.

### ***3.2 Building Description***

As discussed before, in this study, fictitious low-rise (3-storey) and middle-rise (6-storey) CBF office buildings located on site class C in Montreal (Qc.) are proposed for investigation. These fictitious buildings were designed according to NBCC 1980 and CSA S16.1-M78.

The site class C or firm soil is very dense soil or soft rock. The plan view and frame elevations are illustrated in Figure 3.1. The lateral resistance is provided by tension-compression diagonal bracing in the north-south direction (N-S) and chevron bracing in the east-west direction (E-W). In this study, all columns and beams are made of W-shapes, while all braces are made of hollow structural sections, HSS. This type of building structure is common in the 1980s.

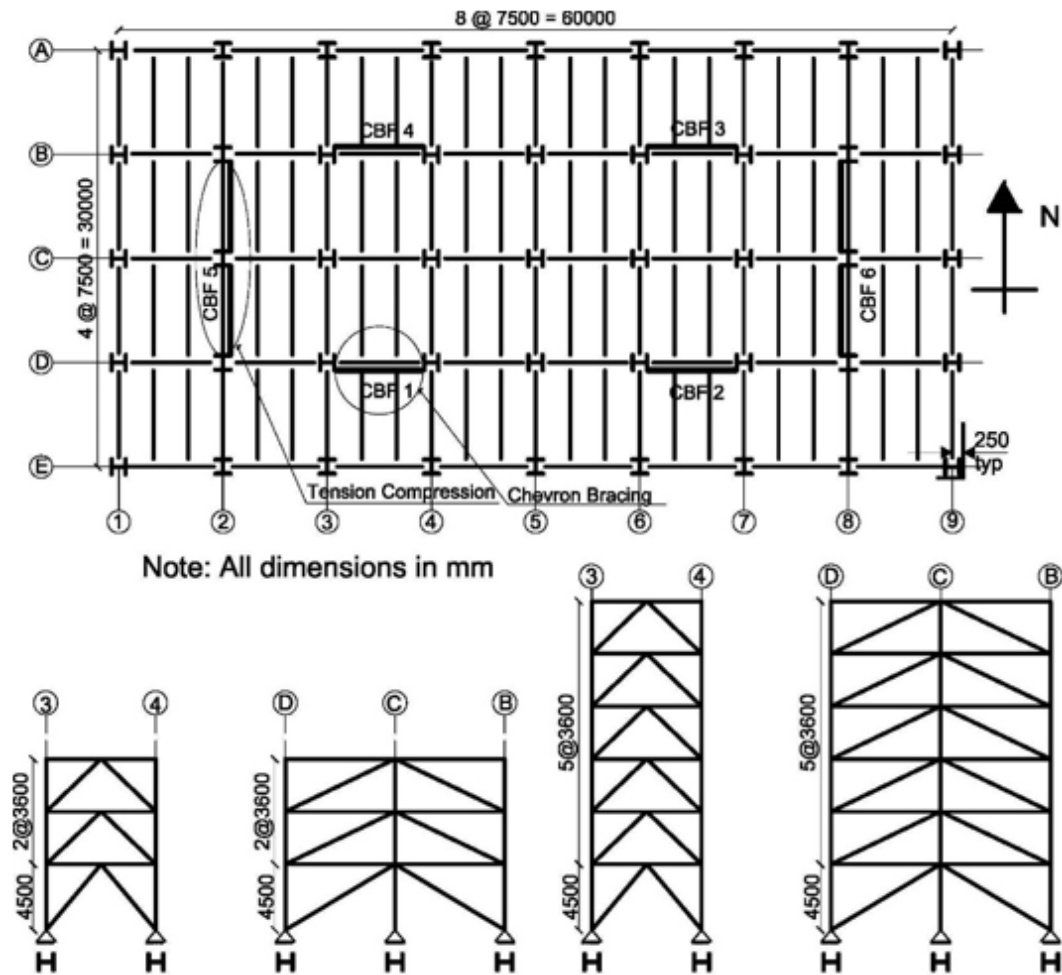


Figure 3.1: Building plan and elevation

### 3.3 Preliminary Design of Concentrically Braced Frame (CBF)

Concentrically braced frames with tension-compression diagonal bracing (N-S) and chevron bracing (E-W) are designed to carry 100% the computed lateral load in addition to the tributary gravity load. In the 1980 provisions, torsional effect was considered, however  $P-\Delta$  effects were introduced only in the 1990 edition of NBCC.

All the gravity loads include dead load, live load, snow load, partitions and cladding wall and are summarized in Table 3.1. The roof and floors were made of a 63 mm thick concrete slab composite with a 38 mm steel deck supported on regularly spaced steel beams, as was done in 1980's.

Table 3.1: Minimum specified gravity loads

Roof Level	
Dead Load	3.0 kPa
Snow Load	2.16 kPa
Typical Floor	
Dead Load (including partitions)	3.4 kPa
Live Load	2.4 kPa
Cladding Wall	1.0 kPa

The snow load was calculated according to the supplement of NBCC 1980 as per Equation (2.1). The basic snow load coefficient ( $C_s$ ) was taken as 0.8 and the ground snow load ( $g$ ) equals to 2.7 kPa.

To calculate the base shear ( $V_{80}$ ), the seismic zone in which the studied building is located should be identified. As can be seen from Figure 2.2, Montreal is located in the seismic zone 2, where  $A = 0.04g$ . The construction factor  $K$  for CBFs with tension/ compression braces is  $K = 1.0$  and the importance factor for office building is equal to 1.0. The soil condition factor ( $F$ ) equals 1.0 for rock, dense and very dense soil. Total seismic weight ( $W$ ) include 100% of dead load plus 25% of the roof snow load is given in Table 3.2. In addition, all the important parameters are summarized in Table 3.2, as well as the resulted seismic force ( $V_{80}$ ) that was calculated using Equation (2.3).

Table 3.2: Summary of seismic coefficients

3-Storey Building										
	$h_n$ (m)	D (m)	$T_{1,80}$ (s)	A (g)	S	K	I	F	W (kN)	$V_{80}$ (kN)
W-E	11.7	60.5	0.136	0.04	1.0	1.0	1.0	1.0	20963	839
N-S	11.7	30.5	0.192	0.04	1.0	1.0	1.0	1.0	20963	839
6-Storey Building										
	$h_n$ (m)	D (m)	$T_{1,80}$ (s)	A (g)	S	K	I	F	W (kN)	$V_{80}$ (kN)
W-E	22.5	60.5	0.261	0.04	0.98	1.0	1.0	1.0	41912	1639
N-S	22.5	30.5	0.370	0.04	0.82	1.0	1.0	1.0	41912	1379

As illustrated in Figure 3.1, the studied building has four CBFs in chevron bracing configuration in the E-W direction and two lines of two adjacent spans of CBFs with diagonal tension/compression brace in the N-S direction. Because all E-W CBFs have the same span

and stiffness, respectively, the base shear is equally distributed and each CBF is designed to carry a shear force equal to  $V_{80}/4$  in addition to the associated lateral force generated from torsion and  $P-\Delta$  effect.

The base shear was distributed over the building height by using Equation (2.6). Because the ratio  $h_n/D_n$  is less than 3 for both 3- and 6-storey buildings (e.g. for 6-storey building in N-S direction  $h_n/D_n = 22.5/30.5 = 0.74$ ) the concentrated force  $F_r=0$ .

Load combinations given in Equation (2.2(a)) were considered. The distribution of factored base shear over the building height is illustrated in Figure 3.2 for a single 3-storey CBF in the E-W direction and for a line of adjacent 3-storey CBF spans in the N-S direction. The factored base shear corresponds to the following combination:  $1.25DL + 1.5Q$  that is given in Equation (2.2(a)). Thus, the factored storey shear is transferred equally to both tension and compression brace ( $T_f$  and  $C_f$ ), where  $T_{f,i} = C_{f,i} = V_i/2\cos\alpha$ , where  $\alpha$  is the angle between the brace and a horizontal line.

Similarly, the distribution of factored base shear over the height of the 6-storey CBF building is given in Figure 3.3.

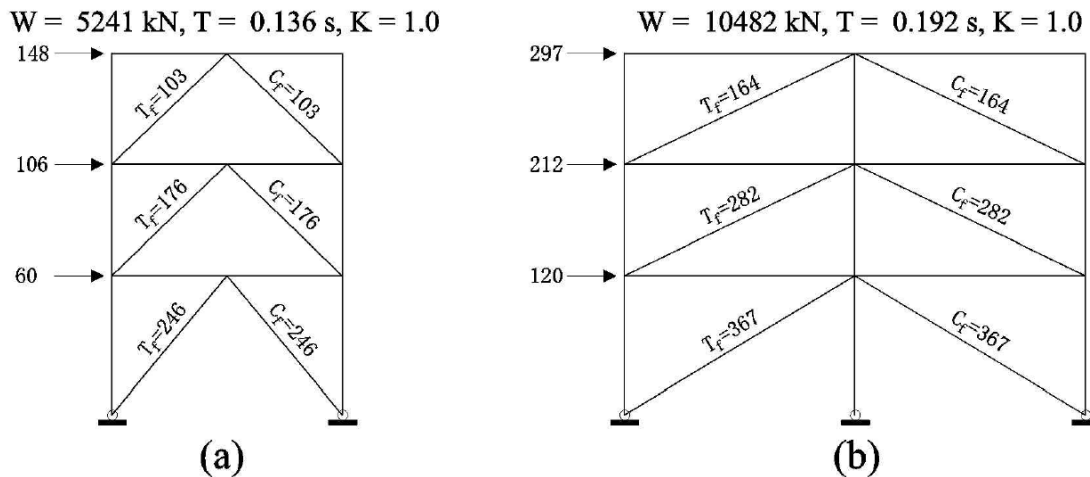


Figure 3.2: Factored load on braces without consideration of torsional and  $P-\Delta$  effects: (a) E-W direction,  $V_{f,80} = 315 \text{ kN}$ ; (b) N-S direction,  $V_{f,80} = 630 \text{ kN}$

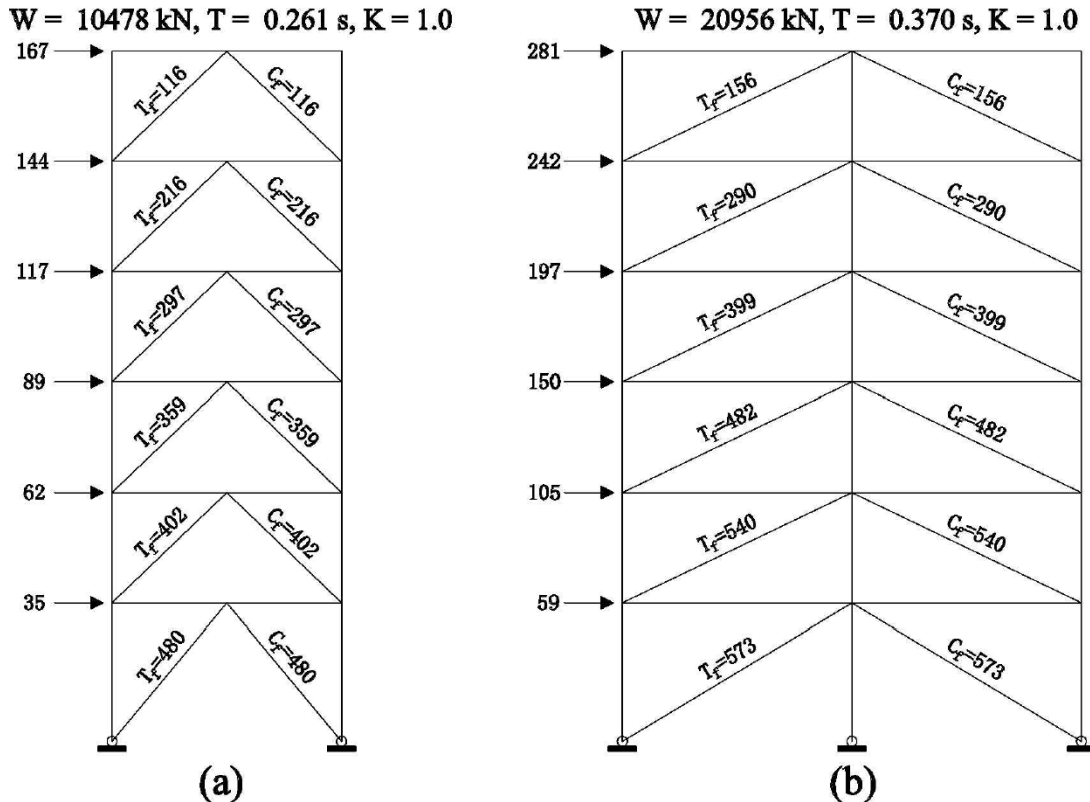


Figure 3.3: Factored load on braces without consideration of torsional and P- $\Delta$  effects: (a) E-W direction,  $V_{f,80} = 614 \text{ kN}$ ; (b) N-S direction,  $V_{f,80} = 1034 \text{ kN}$

All the selected buildings in this study are geometrically symmetric and building mass is uniformly distributed at each floor, so the centre of mass and rigidity is in the same location. In this regard, only the 5% eccentricity is considered. The shear forces due to torsional effect and P- $\Delta$  effect are given in Table 3.3 for the 3-storey building and Table 3.4 for the 6-storey building.

Table 3.3a: Calculation of total unfactored storey shear (3-st E-W direction)

St	Storey shear (seismic force)	Storey shear (torsion)	Storey shear (P- $\Delta$ )	Total Storey Shear (kN)
3	99	0	1	100
2	170	9	3	182
1	210	23	6	239

Table 3.3b: Calculation of total unfactored storey shear (3-st N-S direction)

St	Storey shear (seismic force)	Storey shear (torsion)	Storey shear (P- $\Delta$ )	Total Storey Shear (kN)
3	198	0	19	217
2	339	15	41	396
1	419	40	61	521

Table 3.4a: Calculation of total unfactored storey shear (6-st E-W direction)

St	Storey shear (seismic force)	Storey shear (torsion)	Storey shear (P- $\Delta$ )	Total Storey Shear (kN)
6	111	0	2	113
5	207	8	5	220
4	285	23	8	316
3	345	43	10	398
2	386	67	13	467
1	410	95	16	520

Table 3.4b: Calculation of total unfactored storey shear (6-st N-S direction)

St	Storey shear (seismic force)	Storey shear (torsion)	Storey shear (P- $\Delta$ )	Total Storey Shear (kN)
6	187	0	19	207
5	349	16	41	406
4	480	46	64	590
3	580	88	86	754
2	650	137	108	895
1	689	193	128	1011

Total factored load for each member in the lateral load resisting system is illustrated on Figure 3.4 for the 3-storey building and Figure 3.5 for the 6-storey building.

For preliminary design of brace, gravity load effect is taken into account.

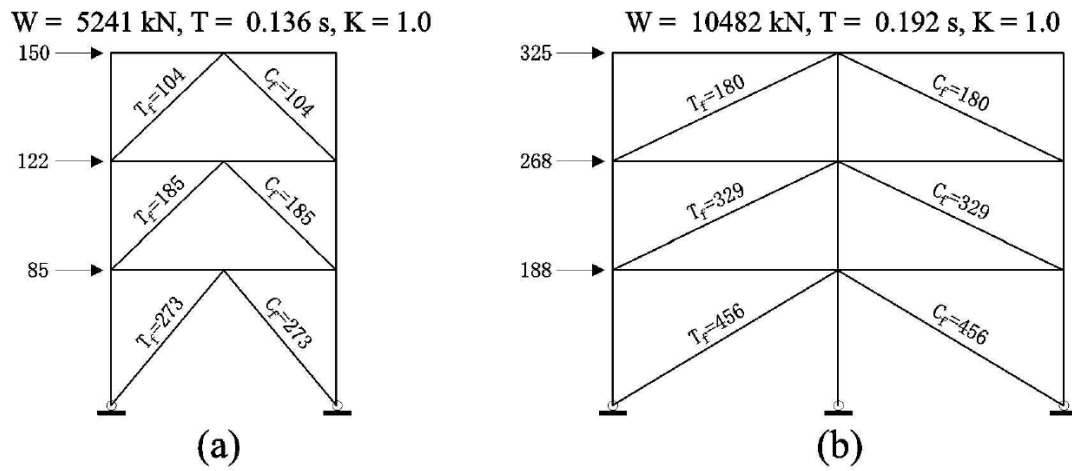


Figure 3.4: Factored load ( $1.5Q$ ) in braces of 3-storey CBF including torsion and P- $\Delta$  effect but without the tributary gravity load: (a) E-W; (b) N-S

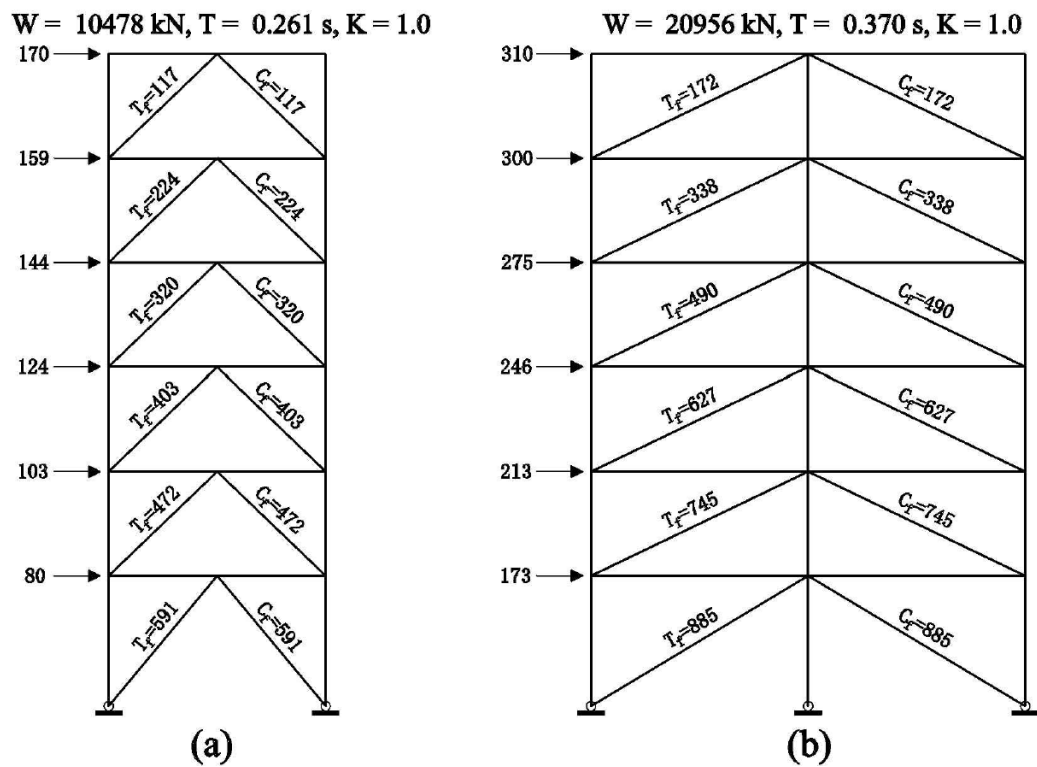


Figure 3.5: Factored load ( $1.5Q$ ) in braces of 3-storey CBF including torsion and P- $\Delta$  effect but without the tributary gravity load: (a) E-W; (b) N-S

At each floor, the beam of CBF in chevron bracing configuration (E-W direction) is the support for two secondary beams. In consequence, a part of the gravity load applied to these secondary beams is transferred to chevron braces. Beams of chevron CBFs are half span loaded in axial compression and bending and the other half in axial tension and bending. For the chevron CBF system (E-W), the calculation of the gravity component transferred to braces that corresponds to Combo 1, 2, and 3 is showed below. It is noted that secondary beams are located at 2.5m distance from each other.

As from the above, the point load comprising the gravity load component  $P_{SB}$  applied to the CBF beam located at the roof level due to the sitting of secondary beams is:

$$\text{Combo 1, } (1.25DL + 1.5Q): P_{SB} = 1.25 \times 3 \times 2.5 \times (7.5/2 + 7.5/2) = 70.3 \text{ kN}$$

$$\text{Combo 2, } (1.25DL + 1.5LL): P_{SB} = 1.25 \times 3 \times 2.5 \times (7.5/2 + 7.5/2) + 1.5 \times 2.16 \times 2.5 \times (7.5/2 + 7.5/2) = 131 \text{ kN}$$

$$\text{Combo 3, } (1.25DL + 1.05LL + 1.05Q): P_{SB} = 1.25 \times 3 \times 2.5 \times (7.5/2 + 7.5/2) + 1.05 \times 2.16 \times 2.5 \times (7.5/2 + 7.5/2) = 112.8 \text{ kN}$$

The point load comprising the gravity load component only which is applied on the main beam of the CBF located at the typical floor due to the sitting of the secondary beam displaced at 2.5m distance from each other, ( $P_{SB}$ ) is:

$$\text{Combo 1, } (1.25DL + 1.5Q): P_{SB} = 1.25 \times 3.4 \times 2.5 \times (7.5/2 + 7.5/2) = 79.7 \text{ kN}$$

$$\text{Combo 2, } (1.25DL + 1.5LL): P_{SB} = 1.25 \times 3.4 \times 2.5 \times (7.5/2 + 7.5/2) + 1.5 \times 2.4 \times 2.5 \times (7.5/2 + 7.5/2) = 147.2 \text{ kN}$$

$$\text{Combo 3, } (1.25DL + 1.05LL + 1.05Q): P_{SB} = 1.25 \times 3.4 \times 2.5 \times (7.5/2 + 7.5/2) + 1.05 \times 2.4 \times 2.5 \times (7.5/2 + 7.5/2) = 126.9 \text{ kN}$$

Then, the gravity load ( $P_G$ ) transferred at the mid-span of the CBF beam where braces are attached is:

- Roof level:

$$\text{Combo 1: } P_G = 70.3 \times 2.5 \times (3 \times 3.75^2 - 2.5^2) / (2 \times 3.75^3) = 60 \text{ kN}$$

$$\text{Combo 2: } P_G = 131 \times 2.5 \times (3 \times 3.75^2 - 2.5^2) / (2 \times 3.75^3) = 112 \text{ kN}$$

$$\text{Combo 3: } P_G = 112.8 \times 2.5 \times (3 \times 3.75^2 - 2.5^2) / (2 \times 3.75^3) = 96 \text{ kN}$$

- Typical floor level:

$$\text{Combo 1: } P_G = 79.7 \times 2.5 \times (3.4 \times 3.75^2 - 2.5^2) / (2 \times 3.75^3) = 68 \text{ kN}$$

$$\text{Combo 2: } P_G = 147.2 \times 2.5 \times (3.4 \times 3.75^2 - 2.5^2) / (2 \times 3.75^3) = 125.4 \text{ kN}$$

$$\text{Combo 3: } P_G = 126.9 \times 2.5 \times (3.4 \times 3.75^2 - 2.5^2) / (2 \times 3.75^3) = 108.1 \text{ kN}$$

Finally, the factored axial compression load component transferred to braces ( $C_{f,g}$ ) is:

- Roof level:

$$\text{Combo 1: } C_{f,g} = P_{SB} / \sin \alpha = 60 / 0.693 = 86 \text{ kN}$$

$$\text{Combo 2: } C_{f,g} = P_{SB} / \sin \alpha = 112 / 0.693 = 161 \text{ kN}$$

$$\text{Combo 3: } C_{f,g} = P_{SB} / \sin \alpha = 96 / 0.693 = 139 \text{ kN}$$

- Typical floor level:

$$\text{Combo 1: } C_{f,g} = P_{SB} / \sin \alpha = 68 / 0.693 = 98 \text{ kN}$$

$$\text{Combo 2: } C_{f,g} = P_{SB} / \sin \alpha = 125.4 / 0.693 = 181 \text{ kN}$$

$$\text{Combo 3: } C_{f,g} = P_{SB} / \sin \alpha = 108.1 / 0.693 = 156 \text{ kN}$$

- Ground floor level:

$$\text{Combo 1: } C_{f,g} = P_{SB} / \sin \alpha = 68 / 0.768 = 88 \text{ kN}$$

$$\text{Combo 2: } C_{f,g} = P_{SB} / \sin \alpha = 125.4 / 0.768 = 163 \text{ kN}$$

$$\text{Combo 3: } C_{f,g} = P_{SB} / \sin \alpha = 108.1 / 0.768 = 141 \text{ kN}$$

Gravity load components,  $C_{f,g}$  triggered in braces of the 3- and 6-storey chevron CBF are summarized in Table 3.5 and Table 3.6, respectively.

Table 3.5: Gravity load component triggered in braces of the 3-st chevron CBF (E-W)

St	$C_{f,g}$	$C_{f,g}$	$C_{f,g}$
	Combo 1 kN	Combo 2 kN	Combo 3 kN
3	86	161	139
2	98	181	156
1	88	163	141

Table 3.6: Gravity load component triggered in braces of the 6-st chevron CBF (E-W)

St	$C_{f,g}$	$C_{f,g}$	$C_{f,g}$
	Combo 1	Combo 2	Combo 3
	kN	kN	kN
6	86	161	139
2-5	98	181	156
1	88	163	142

Therefore, Combo 1 governs brace design.

All gravity load components triggered in the columns of CBFs are summarized in Table 3.7 for the 3-storey building and in Table 3.8 for the 6-storey building. The specified live load due to use and occupancy office was multiplied by the  $[0.3 + (9.8/B)^{0.5}]$  (live load reduction factor) where  $B$  is the tributary area in square meters.

Table 3.7a: Gravity load in the CBF column of the 3-st building (E-W) associated with each load combination

St	Combo 1	Combo 2	Combo 3
	kN	kN	kN
3	151	282	242
2	312	553	481
1	471	781	688

Table 3.7b: Gravity load in the CBF column of the 3-st building (N-S) associated with each load combination

St	Combo 1	Combo 2	Combo 3
	kN	kN	kN
3	211	393	339
2	450	778	679
1	689	1112	985

Table 3.8a: Gravity load in the CBF column of the 6-st building (E-W) associated with each load combination

St	Combo 1 kN	Combo 2 kN	Combo 3 kN
6	151	282	242
5	312	553	481
4	471	781	688
3	631	1003	891
2	790	1221	1092
1	949	1438	1291

Table 3.8b: Gravity load in the CBF column of the 6-st building (N-S) associated with each load combination

St	Combo 1 kN	Combo 2 kN	Combo 3 kN
6	211	393	339
5	450	778	679
4	689	1112	985
3	928	1439	1286
2	1167	1761	1583
1	1406	2081	1879

The summary of design forces resulted from the governing load combination are given in Figure 3.6 for the 3-storey CBF and in Figure 3.7 for the 6-storey CBF.

In the case of 3-storey CBF (E-W), the largest factored compression force in braces of the upper two floors resulted from Combo 3 ( $1.25DL+1.05LL+1.05Q$ ) and in the brace located at the ground floor level from Combo 1 ( $1.25DL + 1.5Q$ ). It is noted that the compression force resulted from Combo 3 that was triggered in the brace at the top floor level is 11% larger than that resulted from Combo 1. This difference is only 5% in the case of 2<sup>nd</sup> floor brace. Referring to the factored tensile force triggered in chevron braces, in the upper two floors, the gravity force component resulted from Combo 3 ( $1.25DL + 1.05LL$ ) that subjects the brace in compression is larger than the associated component  $1.05Q$  that subjects the brace in tension. In this light, the factored tensile force triggered in braces corresponds to Combo 1 because the  $1.5Q$  component is larger than the associated  $1.25DL$  component. These governing factored tensile and compression forces are given in Figure 3.6(a). Because the gravity

components transferred in diagonal braces of the CBF (N-S) are negligible, Combo 1 governs braces design.

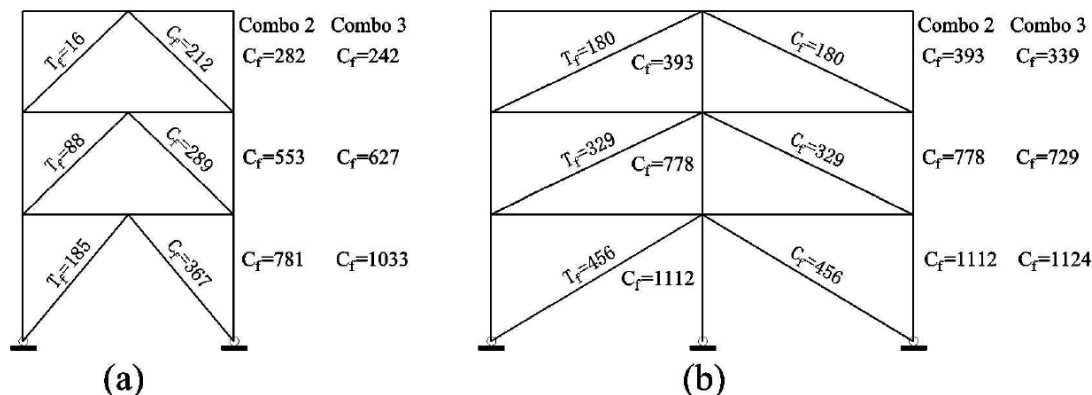


Figure 3.6: Factored load in members of 3-storey CBFs including the gravity component, torsion and  $P-\Delta$  effects

The factored axial load in beam is coming from the horizontal projection of axial load in braces. According to Figure 3.6 (a), the left part of the beam member is in compression and the right part is in tension. The factored axial load and bending moment developed in CBF beams of the 3-storey CBF are summarized in Table 3.9. It can be seen that the maximum factored axial load results from Combo 1 and the maximum bending moment results from Combo 3. In addition, the axial tensile force developed in the CBF (E-W) beams is larger than the axial compression force.

Table 3.9a: Factored axial load and bending moment in beam (3-st E-W)

ST.	Combo. 1			Combo. 2			Combo. 3		
	$M_f$ kN.m	$T_f$ kN	$C_f$ kN	$M_f$ kN.m	$T_f$ kN	$C_f$ kN	$M_f$ kN.m	$T_f$ kN	$C_f$ kN
3	49	78	78	91	0	0	78	52	52
2	55	196	72	102	0	0	88	194	0
1	55	246	104	102	0	0	88	235	10

Table 3.9b: Factored axial load and bending moment in beam (3-st N-S)

ST.	Combo. 1			Combo. 2			Combo. 3		
	M <sub>f</sub>	T <sub>f</sub>	C <sub>f</sub>	M <sub>f</sub>	T <sub>f</sub>	C <sub>f</sub>	M <sub>f</sub>	T <sub>f</sub>	C <sub>f</sub>
	kN.m	kN	kN	kN.m	kN	kN	kN.m	kN	kN
3	66	165	165	123	0	0	106	114	114
2	75	303	303	138	0	0	119	208	208
1	75	398	398	138	0	0	119	273	273

Referring to design compression forces transferred in columns of the 3-storey chevron CBF (E-W), these have resulted from Combo 2 for the upper two floors and Combo 3 for the bottom column. However, there is a small difference in the force magnitude resulted in Combo 3 versus Combo 2. The maximum factored compression forces triggered in the edge column of the 3-storey CBF located in the N-S direction resulted from the same combinations as those resulted for the E-W CBF. The factored compression forces triggered in the middle column resulted from Combo 2.

The factored compression forces triggered in braces of the 6-storey chevron CBF have resulted from Combo 1 for all floor levels but one, the top floor, where the governing combination is Combo 3. These forces are provided in Figure 3.7(a). Factored compression forces triggered in braces of the 6-storey CBF in the N-S have resulted from Combo 1, as well.

The factored compression forces triggered in columns of 6-st. CBFs (E-W) are given in Figure 3.7(a). Thus, forces resulted from Combo 2 are the largest in columns of the upper two floors and those resulted from Combo 3 govern the factored compression force transferred in columns at the remaining floors.

Factored compression forces triggered in columns of 6-st. CBFs (N-S) are given in Figure 3.7(b). Thus, forces resulted from Combo 2 are the largest in the edge columns of the upper two floors and those resulted from Combo 3 governs the design of columns at the remaining floors. For the middle column of the 6-storey CBF (N-S) forces from Combo 2 govern the design.

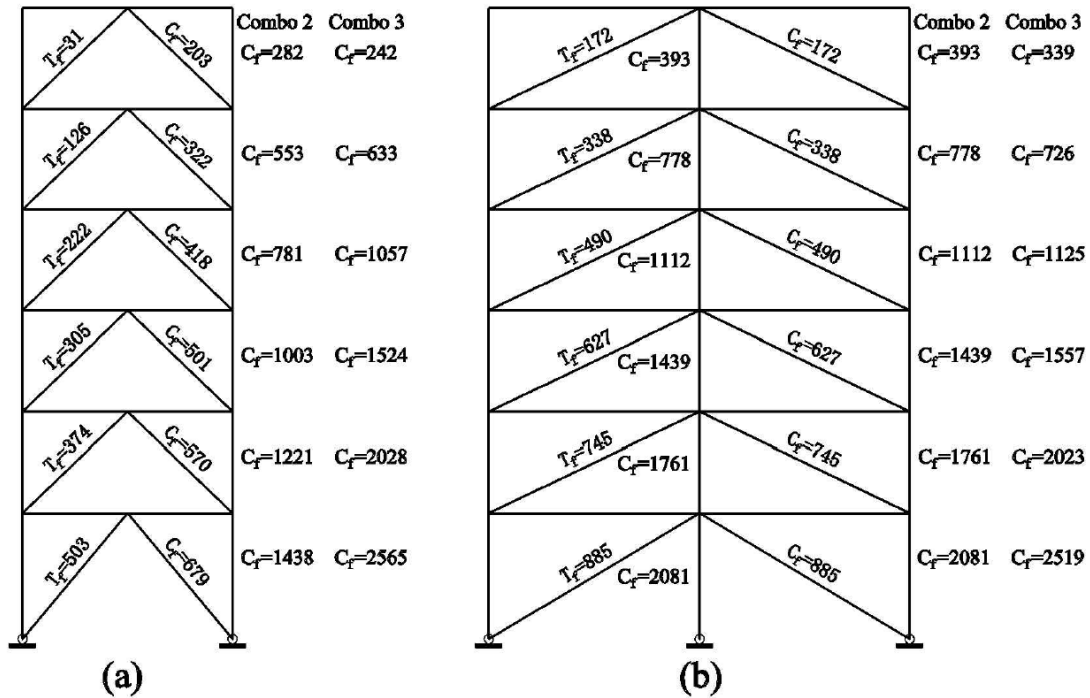


Figure 3.7: Factored load in members of 6-storey CBF including the gravity component, torsion and  $P-\Delta$  effects

Referring to beams of 6-st CBF (E-W), the largest factored bending moment resulted from Combo 3 and the largest axial force developed in beams resulted from Combo 1, whereas the axial tensile force is larger than the axial compression force.

Table 3.10a: Factored axial load and bending moment in beam (6-st E-W)

ST.	Combo 1			Combo 2			Combo 3		
	M <sub>f</sub> kN.m	T <sub>f</sub> kN	C <sub>f</sub> kN	M <sub>f</sub> kN.m	T <sub>f</sub> kN	C <sub>f</sub> kN	M <sub>f</sub> kN.m	T <sub>f</sub> kN	C <sub>f</sub> kN
6	49	84	84	91	0	0	78	58	58
5	55	224	99	102	0	0	88	213	13
4	55	302	160	102	0	0	88	274	49
3	55	361	220	102	0	0	88	316	91
2	55	411	270	102	0	0	88	351	126
1	55	449	308	102	0	0	88	377	152

Table 3.10b: Factored axial load and bending moment in beam (6-st N-S)

ST.	Combo 1			Combo 2			Combo 3		
	M <sub>f</sub> kN.m	T <sub>f</sub> kN	C <sub>f</sub> kN	M <sub>f</sub> kN.m	T <sub>f</sub> kN	C <sub>f</sub> kN	M <sub>f</sub> kN.m	T <sub>f</sub> kN	C <sub>f</sub> kN
6	66	155	155	123	0	0	106	108	108
5	75	305	305	138	0	0	119	213	213
4	75	442	442	138	0	0	119	310	310
3	75	565	565	138	0	0	119	396	396
2	75	672	672	138	0	0	119	470	470
1	75	758	758	138	0	0	119	531	531

### 3.4 Design of Concentrically Braced Frame (CBF)

The design of concentrically braced frame includes: brace design, column design, beam design and brace-to-frame connection design. Thus, the forces in braces and columns showed in Figure 3.6 are used to size the brace and column members of the 3-storey CBFs, while those showed in Table 3.9 are used to size the beam members. Forces in braces and columns showed in Figure 3.7 are used to size the brace and column members of the 6-storey CBFs, while those showed in Table 3.10 are used to size the beam members. The CSA/ S16.1-M78 standard was used for design.

#### 3.4.1 Brace design

The axial compression force triggered in braces governs the brace design because the gravity component is added to the lateral load component. Braces are designed as compression member with HSS cross-section as per Equation (2.19). The nominal yield strength ( $F_y$ ) of HSS members is 345 MPa.

The chevron brace members design is summarized in Table 3.11a and b for the 3- and 6-storey CBFs in the E-W direction, respectively. In the tables are given the gross area of braces, the slenderness ratio ( $KL/r$ ), the brace compression resistance,  $C_{r-80}$  and the reserve capacity in compression  $C_{f-80}/C_{r-80}$  as resulted from the 1980 design provisions. The slenderness ratio of a compression member shall be taken as the ratio of effective brace length to the corresponding radius of gyration ( $r$ ). The slenderness ratio of a compression member

shall not exceed 200. Class of sections were provided in CSA/S16.1-78 and for this study braces were selected to correspond to class 1 section. Similarly, in Table 3.12 are given the brace sizes of the 3- and 6-storey CBFs in the N-S direction.

Table 3.11a: Brace cross-sections of the 3-st CBF (E-W) as per 1980 design

Storey	HSS Section	$A_g(\text{mm}^2)$	KL/r	$C_{r-80}$ (kN)	$C_{f-80}/C_{r-80}$
3	101.6x101.6x7.95	2820	124	269	0.787
2	101.6x101.6x9.53	3280	127	303	0.952
1	127x127x7.95	3620	110	414	0.887

Table 3.11b: Brace cross-sections of the 6-st CBF (E-W) as per 1980 design

Storey	HSS Section	$A_g(\text{mm}^2)$	KL/r	$C_{r-80}$ (kN)	$C_{f-80}/C_{r-80}$
6	101.6x101.6x7.95	2820	124	269	0.755
5	101.6x101.6x9.53	3280	127	303	1.031
4	127x127x7.95	3620	48	489	0.856
3	127x127x9.53	4240	99	559	0.896
2	127x127x9.53	4240	99	559	1.019
1	152.4x152.4x9.53	5210	92	766	0.887

Table 3.12a: Brace cross-sections of the 3-st CBF (N-S) as per 1980 design

Storey	HSS Section	$A_g(\text{mm}^2)$	KL/r	$C_{r-80}$ (kN)	$C_{f-80}/C_{r-80}$
3	127x127x7.95	3620	156	240	0.750
2	152.4x152.4x9.53	5210	130	466	0.705
1	177.8x177.8x9.53	6180	116	653	0.701

Table 3.12b: Brace cross-sections of the 6-st CBF (N-S) as per 1980 design

Storey	HSS Section	$A_g(\text{mm}^2)$	KL/r	$C_{r-80}$ (kN)	$C_{f-80}/C_{r-80}$
6	127x127x7.95	3620	156	240	0.716
5	152.4x152.4x7.95	4430	128	405	0.834
4	177.8x177.8x9.53	6180	110	704	0.702
3	177.8x177.8x11.13	7100	111	795	0.788
2	177.8x177.8x12.7	7970	113	877	0.849
1	203.2x203.2x11.13	8230	101	1051	0.841

### 3.4.2 Beam and column design

All beams and columns were assumed to be Grade G40.21-300W steel with a nominal yield strength of 300 MPa. This is one of the most popular steel used for W shape steel members in the 1980s. The columns were assumed to be continuous over each two-storey for the 6-storey building and continuous for the bottom 2-storey of the 3- storey building. As all the beams and columns are pin-pin connected in CBF system, columns can be designed as a compression member with Equation (2.19). However, beams have to be designed as bending and compression or bending and tension members due to the effect of uniformly distributed gravity load which is the case of beams in CBFs with diagonal bracing system (N-S) and concentrated gravity loads on beams of chevron CBFs (E-W). Using the interaction Equation (2.21) and (2.22), the beam cross-sections are given in Table 3.13a and Table 3.13b for the 3- and 6-storey CBF in the E-W direction, respectively. From both Combo 1 and Combo 3, the *ratio 1* is associated with the interaction equation results involving axial compression and bending while *ratio 2* is associated with the interaction equation results involving axial tension and bending. The gross cross-section area ( $A_g$ ) and the class of sections are also given in the table. Similarly, Table 3.14a and Table 3.14b summarize the beam cross-sections of the 3- and 6-storey CBF, respectively in the N-S direction. It is noted that all beams of CBFs in the N-S direction are laterally supported by the composite steel deck and all beams of chevron CBFs are laterally supported by the secondary beams placed at 2.5 m of each other.

Table 3.13a: Beam cross-sections of the 3-st CBF (E-W) as per 1980 design

Storey	Beam Section	$A_g$ (mm <sup>2</sup> )	Section Class	$C_r$ (kN)	$T_r$ (kN)	$M_r$ (kN.m)	Combo 1		Combo 3	
							ratio1	ratio2	ratio1	ratio2
3	W310X28	3610	1	739	828	110	0.56	0.53	0.80	0.78
2	W310X33	4180	1	862	959	130	0.52	0.63	0.67	0.88
1	W360X33	4170	1	909	957	146	0.51	0.64	0.62	0.85

Table 3.13b: Beam cross-sections of the 6-st CBF (E-W) as per 1980 design

Storey	Beam Section	A <sub>g</sub> (mm <sup>2</sup> )	Section Class	C <sub>r</sub> (kN)	T <sub>r</sub> (kN)	M <sub>r</sub> (kN.m)	Combo 1		Combo 3	
							ratio1	ratio2	ratio1	ratio2
6	W310X28	3610	1	739	828	110	0.58	0.55	0.81	0.78
5	W310X33	4180	1	862	959	130	0.56	0.66	0.70	0.90
4	W310X39	4940	2	1043	1134	165	0.51	0.60	0.59	0.78
3	W310X39	4940	2	1043	1134	165	0.57	0.65	0.64	0.81
2	W310X39	4940	2	1043	1134	165	0.63	0.70	0.68	0.84
1	W360X39	4980	1	1091	1143	179	0.62	0.70	0.65	0.82

Table 3.14a: Beam cross-sections of the 3-st CBF (N-S) as per 1980 design

Storey	Beam Section	A <sub>g</sub> (mm <sup>2</sup> )	Section Class	C <sub>r</sub> (kN)	T <sub>r</sub> (kN)	M <sub>r</sub> (kN.m)	Combo 1		Combo 3	
							ratio1	ratio2	ratio1	ratio2
3	W310X39	4940	2	1043	1134	165	0.58	0.55	0.78	0.74
2	W310X45	5690	1	1205	1306	191	0.68	0.62	0.83	0.78
1	W310X45	5690	1	1205	1306	191	0.77	0.70	0.90	0.83

Table 3.14b: Beam cross-sections of the 6-st CBF (N-S) as per 1980 design

Storey	Beam Section	A <sub>g</sub> (mm <sup>2</sup> )	Section Class	C <sub>r</sub> (kN)	T <sub>r</sub> (kN)	M <sub>r</sub> (kN.m)	Combo 1		Combo 3	
							ratio1	ratio2	ratio1	ratio2
6	W310X39	4940	2	1043	1134	165	0.57	0.54	0.77	0.74
5	W310X45	5690	1	1205	1306	191	0.68	0.62	0.84	0.79
4	W360X45	5730	2	1266	1315	210	0.75	0.69	0.85	0.80
3	W360X51	6450	1	1432	1480	241	0.75	0.69	0.85	0.80
2	W360X51	6450	1	1432	1480	241	0.83	0.76	0.87	0.81
1	W360X57	7220	1	1607	1657	273	0.79	0.73	0.81	0.76

For column design, the effective length ( $KL$ ) was used to calculate the factored compression resistance. Due to the effects of column-beam joints, the effective length factor ( $K$ ) was assumed to be 0.9. The axial forces triggered in columns are shown in Figure 3.6 for the 3-storey building, while for the 6-storey building the forces are given in Figure 3.7. The W-shape column cross-sections of the 3- and 6-st CBFs (E-W) as per the 1980 design are given in Table 3.15a and b, respectively. Similarly, the W-shape middle column cross-sections of the 3- and 6-st CBFs (N-S) as per the 1980 design are given in Table 3.16a and b, respectively.

The W-shape side columns of the 3- and 6-st CBFs (N-S) are given in Table 3.17a and b.

Table 3.15a: Column cross-sections of the 3-st CBF (E-W) as per the 1980 design

Storey	Column	$A_g(\text{mm}^2)$	Section Class	$C_{r-80}$ (kN)	$C_{f-80}/C_{r-80}$
3	W200X31	4000	1	424	0.67
2	W200X52	6650	1	1255	0.50
1	W250X73	9280	2	1748	0.59

Table 3.15b: Column cross-sections of the 6-st CBF (E-W) as per the 1980 design

Storey	Column	$A_g(\text{mm}^2)$	Section Class	$C_{r-80}$ (kN)	$C_{f-80}/C_{r-80}$
5-6	W200X52	6650	1	1255	0.50
3-4	W250X89	11400	1	2444	0.62
1-2	W310X129	16500	1	3471	0.74

Table 3.16a: Middle column cross-sections of the 3-st CBF (N-S) as per the 1980 design

Storey	Middle Column	$A_g(\text{mm}^2)$	Section Class	$C_{r-80}$ (kN)	$C_{f-80}/C_{r-80}$
3	W200X42	5310	1	795	0.49
2	W200X52	6650	1	1255	0.62
1	W250X67	8550	1	1263	0.88

Table 3.16b: Middle column cross-sections of the 6-st CBF (N-S) as per the 1980 design

Storey	Middle Column	$A_g(\text{mm}^2)$	Section Class	$C_{r-80}$ (kN)	$C_{f-80}/C_{r-80}$
5-6	W200X42	5310	1	795	0.98
3-4	W250X67	8550	1	1595	0.90
1-2	W310X107	13600	2	2847	0.73

Table 3.17a: Side column cross-sections of the 3-st CBF (N-S) as per the 1980 design

Storey	Side Column	$A_g(\text{mm}^2)$	Section Class	$C_{r-80}$ (kN)	$C_{f-80}/C_{r-80}$
3	W200X31	4000	1	424	0.93
2	W200X42	5310	1	795	0.98
1	W250X67	8550	1	1263	0.89

Table 3.17b: Side column cross-sections of the 6-st CBF (N-S) as per the 1980 design

Storey	Side Column	$A_g(\text{mm}^2)$	Section Class	$C_{r-80}$ (kN)	$C_{f-80}/C_{r-80}$
5-6	W200X42	5310	1	795	0.98
3-4	W200X71	9100	1	1740	0.89
1-2	W250X115	14600	1	2798	0.90

### 3.4.3 *Brace connection design*

In this study, welding connections were selected for brace-to-frame. In this respect, the gusset plate transfer the forces from the HSS brace to frame as depicted in Figure 3.8 for the chevron brace. From the HSS to the gusset the axial force is transferred by means of four fillet welds. On the other side, the gusset plate is welded to the beam and column. It is noted that chevron brace forms an angle of about  $45^\circ$  with a horizontal line, while the diagonal brace (N-S) shown in Figure 3.9 forms an angle of about  $28^\circ$ . The connection of chevron braces to the beam middle span is given in Figure 3.10. Brace connection design should consider factored resistance of weld, gusset plate and connected brace. Design of each component should follows the possible failure modes examined with CSA/ S16.1-M78 requirements for connections. For weld, shear failure has to be checked. For gusset plate and connected brace, the failure models include ultimate strength and tension rupture on the net section. Welding connection was used in this study, steel type used for gusset plate is G40.21-300W as other structural members. E480 electrodes were used for welding, the electrode ultimate strength ( $X_u$ ) was taken as 480 MPa, the weld leg width ( $D_w$ ) was taken as 8.0 mm. The brace connection was designed to take the factored axial load transferred from brace.

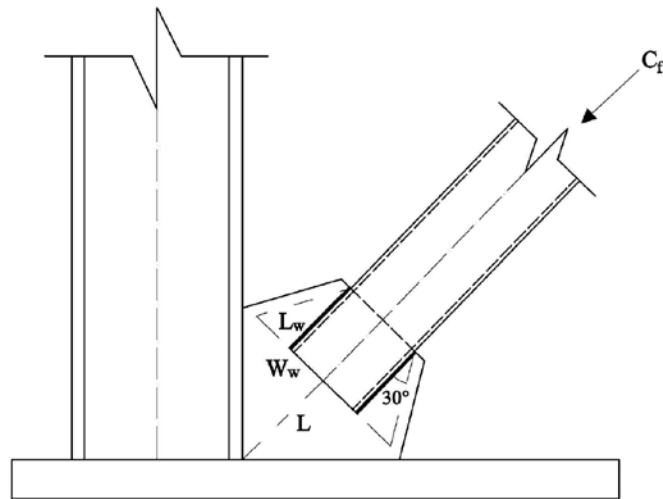


Figure 3.8: Brace-to-frame gusset plate connection (CBF E-W direction)

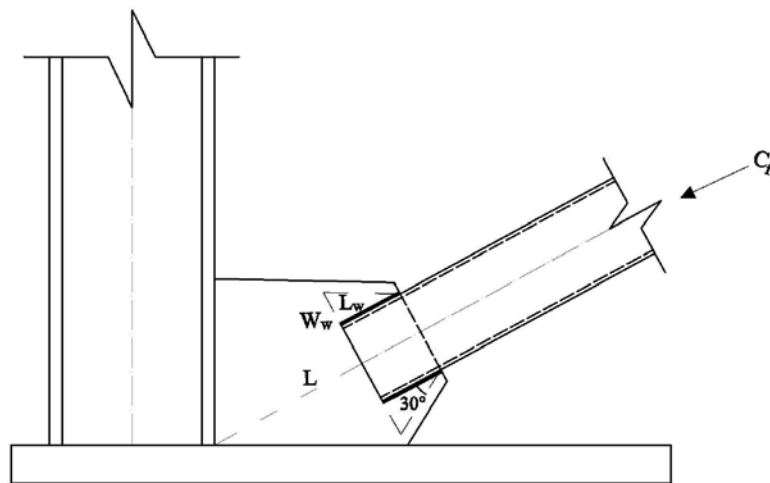


Figure 3.9: Brace-to-frame gusset plate connection (CBF N-S direction)

In the given example, the connection of the ground floor brace of the 6-storey CBF (E-W) to the column and base plate is considered (See Figure 3.8). The required length of the weld of HSS 152.4x152.4x9.53 brace to gusset plate is:

$$L_w = \frac{C_f/4}{0.66\Phi D_w F_y} = \frac{679/4}{0.66(0.9)(8.0)(300)/1000} \cong 120 \text{ mm}$$

The required length of fillet weld should be the calculated length, 120 mm, plus 2

times of weld leg width, 32mm, and finally the length of weld was rounded to 160 mm for construction convenience (including 20mm HSS interior welding).

Next, the factored shear resistance of fillet weld results from the consideration of two failure modes: fracture of the weld metal through the weld throat and yielding at the weld-to-base metal interface. The respective equations are: i)  $V_r = 0.50\phi A_w X_u$  and ii)  $V_r = 0.66\phi A_m F_u$ . The shear area is  $A_w = 0.707D_w L_w$  and the interface area is  $A_m = D_w L_w$ . Thus, the fracture of the weld metal computed for a fillet weld with an effective length of 160 – 40 = 120 mm is:

$$V_r = 0.50\phi A_w X_u = \frac{0.50(0.9)(120)(0.707)(8.0)(480)}{1000} = 147 \text{ kN}$$

$$< \left(\frac{679}{4}\right) \text{ kN} \quad \text{No good.}$$

Therefore, the effective length of fillet weld needs to be increased from 120 mm to 150 mm for which it results  $V_r = 183$  kN. By considering that the HSS is attached to the gusset plate by four fillet welds, the value of  $V_r = 183 \times 4 = 732$  kN > 679 kN. It is noted that the  $C_f$  force developed in the brace is 679 kN, while the tensile force  $T_{f\text{brace}} = 503$  kN.

Checking the yielding at the weld-to-base metal interface:

$$V_r = 0.66\phi A_m X_u = \frac{0.66(0.9)(150)(8.0)(300)}{1000} = 214 \text{ kN} > \left(\frac{679}{4}\right) \text{ kN} \quad \text{OK.}$$

After the effective welding length was computed as 150 mm the gusset plate thickness was based on Whitmore width cross-section. The Whitmore width ( $W_w$ ) can be found using the following equation:

$$W_w = 2L_w \tan 30^\circ + b = 2(170)\tan 30^\circ + 152.4 = 349 \text{ mm}$$

It is noted that at the end of HSS brace, the fillet weld was returned inside the HSS and only 16 mm were added to the 150 mm welding length (170 mm rounded) in order to calculate the Whitmore width.

Next, a preliminary gusset plate thickness was estimated based on yielding of the Whitmore width cross-section:

$$t_g = \frac{C_f}{0.85\phi_w F_y} = \frac{679}{0.85(0.9)(349)(300)/1000} = 8.5 \text{ mm}$$

Consider  $t_g = 9.5 \text{ mm}$ .

The tensile resistance of metal base (gusset plate) is equal to

$$\phi t_g L_w F_y = 0.9 \times 2(9.5 \times 160) \times 300/1000 = 770 \text{ kN} > 503 \quad \text{OK.}$$

Then, the compression resistance of gusset plate was calculated. In this light, the slenderness is given below, where  $r$  is the radius of gyration of Whitmore cross-section and it corresponds to out-of-plan buckling.

$$\lambda = \frac{KL}{r} \sqrt{\frac{F_y}{\pi^2 E}} = \frac{0.67(178)}{(2.74)} \sqrt{\frac{300}{\pi^2 E}} = 0.536$$

The effective length of gusset plate ( $L$ ) is the geometric length from end of brace to the end of gusset plate as shown on Figure 3.8. The compressive Whitmore resistance ( $C_r$ ) was then calculated based on Equation (2.19):

$$\begin{aligned} C_{rGP} &= 0.9 \times 349 \times 9.5 \times \frac{300(1.035 - 0.202 \times 0.536 - 0.222 \times 0.536^2)}{1000} \\ &= 772 \text{ kN} > C_f = 679 \text{ kN} \end{aligned}$$

The thickness of gusset plate of 9.5 mm is OK. The tensile resistance of gusset plate,  $T_{rGP}$  equals to  $0.9 \times 349 \times 9.5 \times 300/1000 = 895 \text{ kN}$  which is larger than  $T_{f,brace} = 503 \text{ kN}$ . In addition, the tensile resistance of gusset plate should be larger than the 50% of brace tensile resistance which is 703 kN and its compressive resistance should be larger than 50% of brace compression resistance which is  $50\%(766) = 383 \text{ kN}$ . It is noted that the block shear check was introduced in the provisions later than 1980. Net rupture of brace due to the reduction of cross section area for the gusset plate slot was checked:

$$\begin{aligned} T_{rb} &= 0.85\phi A_{nb} F_y = \frac{0.85(0.9)(5210 - 2 \times 9.53 \times 11)(345)}{1000} \\ &= 1320 \text{ kN} > 681 \text{ kN} \quad \text{OK.} \end{aligned}$$

To summarize, the compression resistance of gusset plate  $C_{rGP} = 772$  kN is larger than the axial compression force transferred from the brace ( $C_{fbrace} = 679$  kN) Therefore, it satisfies the 1980 requirements. However, from Table 3.11b it results that the compression resistance of the HSS 152.4x152.4x9.53 chevron brace is  $C_{r-80} = 927$  kN. The recalculate  $C_{r-80}$  value was obtained after the dimensions of gusset plates were known and the length of brace was obtained. In these circumstances,  $C_{rGP} < C_{r-80}$  which means that buckling of braces cannot be sustained under increased seismic demand. Then, if the force in the tensile brace increases by 20% due to the asymmetric response, the tensile resistance of metal base (gusset plate) will be reached and failure at the level of welds will occur.

The middle gusset plate design shown in Figure 3.10 is similar to that of a corner gusset plate, one or two stiffener are required to sustain buckling of braces if occurs.

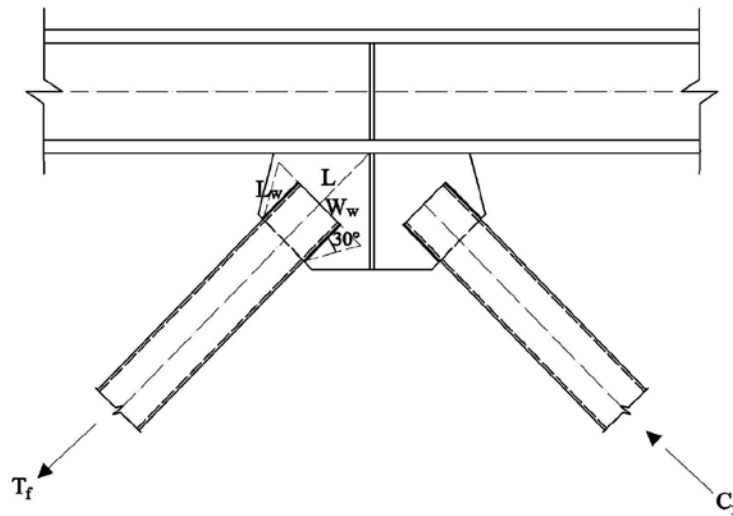


Figure 3.10: Middle brace connection

The summary of corner brace connections is given in Table 3.18a for the 3-storey building (E-W) and Table 3.18b for the 6-storey.

Table 3.18a: Brace-to-frame connections design (3-st E-W) (unit: mm)

Storey	$L_w$	$t_{gusset}$	$W_w$	$L$
3	100	9.5	217	149
2	100	9.5	217	149
1	100	9.5	242	134

Table 3.18b: Brace-to-frame connections design (6-st E-W) (unit: mm)

Storey	$L_w$	$t_{\text{gusset}}$	$W_w$	L
6	100	9.5	217	149
5	100	9.5	217	149
4	110	9.5	254	168
3	130	9.5	277	180
2	150	9.5	300	192
1	170	9.5	349	178

The summary of diagonal brace connections is given in Table 3.19a for the 3-storey building (N-S) and Table 3.19b for the 6-storey.

Table 3.19a: Brace-to-frame connections design (3-st N-S) (unit: mm)

Storey	$L_w$	$t_{\text{gusset}}$	$W_w$	L
3	100	9.5	242	311
2	100	9.5	268	337
1	120	9.5	316	312

Table 3.19(b): Brace-to-frame connections design (6-st N-S) (unit: mm)

Storey	$L_w$	$t_{\text{gusset}}$	$W_w$	L
6	100	9.5	242	311
5	100	9.5	268	337
4	130	12.7	328	400
3	160	12.7	363	436
2	180	15.9	386	460
1	210	12.7	446	372

The reserve capacity of corner connections based on 1980 design is given in Table 3.20a and Table 3.20b for the 3-st and 6-st CBF (E-W), respectively. The results are the same for the corresponded middle brace-to-frame connections. The reserve capacity of diagonal brace to frame connections based on 1980 design is given in Table 3.21a and Table 3.21b for the 3-st and 6-st CBF (N-S).

Table 3.20a: Brace-to-frame connection capacity based on 1980 design (3-st E-W)

St	Shear Resistance of Welding		Tensile Resistance of Metal Base		Yielding of Gusset Plate		Buckling of Gusset Plate		Net Fracture of Brace	
	$V_r$	$C_{f,br}/V_r$	$T_{r,MB}$	$T_{f,br}/T_{r,MB}$	$T_{r,GP}$	$T_{f,br}/T_{r,GP}$	$C_{r,GP}$	$C_{f,br}/C_{r,GP}$	$T_{r,b-net}$	$T_{f,br}/T_{r,b-net}$
	3	391	0.54	410	0.04	557	0.03	513	0.41	692
2	391	0.74	410	0.21	557	0.16	513	0.56	803	0.11
1	391	0.94	410	0.45	622	0.30	584	0.63	903	0.20

Table 3.20b: Brace-to-frame connection capacity based on 1980 design (6-st E-W)

St	Shear Resistance of Welding		Tensile Resistance of Metal Base		Yielding of Gusset Plate		Buckling of Gusset Plate		Net Fracture of Brace	
	$V_r$	$C_{f,br}/V_r$	$T_{r,MB}$	$T_{f,br}/T_{r,MB}$	$T_{r,GP}$	$T_{f,br}/T_{r,GP}$	$C_{r,GP}$	$C_{f,br}/C_{r,GP}$	$T_{r,b-net}$	$T_{f,br}/T_{r,b-net}$
	6	391	0.52	410	0.07	557	0.05	513	0.40	692
5	391	0.82	410	0.31	557	0.23	513	0.63	803	0.16
4	440	0.95	462	0.48	652	0.34	583	0.72	739	0.30
3	538	0.93	564	0.54	711	0.43	622	0.80	1056	0.29
2	635	0.90	667	0.56	770	0.49	659	0.86	1056	0.35
1	732	0.93	770	0.65	895	0.56	772	0.88	1320	0.38

Table 3.21a: Brace-to-frame connection capacity based on 1980 design (3-st N-S)

St	Shear Resistance of Welding		Tensile Resistance of Metal Base		Yielding of Gusset Plate		Buckling of Gusset Plate		Net Fracture of Brace	
	$V_r$	$C_{f,br}/V_r$	$T_{r,MB}$	$T_{f,br}/T_{r,MB}$	$T_{r,GP}$	$T_{f,br}/T_{r,GP}$	$C_{r,GP}$	$C_{f,br}/C_{r,GP}$	$T_{r,b-net}$	$T_{f,br}/T_{r,b-net}$
	3	391	0.46	410	0.44	622	0.29	395	0.46	903
2	391	0.84	410	0.80	687	0.48	403	0.82	1312	0.25
1	489	0.93	513	0.89	811	0.56	514	0.89	1568	0.29

Table 3.21b: Brace-to-frame connection capacity based on 1980 design (6-st N-S)

St	Shear Resistance of Welding		Tensile Resistance of Metal Base		Yielding of Gusset Plate		Buckling of Gusset Plate		Net Fracture of Brace	
	$V_r$	$C_{f,br}/V_r$	$T_{r,MB}$	$T_{f,br}/T_{r,MB}$	$T_{r,GP}$	$T_{f,br}/T_{r,GP}$	$C_{r,GP}$	$C_{f,br}/C_{r,GP}$	$T_{r,b-net}$	$T_{f,br}/T_{r,b-net}$
6	391	0.44	410	0.42	622	0.28	395	0.44	903	0.19
5	391	0.86	410	0.82	687	0.49	403	0.84	1117	0.30
4	538	0.91	754	0.65	1124	0.44	738	0.66	1552	0.32
3	684	0.92	960	0.65	1243	0.50	753	0.83	1782	0.35
2	782	0.95	1374	0.54	1656	0.45	1163	0.64	1977	0.38
1	929	0.95	1303	0.68	1528	0.58	1064	0.83	2080	0.43

Therefore, the shear resistance of welding governs, followed by buckling of gusset plate and tensile resistance of metal base. Yielding of gusset plate is more likely to occur at lower floors of the 6-storey building and in CBFs with diagonal tension/compression braces.

## **CHAPTER 4. SEISMIC ASSESSMENT OF STUDIED BUILDINGS ACCORDING TO CURRENT CODE DEMAND**

In this chapter, the fictitious buildings designed in 1980 were assessed based on the design provisions of NBCC 2010 and CSA S16.1-09 standard in order to detect their strength deficiencies under seismic loads. Seismic assessment of CBF systems focused on the evaluation of braces, columns, beams and brace-to-frame connections. Cost- efficient retrofitted strategies are proposed in order to improve the structural response.

### ***4.1 Results from Static Equivalent Method (NBCC 2010)***

Generally, seismic weight ( $W$ ) and the fundamental period ( $T_a$ ) are the key factors in the calculation of shear forces resulted from the designed seismic load. For existing buildings, their seismic weight was slightly increased due to the increase in the snow load. Thus, the snow load of 2.16 kPa calculated from Equation (2.1) as per 1980 has increased to 2.48 kPa. In consequence, a 1% increase in the seismic weight resulted for both 3- and 6-storey buildings. More precisely, the total seismic weight of the 3-storey building increases from 20963 kN to 21107 kN and that of the 6-storey building from 41912 kN to 42056kN.

The empirical fundamental period ( $T_{emp.}$ ) of the 3-storey building in the E-W direction has increased from 0.136s to 0.293s and that in the N-S direction has increased from 0.192s to 0.293s. In the case of the 6-storey building in the E-W direction the fundamental period has increased from 0.261s to 0.563s and that in the N-S direction from 0.370 s to 0.563s. It is noted that the fundamental period computed for both 3- and 6-storey buildings was calculated based on Equation (2.13) as provided in NBCC 2010. In addition, according to the NBCC 2010 provisions, the base shear of CBF should not be lower than that corresponding to  $2T_{emp.}$ . In order to estimate the ductility-related force modification factor,  $R_d$  and the overstrength-related force modification factor  $R_o$ , both fictitious buildings were considered as being conventional constructions (CC Type). In this light, the assigned values are:  $R_d = 1.5$  and  $R_o = 1.3$ . In agreement with the requirements of S16-2009, for buildings located in areas where

the specified short-period spectral acceleration ratio  $IEF_aSa(0.2) \geq 0.35$ , the height of buildings in the category “other occupancy” rather than “assembly occupancy” is limited to 60 m. The height of the 6-storey building is 22.5 m, therefore lower than 60 m. Because the studied buildings were subjected to dynamic analysis, for the preliminary design, their fundamental period was considered equal to  $2T_{emp} = 2 \times 0.025h_n$ . It resulted:  $T_1 = 0.585s$  for the 3-storey and 1.125s for the 6-storey CBF. With these assumptions,  $M_v = 1.0$  for the 3-storey building and  $M_v = 1.07$  for the 6-storey building. The importance factor for offices buildings is:  $I_E = 1.0$ .

Site coefficient factors,  $F_a$  and  $F_v$ , are equal to unity for site class C. The design spectral response acceleration,  $S(T_a)$ , was calculated based on the acceleration spectrum for Montreal provided by geological survey of Canada and the fundamental period of the building. The calculated base shear ( $V_{f,10}$ ) has to be larger than the base shear determined at a period of 2.0s ( $V_{min}$ ) and should not exceed 2/3 of the computed base shear at a period of 0.2s ( $V_{max}$ ). A summary of base shear calculation based on the static equivalent method is shown in Table 4.1.

Table 4.1: Seismic load calculation based on static design method

Building	$2T_{emp}$	$S_a(T_1)$	$M_v$	$I_E$	$R_d$	$R_o$	W(kN)	$V_{f,10}$ (kN)
6-Storey	1.125s	0.129g	1.07	1	1.5	1.3	42056 kN	2965 kN
3-Storey	0.585s	0.281g	1	1	1.5	1.3	21107 kN	3043 kN

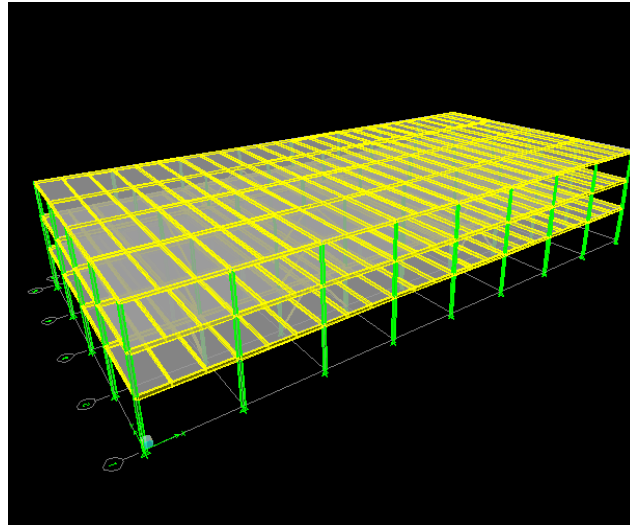
Referring to load combinations, important changes were made. In the 1980 code, the factored load coefficient was 1.5 for earthquake, versus 1.0 in NBCC 2010 where the load combination is:  $1.0D + 0.5L + 0.25S + 1.0E$ .

## 4.2 Results from Modal Response Spectrum Method

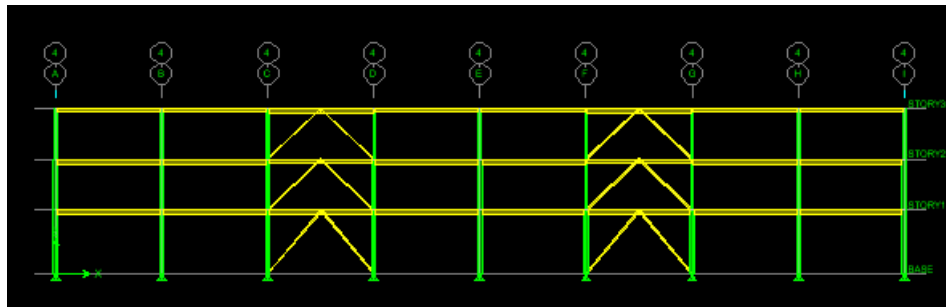
In this study, a numerical model of the fictitious buildings was developed in ETABS (CSI, 2009) and a linear dynamic analysis following the modal response spectrum method was carried out.

All gravity load and the acceleration spectrum data for Montreal were inputted into ETABS model and the torsion effect was considered with a 10% accidental eccentricity. The 3D view and elevation view of braced frame in each direction is shown in Figure 4.1 for the 3-

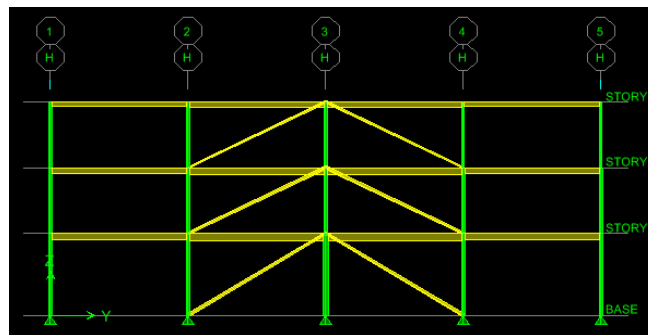
storey building and Figure 4.2 for the 6-storey building.



(a)

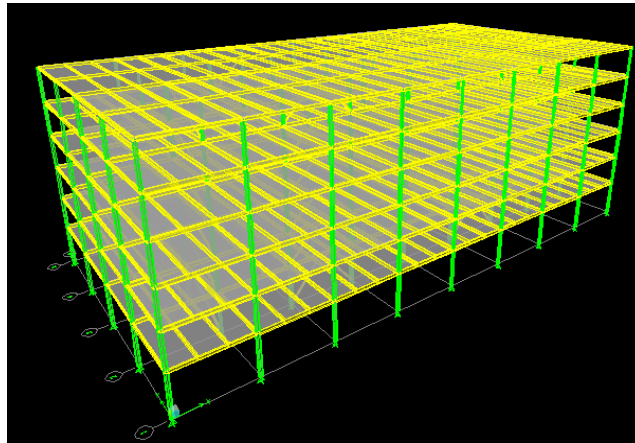


(b)

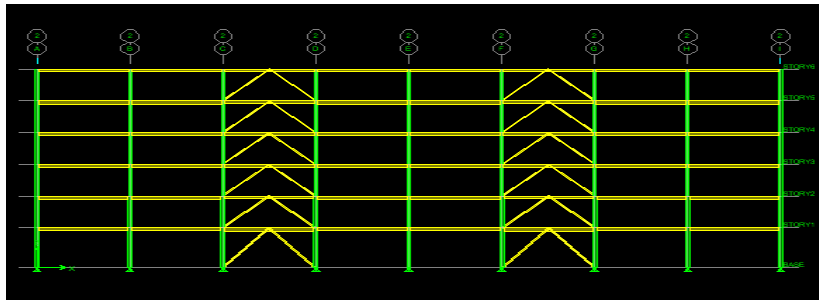


(c)

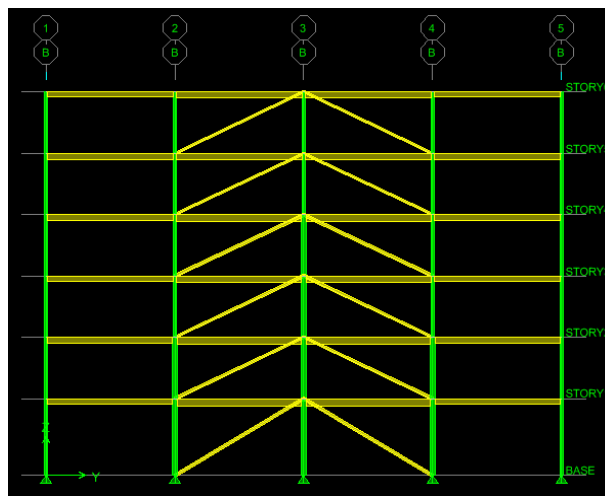
Figure 4.1: ETABS model of the 3-st. building: a) 3-D view, b) elevation E-W; c) elevation N-S



(a)



(b)



(c)

Figure 4.2: ETABS model of the 6-st. building: a) 3-D view, b) elevation E-W; c) elevation N-S

The design base shear ( $V_{dyn,10}$ ) was obtained by multiplying the elastic base shear ( $V_e$ ) resulted from linear dynamic analysis with the ratio of  $I_E/(R_d R_o)$ . Then, for a regular building, the resulted  $V_{dyn,10}$  value should not be lower than  $80\%(V_{f,10})$ , as shown in Table 4.1. The fundamental period resulted from the linear dynamic analysis  $T_{1,dyn}$  is given in Table 4.2 in addition to the empirical fundamental period,  $2T_{emp}$ ,  $V_e$ ,  $V_{dyn,10}$  and  $V_f$ . In the case that  $V_{dyn,10} \geq 80\%V_{f,10}$ , the results from linear dynamic analysis (ETABS), such as: elastic storey shear, member forces, deflections should be multiplied by the ratio  $I_E/(R_d R_o)$ . If the building is irregular and is torsional sensitive (irregularity type 7) the resulted base shear  $V_{dyn,10}$  should be magnified to reach at least  $100\% V_{f,10}$ .

The building located in seismic area with  $I_E F_a S_a(0.2) \geq 0.35$  is classified as torsional sensitive if the ratio of maximum storey displacement at the extreme points of the structure and the average of the displacements at the extreme points of the structure at the same level under a torsional effects with 10% of eccentricity is larger than 1.7. Both 3-storey and 6-storey building show a ratio of 1.16, therefore they are not torsional sensitive.

Table 4.2: Base shear comparisons. (Unit: s, kN)

Building	W-E Direction					N-S Direction				
	$2T_{1,emp}$	$V_e$	$T_{1,dyn}$	$V_d$	0.8V	$2T_{1,emp}$	$V_e$	$T_{1,dyn}$	$V_d$	0.8V
6-Storey	1.125	5709	1.107	2928	2372	1.125	5543	1.075	2842	2372
3-Storey	0.585	5602	0.594	2873	2434	0.585	5341	0.619	2739	2434

For both buildings,  $V_{dyn,10}$  is larger than  $0.8V_{f,10}$ , so the base shear was taken as  $V_{dyn,10}$ . It is noted that, the torsional effect due to accidental eccentricity is not included in the base shear ( $V_e$ ) obtained from ETABS in order to compare it with that calculated from the equivalent static force procedure.

In addition, according to conventional constructions (clause of CSA/S16 2009), the ductility-related force modification factor should be considered as  $R_d = 1.0$  instead of  $R_d = 1.5$  if the failure mode of brace-to-frame connections is a brittle failure mode like welds fracture, gusset plate fracture, etc. In all the following verifications referring to the demand to capacity ratios,  $R_d = 1.5$  was considered.

As mentioned above, the evaluation of all buildings were conducted using the 2010

NBCC and S16-2009 standard. Regarding the demand to capacity ratio of storey shear computed as:  $\max(V_{dyn,10}; 0.8V_{f,10})/V_{f,80}$ , the results are shown in Figure 4.3. It is illustrated that this ratio is larger for the 3-storey building and especially for the chevron CBFs (E-W).

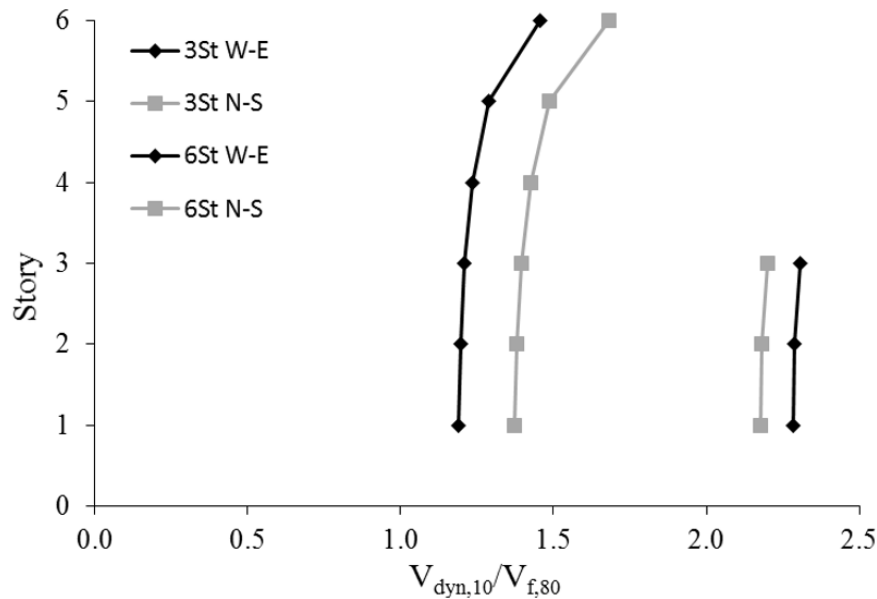
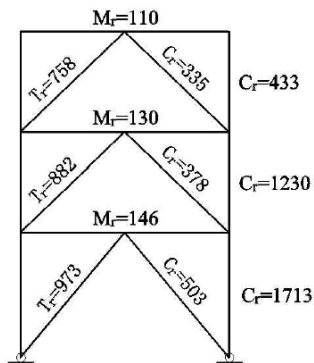


Figure 4.3: Demand to capacity ratio of storey shear  $V_{dyn,10}/V_{f,80}$

According to CSA/S16 2009 standard, the lateral-load-resisting system is designed based on the capacity design principle, which means that all remaining members of CBFs should sustain the probable tensile and compressive forces developed in braces. The tensile and compression resistance of HSS brace members ( $T_{r,br}$  and  $C_{r,br}$ ) computed according to Equations (2.27) and (2.25) are given in Figure 4.4, as well as the compression resistance of columns and the flexural resistance of beams,  $M_r$ . It is noted that the  $C_r$  of the ground floor column of the 6-storey CBF is lower than that of the column above because of its larger height, even if their cross-section is the same. The length of brace used in the equation of brace compression strength ( $C_{r,br}$ ) was computed as being the geometric length minus two times the distance between the working point and the end of brace projected on the gusset plate.

$V_{dyn,10} = 2873 \text{ kN}, T_{1,dyn} = 0.594 \text{ s}, R_d = 1.5$



$V_{dyn,10} = 2739 \text{ kN}, T_{1,dyn} = 0.619 \text{ s}, R_d = 1.5$

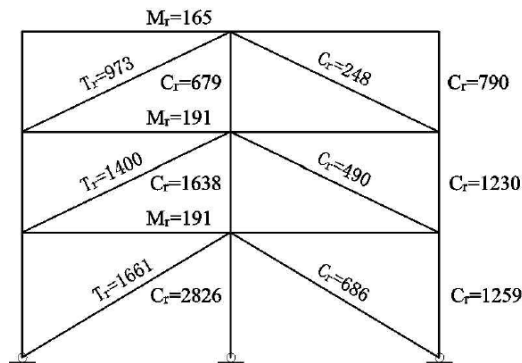
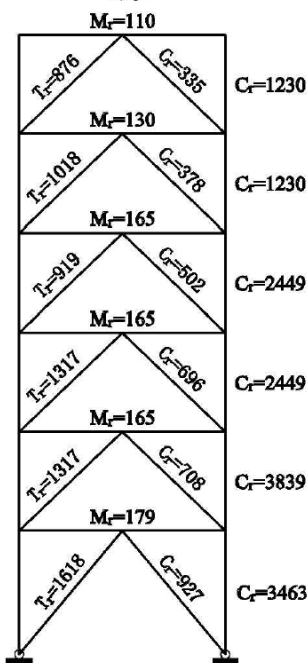


Figure 4.4a: Structural members' resistance, 3-Storey

$V_{dyn,10} = 2928 \text{ kN}, T_{1,dyn} = 1.107 \text{ s}, R_d = 1.5$



$V_{dyn,10} = 2842 \text{ kN}, T_{1,dyn} = 1.125 \text{ s}, R_d = 1.5$

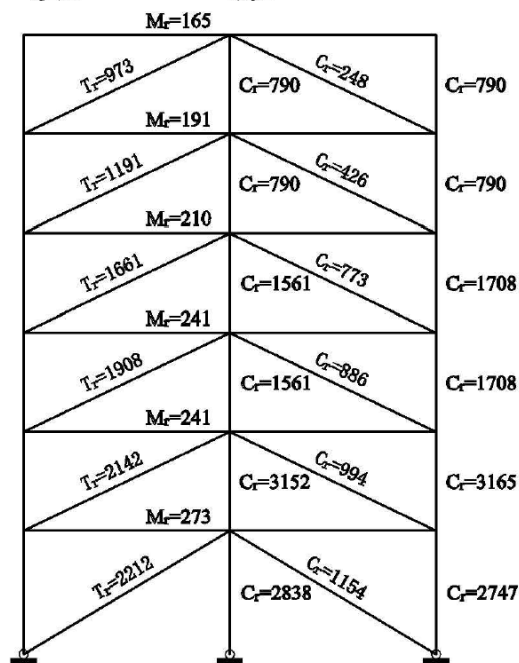


Figure 4.4b: Structural members' resistance, 6-Storey

All members of the CBFs should be able to sustain the design seismic force in addition to the gravity load. It is noted that forces triggered in braces due to earthquake loading were obtained from dynamic analysis. Due to the increasing of base shear in the current code the demand is more than twice for the 3-storey building and about 1.4 for the 6-storey building,

Figure 4.3, meaning that the seismic deficiency of the 3-storey building is higher than that of the 6-storey building.

The demand to capacity ratio for bracing members is given for both buildings in Table 4.3 (E-W direction) and Table 4.4 (N-S direction) in terms of  $C_{f,10}/C_{r,10}$  and  $T_{f,10}/T_{r,10}$  according to Equation (2.26). It is noted that for the seismic assessment of braces, in the expression of  $C_{r,10}$  it was considered  $\Phi = 1.0$  instead of  $\Phi = 0.9$ . Even though, the compression resistance of braces is lower than the demand for the 3-storey building in both E-W and N-S directions. In this regards,  $C_{f,10}/C_{r,10}$  is in the ranges of 1.10 to 1.49 (N-S) and 1.35 to 1.38 (E-W). If we considered  $C_{f,10}$  reported to the probable compression strength,  $C_{u,10}$  calculated with  $\Phi = 1.0$  and  $R_y = 1.1$ , the demand to capacity ratios,  $C_{f,10}/C_{u,10}$  have slightly improved but is still larger than 1.08 for braces of the 3-storey building. Therefore, by following the equivalent static force distribution over the building height, the compression resistance of braces is not sufficient. For both buildings, the  $C_{f,10}/C_{r,10}$  ratio is shown in Figure 4.5. In the case of the 6-storey building, in both E-W and N-S directions, the  $C_{f,10}/C_{u,10}$  ratios are less than 1.0. As resulted from Table 4.3 and Table 4.4, the tensile capacity of braces is adequate. It is noted that the effect of torsion due to accidental eccentricity and  $P-\Delta$  effect were included in the demand.

Table 4.3a: Demand to capacity ratio of brace (3-st E-W)

St	$C_{f,10}/C_{r,10}$	$C_{f,10}/C_{u,10}$	$T_{f,10}/T_{r,10}$	$T_{f,10}/T_{u,10}$
3	0.97	0.88	0.26	0.21
2	1.38	1.26	0.42	0.34
1	1.35	1.23	0.58	0.47

Table 4.3b: Demand to capacity ratio of brace (6-st E-W)

St	$C_{f,10}/C_{r,10}$	$C_{f,10}/C_{u,10}$	$T_{f,10}/T_{r,10}$	$T_{f,10}/T_{u,10}$
6	0.83	0.68	0.13	0.10
5	1.01	0.92	0.21	0.17
4	0.94	0.86	0.34	0.28
3	0.78	0.71	0.30	0.24
2	0.83	0.76	0.34	0.28
1	0.73	0.66	0.34	0.28

Table 4.4a: Demand to capacity ratio of brace (3-st N-S)

St	$C_{f,10}/C_{r,10}$	$C_{f,10}/C_{u,10}$	$T_{f,10}/T_{r,10}$	$T_{f,10}/T_{u,10}$
3	1.49	1.35	0.42	0.34
2	1.28	1.16	0.50	0.41
1	1.19	1.08	0.55	0.45

Table 4.4b: Demand to capacity ratio of brace (6-st N-S)

St	$C_{f,10}/C_{r,10}$	$C_{f,10}/C_{u,10}$	$T_{f,10}/T_{r,10}$	$T_{f,10}/T_{u,10}$
6	1.09	0.99	0.31	0.25
5	1.04	0.95	0.41	0.34
4	0.76	0.69	0.39	0.32
3	0.78	0.71	0.40	0.33
2	0.77	0.70	0.40	0.33
1	0.74	0.67	0.43	0.35

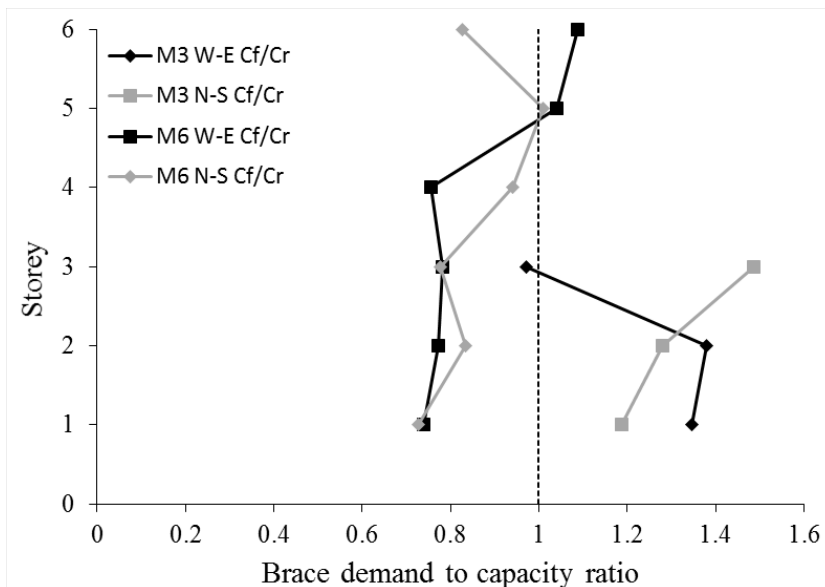


Figure 4.5: Seismic assessment of bracing members of the CBF systems

In this study the beams of CBF systems were verified as beam-column element for three limit states such as: cross-sectional strength (*CSS*), overall member strength (*OMS*) and combined tensile axial force and bending moment (*AT&B*). The torsional buckling strength was not verified because the beam is laterally supported by the composite steel deck. In CSA

S16-09, the interaction equation used to check member strength and stability under axial compression force and bending for class 1 and class 2 W-shape cross-sections has been changed and the interaction equation for bending about strong axis is given in Equation (2.21). The same interaction equation is used to verify the capacity of the member for cross-sectional strength (*CSS*) and overall member strength (*OMS*). In this study, the factored bending moment ( $M_f$ ) developed at the mid-span of CBF beams governs and all beams have a W-shape cross-section and are Class 1 or 2. Thus, to check the cross-sectional member strength, the maximum cross-sectional compressive resistance was calculated by using the following equation:  $C_r = \Phi A F_y$ , where  $\lambda = 1.0$ . For cross-sectional strength,  $U_{1x} = 1.0$ . The overall member strength (*OMS*) or the in-plan bending strength is affected by member's slenderness,  $\lambda$ . See Equation (2.27) for  $C_r$  calculation. For both limit states,  $M_r = \Phi Z_x F_y$ . For overall member strength,  $U_{1x}$  is obtained from the following equation:  $U_1 = \omega_l / (1 - C_f / C_e)$ , where  $\omega_{1x} = 1.0$  for uniformly distributed load and  $C_{ex} = A F_{ex}$ . Beams of CBFs are also subject to tension and bending (*AT&B*) and the interaction Equation (2.22) was applied. The seismic assessment of beam members of CBFs given in terms of demand to capacity ratio corresponding to the following limit states: *CSS*, *OMS* and *AT&B* is shown in Figure 4.6. Thus, none of the beams have sufficient capacity to withstand the required limit states. For both buildings, the larger demand resulted for the *OMS* limit state. Conversely, for beams of 6-storey CBF (N-S), the larger demand occurs at the lower floors and for the CBF in the E-W direction at the upper floors. In this case, the demand to capacity ratio is between 1.5 and 2.0 due to the projection of compression and tension resistance on the beam axis.

Regarding the column assessment, the demand to capacity ratio for the columns of the CBF systems is illustrated in Figure 4.7. Only the governing compression load was considered for the seismic assessment of the side column (*SC*) and middle column (*MC*) of CBF in the N-S direction. As illustrated, the compression resistance of the 3- and 6-storey braced frame columns in the N-S direction, especially the middle column does not have sufficient strength and it shows a demand to capacity compression strength ratio of 2.0. However, the compression strength of all other braced frame columns is adequate.

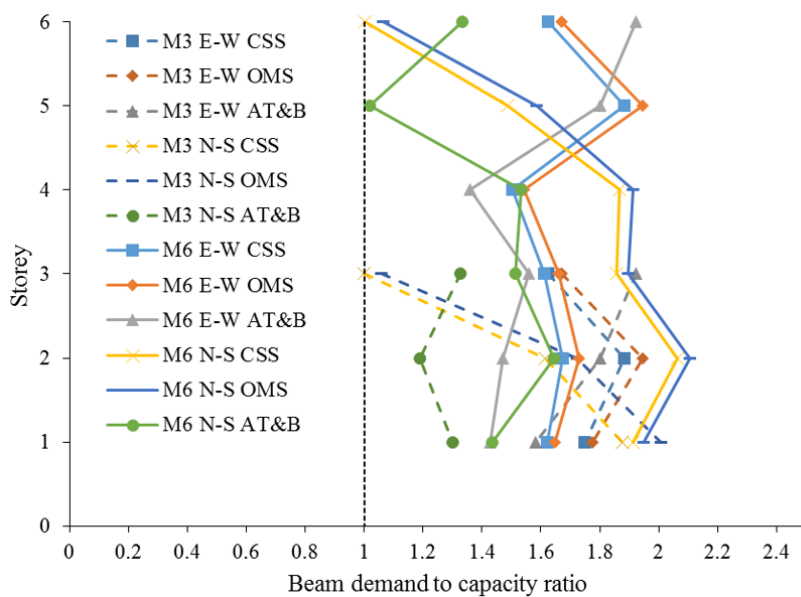


Figure 4.6: Seismic assessment of beams of the CBF systems.

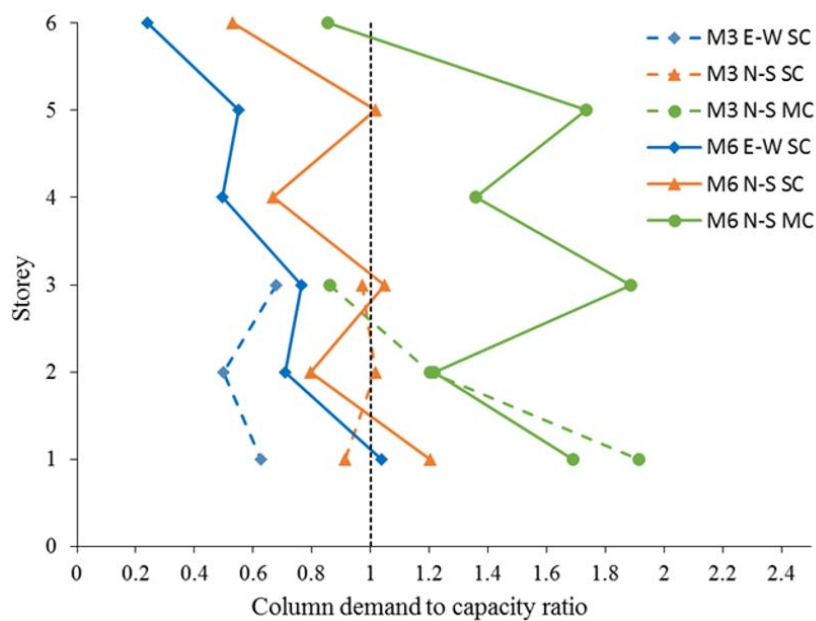


Figure 4.7: Seismic assessment of columns of the CBF systems

Brace to frame connections are the structural component that are more likely to fail when the capacity design principle applies. The  $2t_g$  linear clearance required to be provided at

the level of gusset plate, as well as, the addition of cover plate at the location of slotted HSS were not demanded in 1980. Based on the current standard requirements, the brace-to-frame connection detail is illustrated in Figure 4.8 for chevron brace and in Figure 4.9 for the tension/compression diagonal brace. In addition, block shear failure is a new check required by the CSA S16.1-09 standard.

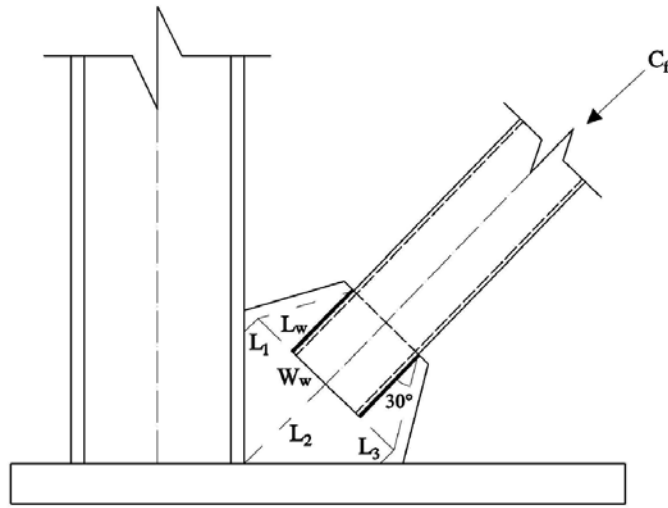


Figure 4.8: Corner brace to frame connection (E-W direction, 2010)

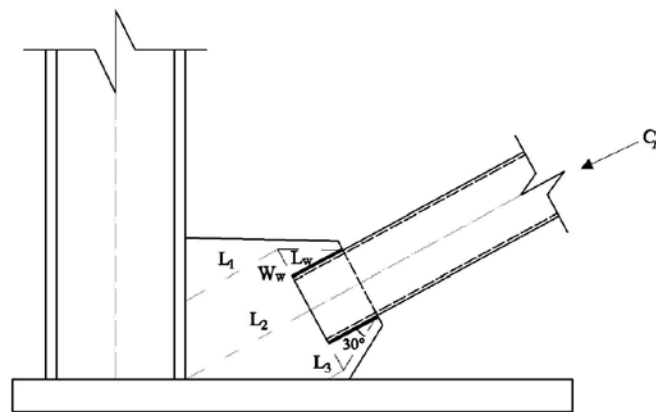


Figure 4.9: Corner brace to frame connection (N-S direction, 2010)

For seismic assessment of brace-to-frame connections, the connections designed according to CSA/S16.1-M78 requirements are checked against the CSA/S16-09 requirements.

Thus, for the given brace-to-frame connection design example given in Chapter 3 (ground floor brace of the 6-storey building, E-W) the resulted parameters are summarized: welding length,  $L_w = 150 \text{ mm}$ ; high of fillet weld,  $D_w = 8.0 \text{ mm}$ ; and Whitmore width,  $W_w = 349 \text{ mm}$ . According to the current standard, the length of the gusset plate ( $L_g$ ) is calculated as the average of  $L_1$ ,  $L_2$  and  $L_3$  lengths which are illustrated in Figure 4.8 and Figure 4.9 and were calculated based on the gusset plate geometry. From the gusset plate geometry, the value of  $L_g$  computed for the aforementioned example is 63.4 mm versus 178 mm previously calculated (CSA/S16.1-M78).

The equation for tension resistance of gusset plate is the same as that calculated according to CSA/S16.1-M78 standard and  $T_{rGP} = 894 \text{ kN}$ . The calculation of gusset compression resistance ( $C_{rGP}$ ) was conducted in accordance with Equation (2.27) of CSA/S16-09 standard. Because of the slight changes in the expression of  $C_r$  equation and a smaller  $L_g$  value, the resulted compression strength is  $C_{rGP} = 887 \text{ kN}$  which is 14.9% larger than that computed according to CSA/S16.1-M78 standard.

The expression of shear resistance of welding metal and base metal  $V_r$  that is given in Equation (2.32) as per the current code was slightly changed from its previous form (CSA/S16-78). Thus, the factored coefficient has changed from 0.66 (base metal) and 0.5 (weld metal) to 0.67 in CSA/S16-09 standard. In addition, the welding resistance factor  $\Phi_w$  has changed from 0.9 in CSA/S16.1-M78 standard to 0.67 in CSA/S16-09 standard. Overall, it resulted a slight change of 0.1%:  $V_{r,10} = 731 \text{ kN}$  versus  $V_{r,80} = 733 \text{ kN}$ .

The tensile resistance of HSS brace due to block shear failure is checked according to the current code demand as per Equation (2.22) and the calculation is given below:

$$\begin{aligned} T_{rBS} &= \Phi_u \left[ U_t A_n F_u + 0.6 A_{gv} \frac{(F_y + F_u)}{2} \right] \\ &= 0.75 \left[ (1.0)(0)(345) + (0.60)(5718) \frac{(345 + 448)}{2} \right] / 1000 = 1020 \text{ kN} \end{aligned}$$

where  $A_n$  is the net area of the failure plane subjected to tension, as gusset plate is not welded to the brace at the end ( $A_n = 0 \text{ mm}^2$ ) and  $A_{gv}$  is the net area along the shear failure plane,  $A_{gv} = 4 \times 150 \times 9.53 = 5718 \text{ mm}^2$ . Thus, “for shorter weld (insertion) lengths, the failure mode changes

to *block shear*, wherein the gusset plate tears out of the HSS by forming a fracture path through the HSS wall (on two opposite sides of the HSS) immediately adjacent the fillet weld toes.” (Packer, 2014). Although the *block shear* may control the tensile limit state, the “circumferential” fracture of the HSS with the consideration of shear lag effect is checked below.

To verify the tensile rupture in the net section of HSS brace that is also known as the *circumferential fracture of the HSS brace*, the following equation should be satisfied:  $T_u = 0.85\phi A_{ne}F_u$  where  $A_{ne}$  is the effective net area given in clause 12.3.3.3 of S16-09 standard. For elements connected by longitudinal welds along two parallel edges  $A_{n2} = 0.5wt + 0.25L_w t$  when  $2w > L_w \geq w$ . In the case study  $L_w = 170$  mm and  $w = 152$  mm, while the brace is HSS 152.4 x152.4 x9.53. Thus,  $A_{n2} = 1131.2 \times 4 = 4525$  mm<sup>2</sup>. When the effective net area is affected by the shear lag effect, it is reduced with the shear lag factor  $U$  computed below. Because of the eccentricity of center of gravity resulted for the half cross-section of brace as shown in Figure 4.10, the shear lag may influence the net rupture of the brace.

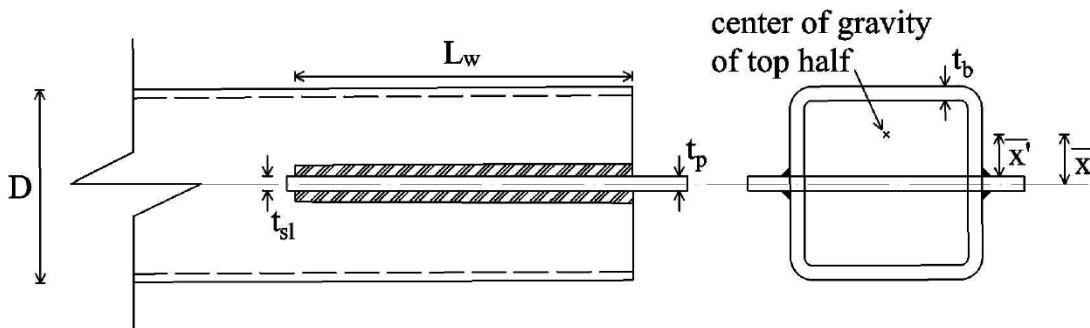


Figure 4.10: Slotted-end HSS welded connection

Based on the research conducted by Martinez-Saucedo and Packer (2009), a new clause 12.3.3.4 has been added in the upcoming edition of CSA/S16-14 standard in order to specifically address the shear lag factor,  $U$ , for all slotted HSS welded connections with a single concentric gusset plate. Thus,  $U = 1.1 - \bar{x}'/L_w$  but  $\geq 0.8$ , when  $0.1 < \bar{x}'/L_w \leq 0.3$  the shear lag factor  $U$  results from the following expression  $U = 1.1 - \bar{x}'/L_w$ , but it cannot be considered less or equal to  $0.8$ . When  $\bar{x}'/L_w \leq 0.1$ , the shear factor  $U$  is  $U = 1.0$ .

Applying the given explanations to the given example, the shear lag factor  $U$  is

calculated from Equation (2.34):

$$\bar{x}'/L_w = (49.7 - 9.5/2)/170 = 0.265, U = 1.1 - 0.265 = 0.835$$

Then, the effective net area is modified as  $A_{ne} = A_{n2}U = 4525 \times 0.835 = 3780 \text{ mm}^2$  and the nominal capacity for tensile rupture in the net section of HSS brace is:

$$T_u = 0.85\phi A_{ne}F_u = 0.85 \times 0.9 \times 3780 \times 448/1000 = 1296 \text{ kN}$$

Therefore, the block shear governs the tensile limit state.

For middle brace connection, the seismic assessment procedures are the same as the corner brace connection.

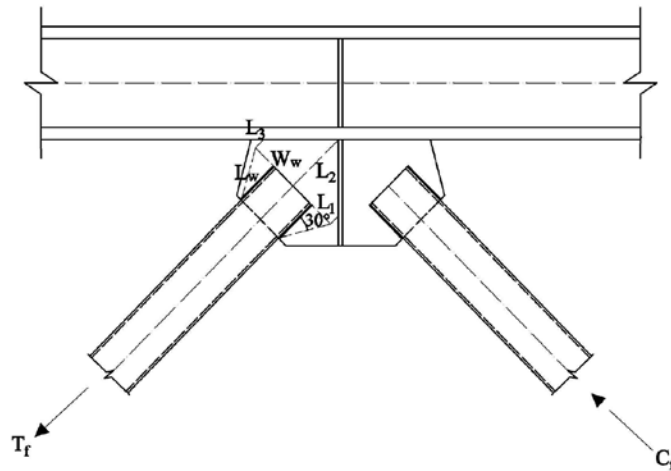


Figure 4.11: Middle brace to frame connection (2010 design)

The seismic assessment of brace to frame connections is summarized in Table 4.5a and Table 4.5b for the 3- and 6-storey building in the E-W direction and in Table 4.6a and Table 4.6b for brace connections of the 3- and 6-storey building when loading is applied in the N-S direction.

In general, for all case studied failure occurs due to the shear failure of welding followed by the tensile resistance of metal base. Braces of the lower two floors of the 3-storey building (E-W and N-S) and the lower three floors of the 6-storey building (E-W) cannot reach buckling because the gusset plate buckling occurs first. The yielding resistance of gusset plate and the resistance of block shear are almost equal at the 2<sup>nd</sup> floor of the 3-storey building (E-

W), at the 5<sup>th</sup> and 3<sup>rd</sup> floor of the 6-storey building (E-W) and at the 1<sup>st</sup> floor of the 6-storey building (N-S). It is noted that larger tensile force demand exists in braces of diagonal tension/compression braces than in chevron braces. In this regard, the risk of brace to frame connections that are controlled by the tensile force is higher in the case of diagonal tension/compression brace than in the case of chevron brace. In the case of chevron brace connections, the beam to which the braces are attached and the brace to beam gusset plate connection should have the strength to sustain the development of brace buckling and yielding forces.

The brace-to frame connections of the 3-storey building show a high risk because the demand in connections due to the development of  $T_u$  in braces is much larger than the connections strength. In addition, as per Table 4.3a and Table 4.4a braces of the 3-storey building are under designed by about 30%.

Therefore, all brace-to-frame connections should be re-designed and re-placed in order to provide the  $2t_g$  clearance, sufficient welds to carry the brace capacity, as well as sufficient strength to sustain brace buckling and yielding.

Table 4.5a: Seismic assessment of brace connection (3-st, W-E) (unit: kN)

St	Shear Resistance of Welding			Tensile Resistance of Metal Base		Yielding of Gusset Plate		Buckling of Gusset Plate		Net Rupture and block shear of brace with shear lag		
	$V_r$	$C_u/V_r$	$T_u/V_r$	$T_{rMB}$	$T_u/T_{rMB}$	$T_{rGP}$	$T_u/T_{rGP}$	$C_{rGP}$	$C_u/C_{rGP}$	$T_{u-NR}$	$T_{r-BS}$	$T_u/\min(T_{u-NR}, T_{r-BS})$
3	390	1.05	2.74	410	2.61	557	1.92	550	0.74	683	454	2.36
2	390	1.18	3.19	410	3.03	557	2.24	550	1.05	824	544	2.29
1	390	1.58	3.52	410	3.35	622	2.21	619	1.22	654	454	3.03

Table 4.5b: Seismic assessment of brace connection (6-st, W-E) (unit: kN)

St	Shear Resistance of Welding			Tensile Resistance of Metal Base		Yielding of Gusset Plate		Buckling of Gusset Plate		Net Rupture and block shear of brace with shear lag		
	$V_r$	$C_u/V_r$	$T_u/V_r$	$T_{rMB}$	$T_u/T_{rMB}$	$T_{rGP}$	$T_u/T_{rGP}$	$C_{rGP}$	$C_u/C_{rGP}$	$T_{u-NR}$	$T_{r-BS}$	$T_u/\min(T_{u-NR}, T_{r-BS})$
6	390	1.05	2.74	410	2.61	557	1.92	550	0.74	683	454	2.36
5	390	1.18	3.19	410	3.03	557	2.24	550	0.84	824	544	2.29
4	439	1.40	2.56	462	2.43	652	1.72	641	0.96	575	408	2.75
3	536	1.59	3.00	564	2.85	711	2.26	698	1.22	1038	748	2.15
2	634	1.36	2.54	667	2.41	770	2.09	754	1.15	1140	884	1.82
1	731	1.55	2.70	770	2.57	894	2.21	887	1.28	1296	1020	1.94

Table 4.6a: Seismic assessment of brace connection (3-st, N-S) (unit: kN)

St	Shear Resistance of Welding			Tensile Resistance of Metal Base		Yielding of Gusset Plate		Buckling of Gusset Plate		Net Rupture and block shear of brace with shear lag		
	$V_r$	$C_u/V_r$	$T_u/V_r$	$T_{rMB}$	$T_u/T_{rMB}$	$T_{rGP}$	$T_u/T_{rGP}$	$C_{rGP}$	$C_u/C_{rGP}$	$T_{u-NR}$	$T_{r-BS}$	$T_u/\min(T_{u-NR}, T_{r-BS})$
3	390	0.78	3.52	410	3.35	622	2.21	526	0.78	654	454	3.03
2	390	1.54	5.07	410	4.82	687	2.88	563	1.24	784	544	3.63
1	488	1.72	4.81	513	4.57	811	2.89	708	1.28	941	680	3.45

Table 4.6b: Seismic assessment of brace connection (6-st, N-S) (unit: kN)

St	Shear Resistance of Welding			Tensile Resistance of Metal Base		Yielding of Gusset Plate		Buckling of Gusset Plate		Net Rupture and block shear of brace with shear lag		
	$V_r$	$C_u/V_r$	$T_u/V_r$	$T_{rMB}$	$T_u/T_{rMB}$	$T_{rGP}$	$T_u/T_{rGP}$	$C_{rGP}$	$C_u/C_{rGP}$	$T_{u-NR}$	$T_{r-BS}$	$T_u/\min(T_{u-NR}, T_{r-BS})$
6	390	0.78	3.52	410	3.35	622	2.21	526	0.58	654	454	3.03
5	390	1.34	4.31	410	4.10	687	2.45	563	0.93	654	454	3.70
4	536	1.76	4.37	754	3.11	1124	2.09	974	0.97	1019	748	3.13
3	683	1.59	3.95	960	2.81	1243	2.17	1045	1.04	1465	1112	2.42
2	780	1.56	3.88	1374	2.20	1656	1.83	1479	0.82	1941	1450	2.09
1	926	1.52	3.37	1303	2.40	1528	2.04	1343	1.05	1905	1509	2.07

### ***4.3 Results from Non-Linear Dynamic Analysis***

Non-linear time-history analysis was conducted in the OpenSees environment. A numerical 2D model with the option for braces to deform out-of-plane as per a 3-D model was built in order to study the response of CBFs in the non-linear range. Due to the building symmetry, the structural system in the N-S direction was developed for half of the building and in the E-W direction for  $\frac{1}{4}$  of building. The OpenSees model is explained in the part 4.3.1, the selection of ground motions in 4.3.2 and the applied incremental dynamic analysis in the part 4.3.3. To observe the behaviour of CBFs under free vibrations and to record the residual interstorey drift, the accelerograms were elongated by 5.0 s of zero acceleration amplitude. To compute the IDA curves, the selected ground motions were incremented with a step of 0.05g until failure was reached. Then the fragility of the structural system designed according to 1980 codes was studied in Chapter 5.

#### ***4.3.1 OpenSees modelling***

The OpenSees model is shown in Figure 4.12a for the CBF in the E-W direction and in Figure 4.12b for the CBF in the N-S direction. As illustrated, the tributary leaning columns were added to the model in order to account for the real stiffness, to consider the afferent gravity loads and to account on the  $P-\Delta$  effects. These columns are connected at each floor by rigid link beams in order to simulate the rigid diaphragm effect. As mentioned in Chapter 3, all beams are pin connected to the column by means of shear-tab connections. Additionally, columns of the 6-storey building as well as the leaning columns are continuous over two storey, while those of the 3-storey are pin connected at each floor. Braces, beams and columns were modelled as non-linear force-based beam-column elements with distributed plasticity. The leaning columns, link beams and all rigid link segments described below were modeled with elastic beam-column elements. Brace connections and beam-column connections were modeled as Zero-Length element. The seismic mass was applied to the node of each CBF column and the associated lumped gravity load was applied to each column including the leaning columns and to the beams of CBFs.

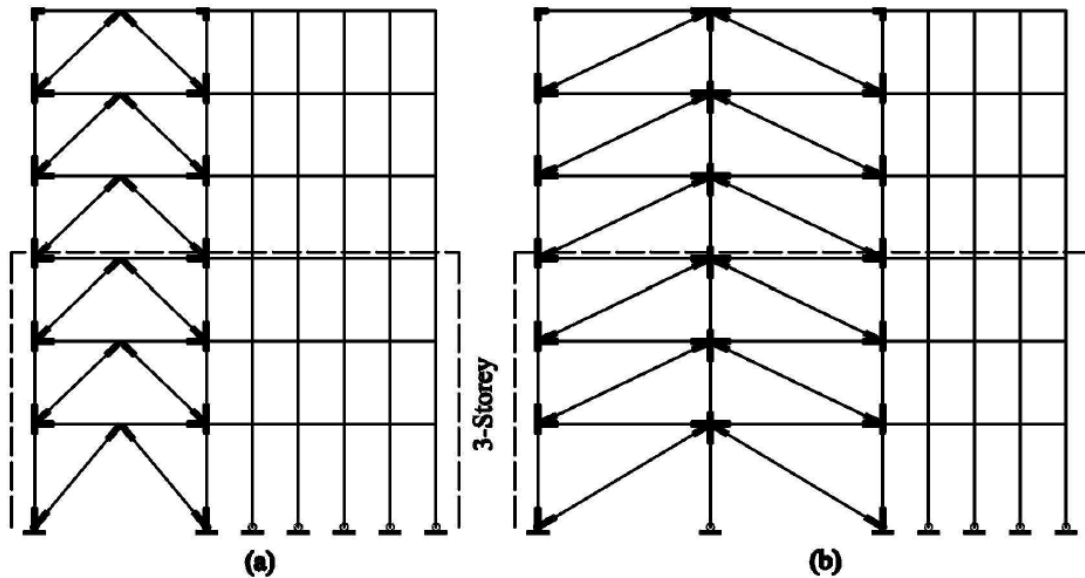


Figure 4.12: OpenSees model of the 3- and 6-storey CBF together with their tributary leaning columns a) E-W direction and b) N-S direction

To explain the OpenSees model more in detail, a single storey, single bay chevron braced frame is shown in Figure 4.13. As mentioned above, all braces were modelled as nonlinear force-based beam-column elements with distributed plasticity. As per Hsiao et al. (2013) recommendation, each brace member is made of 16 elements ( $n_e = 16$ ) with 3 integration points per element and fiber cross-section formulation. To simulate the out-of-plan buckling of HSS braces, a quadratic out-of-plan imperfection of  $L_{br}/500$  was assigned.

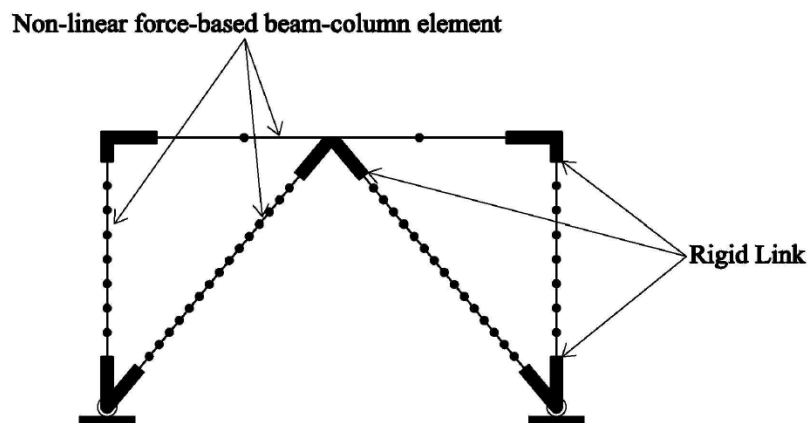


Figure 4.13: Model of one bay and one storey chevron braced frame

The uniaxial Giuffr -Menegotto-Pinto steel material known as Steel02 was assigned to braces. To simulate the failure of braces by fracture due to low-cycle fatigue, the fatigue material developed in OpenSees was wrapped to the Steel02 material. Parameters used to define the fatigue material were calculated using Equation (2.40).

The cross-section of each element was discretized in fibers as illustrated in Figure 4.14a, whereas the round corners of the rectangular HSS cross-section were modelled with circular fibers. As shown in the figure, there are 40 fibers used for each web and flange of HSS and 20 circular fibers used for each rounded corner.

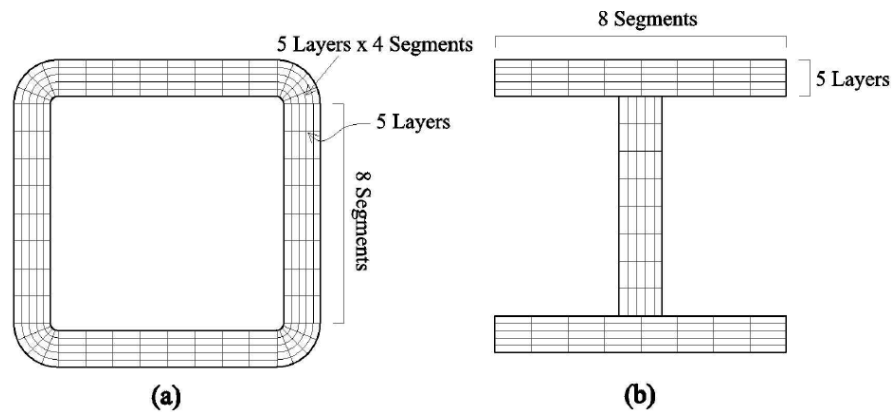


Figure 4.14: Fiber cross-section discretization a) HSS and b) W-shape

Columns were built up with 8 nonlinear force-based beam-column elements with distributed plasticity and beams were built up with 4 nonlinear force-based beam-column elements. Similar with HSS cross-section modelling, all the W-sections used for columns and beams were discretized using fiber cross-section formulation. There are 40 fibers used for the web and 40 fibers used for each flange, as shown in Figure 4.14b. The initial out-of-straightness for columns was considered 1/1000 of the effective length of columns.

Columns and beams were also modelled with the uniaxial Giuffr -Menegotto-Pinto (Steel02) steel material to produce the nonlinear material response. It is noted that Bauschinger effect and the residual stresses can be well accounted by using the Steel02 material (Lamarche and Tremblay, 2008). Parameters to define Steel02 material are the same as those used in Agüero et al. (2007).

The beam-column connections were modelled as shear-tab connections. In the model, one rotational spring was added in the zero-length element in the plan of beam bending. This rotational spring was designed to transfer up to 20% of the plastic bending capacity of the beam to the rigid link as shown in Figure 4.13 (Liu and Astanah-Asl, 2004).

Regarding the brace connections, these were modelled by defining two rotational springs and one torsional spring in the Zero-length element (Uriz and Mahin, 2008). The first rotational spring is assigned to behave out-of-plan while the rotational stiffness is calculated according to Hsiao et al. (2012) proposal given in Figure 4.15.

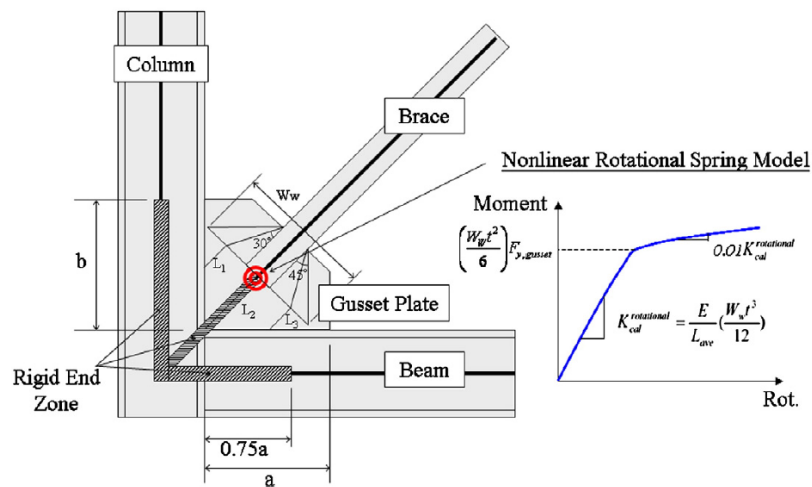


Figure 4.15: Brace to frame connection model (Hsiao et al., 2012)

The second rotational spring was assigned to control the in-plan buckling. However, its rotational stiffness was assigned larger than that of the brace. The torsional spring was assigned to prevent torsion of brace. All rotational springs were made of Steel02 material and the torsional spring was made of elastic material.

The MinMax material given in OpenSees is defined in term of stress-strain or force-displacement and was assigned to Steel02 material which controls the behavior of gusset plates. As explained before, shearing of welds is the controlling failure mode of brace-to-frame connections. When the axial elongation of gusset plate corresponding to the maximum capacity of connection occurs, or in other words, the axial deformation of gusset plate falls below or above the pre-defined threshold value, the MinMax material turns the stress to zero and the

gusset plate is decoupled from the CBF. In the case of a strong gusset plate, the failure occurs at the level of braces. Brace fracture failure due to low-cycle fatigue is the desirable failure mode (Hsiao et al., 2012). When braces fail due to low-cycle fatigue, stresses in that extreme fibers turn to zero and brace is not able to sustain further loading.

### 4.3.2 *Ground motion selection*

Seismic events registered in Eastern Canada occur at depths varying from surface to 30 km and are mainly concentrated in specific clusters defined as Western Quebec zone, Charlevoix zone, etc. (Atkinson, 2009). According to Earthquake Canada (2011), the pattern of recorded events shows concentrations along the Maniwaki – Montreal axis and the St- Laurent River axis. Thus, the urban area of Montreal, Ottawa-Hull, and Quebec, characterized by larger population density and vulnerable building stock is exposed to high seismic risk. Statically, in Eastern Canada, about three seismic events above magnitude 5 were recorded over a ten-year period (Adams and Atkinson, 2003).

For Eastern Canada, the contributions to hazard are moderate crustal earthquakes of magnitudes  $M_6 - M_7$ , which are compatible with the NBCC 2010 uniform hazard spectrum (*UHS*) developed for 2% probability of exceedance in 50 years (Atkinson, 2009), as shown in Table 4.8. In this study, the crustal ensemble is composed of 10 records given in Table 4.7. Among them, seven are simulated records selected from ground motion database provided by Atkinson ([www.seismotoolbox.ca](http://www.seismotoolbox.ca)) and three are historical records (Saguenay 1988). The value of peak ground velocity, *PHV*, peak ground acceleration, *PHA*, the Trifunac duration,  $t_D$ , the main and average period of ground motion  $T_p$  and  $T_m$ , respectively, are given in Table 4.7 together with ratio *PHV/PHA*. According to the NBCC 2010 provisions, all ground motions must be scaled to match the code design spectrum ordinate at the fundamental period of the building,  $S(T_1)$ , and to be equal to or be above the code design spectrum at all points corresponding to the period of higher modes. Alternatively, according to ASCE/SEI-7, ground motions must be scaled such that the mean of the 5% damped response spectra of a minimum of seven ground motions to match or be above the code design spectrum in any point over the interval  $0.2T_1 - 1.5T_1$ . The acceleration response spectrum of the scaled ground motions are

plotted against the code design spectrum in Figure 4.16. As illustrated, slightly larger scale factors are required to fit the design spectrum over the interval  $0.2T_l - 1.5T_l$ , when  $T_l$  of the 6-storey building is 1.1s. For scaling ground motions, the methodology proposed by Reyes and Kalkan (2011) was employed.

Table 4.7: Seismic ground motions

Event	$M_w$	Station	R	Comp	PHV	PHA	PHV/ PHA	$t_D$	$T_p$	$T_m$
			(km)	(°)	(cm/s)	(cm/s <sup>2</sup> )	(s)	(s)	(s)	(s)
M6C1-10.7	6.0	simulated	10.7	-	18.93	547.0	0.035	2.39	0.06	0.20
M6C1-12.8	6.0	simulated	12.8	-	30.58	753.0	0.041	1.29	0.12	0.19
M6C1-16.6	6.0	simulated	16.6	-	17.43	429.0	0.041	1.95	0.12	0.23
M7C1-20.1	7.0	simulated	20.1	-	22.39	467.0	0.048	6.81	0.12	0.26
M7C1-25.2	7.0	simulated	25.2	-	18.65	379.0	0.049	7.32	0.06	0.24
M7C1-25.8	7.0	simulated	25.8	-	17.56	288.0	0.061	7.31	0.08	0.28
M7C2-41.6	7.0	simulated	41.6	-	14.49	224.0	0.065	7.61	0.14	0.31
Saguenay	5.8	La Malbaie		63	4.37	126.8	0.034	10.5	0.12	0.19
Saguenay	5.8	St-Pascal		0	2.61	45.7	0.057	21.5	0.14	0.23
Saguenay	5.8	Riviere-Quelle		270	3.83	56.3	0.068	12.5	0.14	0.27

Because this study employs the performance-based design method that is presented in Chapter 5, the *UHS* computed for the following hazard levels: 2%/ 50 yrs., 10%/ 50 yrs. and 50%/50 yrs. is required. The *UHS* computed for Montreal for different hazard levels is given in Table 4.8 It is noted that the *UHS* corresponding to 5%/50 yrs., 10%/50 yrs., and 50%/50 yrs. was derived from that provided for 2%/50 yrs. probability of exceedance. Herein, the *UHS* corresponding to 5%/50 yrs. probability of exceedance was provided for comparison purposes.

Table 4.8: Uniform hazard spectrum (*UHS*) computed for different hazard level

Hazard Level	Sa(0.2)	Sa(0.5)	Sa(1.0)	Sa(2.0)
2%/50 yr.	0.641	0.313	0.137	0.047
5%/50 yr.	0.389	0.191	0.087	0.029
10%/ 50 yr.	0.251	0.124	0.057	0.019
50%/ 50 yr.	0.072	0.035	0.014	0.005

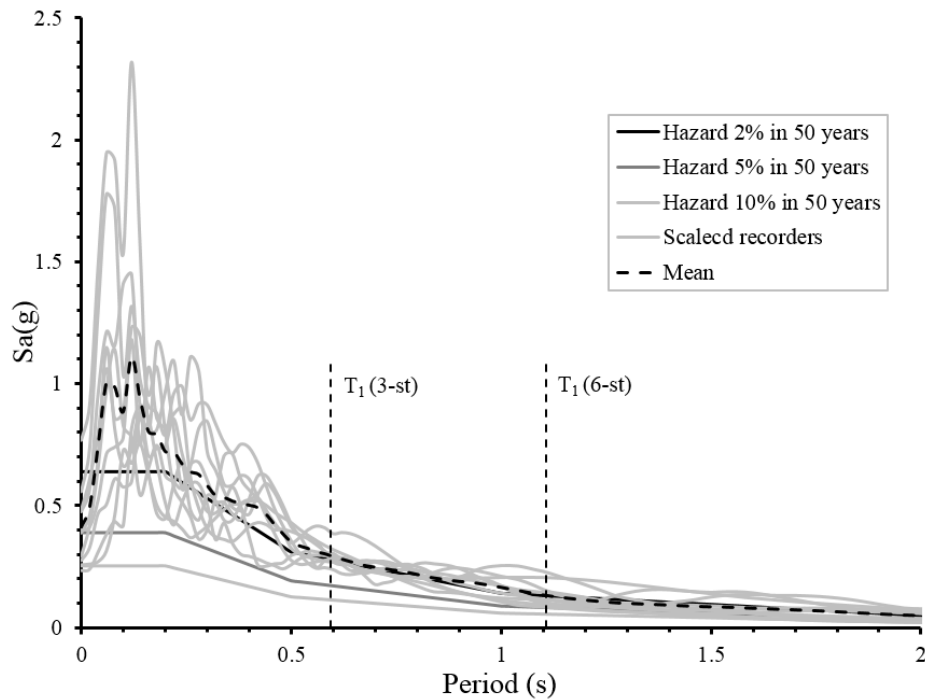


Figure 4.16: Response spectrum of scaled ground motions

### 4.3.3 Results from OpenSees

The selected ground motions were scaled as explained above and the nonlinear time-history dynamic analysis was conducted using OpenSees. The fundamental building period of first two modes  $T_1$  and  $T_2$  resulted from OpenSees is summarized in Table 4.9 together with the  $S_a(T_1)$  value. For comparison purpose, the fundamental building period obtained from the equivalent static force procedure ( $2T_{1,emp}$ ) and the associated  $S_a(2T_{1,emp})$  value is also provided.

Table 4.9: Dynamic properties of buildings

Building	$T_1$	$T_2$	$S_a(T_1)$	$2T_{1,emp}$	$S_a(2T_{1,emp})$	$T_{1,dyn}$	$S_a(T_{1,dyn})$
	(s)	(s)	(g)	(s)	(g)	(s)	(g)
	OpenSees		Equivalent static force method		ETABS		
3-st E-W	0.611	0.225	0.273	0.585	0.281	0.594	0.278
3-st N-S	0.727	0.269	0.233	0.585	0.281	0.619	0.270
6-st E-W	1.060	0.377	0.135	1.125	0.129	1.107	0.130
6-st N-S	1.243	0.454	0.118	1.125	0.129	1.075	0.133

The fundamental period  $T_1$  resulted from the OpenSees model analysed in the E-W

direction (see Table 4.9) is almost the same with that resulted from the ETABS model ( $T_{1, dyn}$ ). However, in the N-S direction there is a 10% difference in both 3- and 6-storey building.

To capture the failure of the studied buildings, both the 3- and 6-storey buildings in the E-W and N-S direction were subjected to the incremental dynamic analysis.

#### **4.3.4 Incremental dynamic analysis using OpenSees**

To assess the failure of existing braced frames, the Incremental Dynamic Analysis (*IDA*) method was employed. In this light, pairs of the maximum inter-storey drift among floors express as  $\%h_s$  and the corresponding 5% damped spectral response acceleration  $S_a(T_{1, dyn}, 5\%)$  corresponding to  $T_1$  is given in Figure 4.17. For each seismic ground motion incremented in 0.05g steps, pairs of points ( $\%h_s; S_a(T_1, 5\%)$ ) were computed and plotted. The ensemble of these points forms the IDA curve of a given ground motion. The collapse prevention or damage-tolerate limit state was defined when the slope of the IDA curve becomes equal to or less than 20% of the initial (elastic) slope. The 20% slope approach was proposed by Vamvatsikos and Cornell (2002) and adopted by FEMA-350 (2000). Further, it indicates the formation of storey mechanism because large maximum interstorey drift results for small increase of the intensity measure parameter. When there are not convergence problems, the flattening of the end segment of IDA curve it results.

All ten IDA curves computed for the 3-storey and 6-storey pre-retrofit CBF building subjected to earthquake loading in the E-W and N-S direction are illustrated in Figure 4.17a-b and Figure 4.18a-b, respectively. The variation between IDA curves reflects the differences between seismic ground motions.

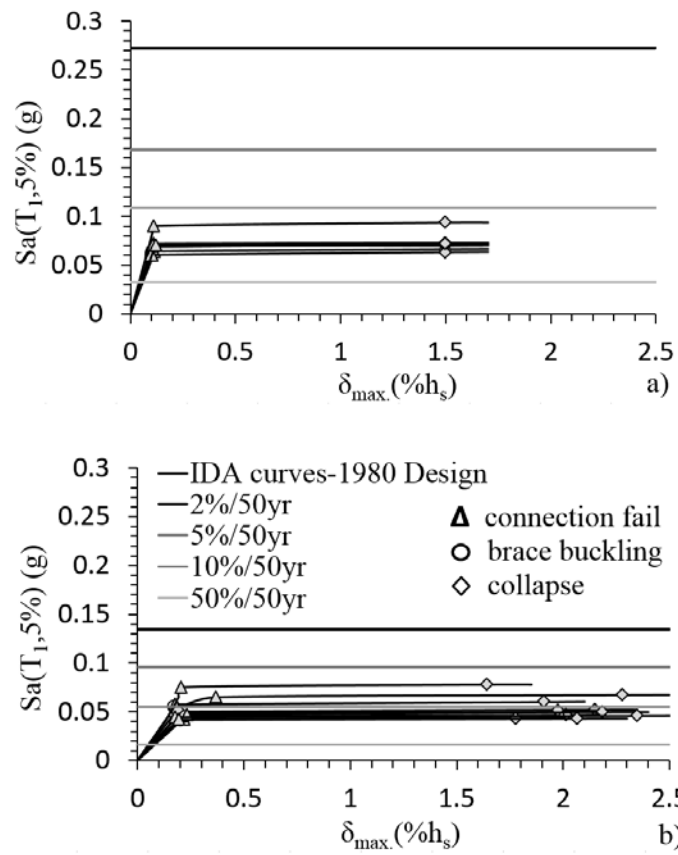


Figure 4.17: IDA curves: a) 3-Storey, W-E direction; b) 6-Storey, W-E direction

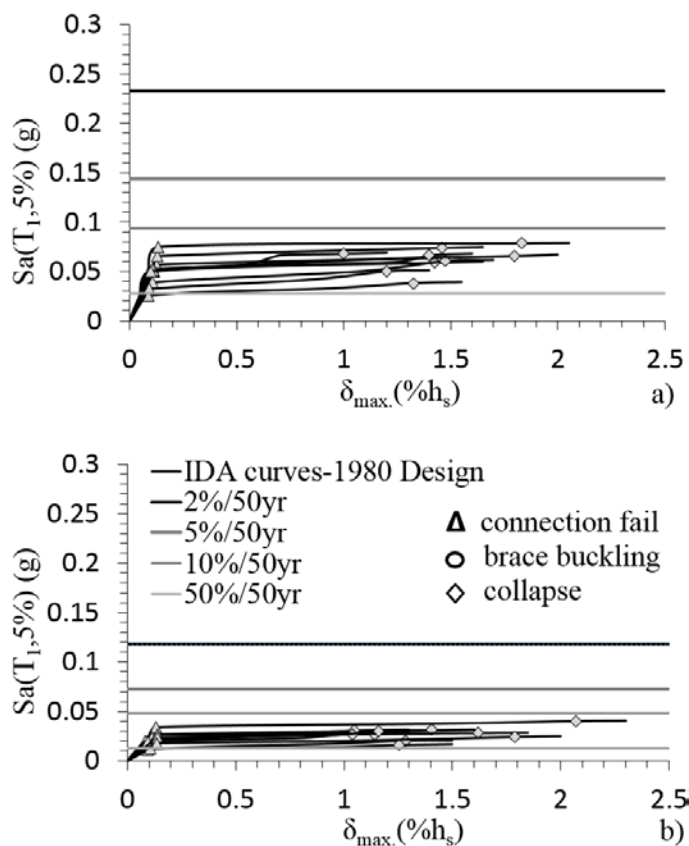


Figure 4.18: IDA curves: a) 3-Storey, N-S direction; b) 6-Storey, N-S direction

The seismic demand corresponding to the fundamental building period,  $S_a(T_1)$  computed for different hazard levels is given in Table 4.10.

Table 4.10: Seismic demand on each hazard level

Hazard Level	3-st E-W	6-st E-W	3-st N-S	6-st N-S
	$S_a(T_1)$	$S_a(T_1)$	$S_a(T_1)$	$S_a(T_1)$
2%/50 years	0.292	0.155	0.252	0.129
5%/50 years	0.180	0.096	0.155	0.080
10%/50 years	0.117	0.063	0.101	0.052
50%/50 years	0.033	0.016	0.028	0.013

The response of the studied buildings when subjected to the records given in Table 4.7 is discussed below. Thus, a captured image of the 3-storey building response under record M6C1-10.7 is illustrated in Figure 4.19a-b and that of the 6-storey CBF subjected to record S8EN1 in Figure 4.19c-d. As resulted, in these cases, the higher demand occurs at the ground

floor level.

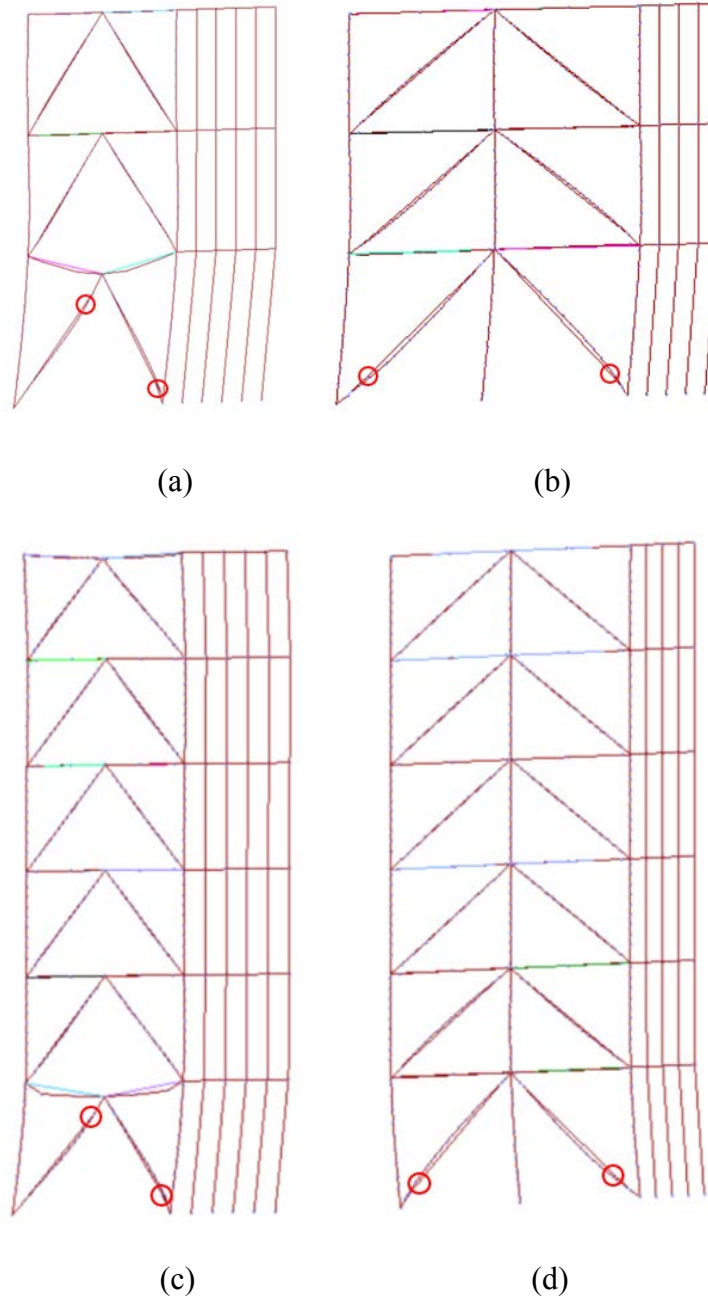


Figure 4.19: Seismic response of CBFs: a) 3-storey building (E-W) under recorder M6C1-10.7; b) 3-storey building (E-W) under recorder M6C1-10.7; c) 6-storey building under recorder S8EN1; d) 6-storey building under recorder S8EN1

The collapse margin ratio (*CMR*) defined in FEMA P695 (2009) as the ratio between

the ground motion intensity at which the median collapse capacity is reached and the acceleration spectrum intensity corresponding to the fundamental period of the building. The *CMR* is a consistent parameter which is able to quantify the collapse safety of building structures. The median collapse capacity of the ten collapse points,  $S_{MC}$ , and the collapse margin ratio, *CMR*, are given in Table 4.11. In addition, the median value of the ten points characterised by failure of connections that characterises the damage state  $S_{MD}$  and the ratio between the ground motion intensity at which the median damage state is reached and the acceleration spectrum intensity corresponding to the fundamental period of the building, *DMR* is also given. Herein *DMR* means damage margin ratio.

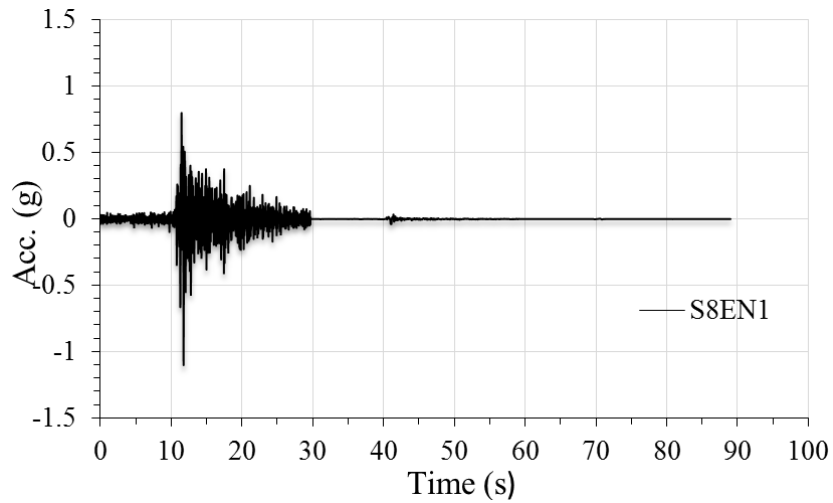
Table 4.11: Collapse margin ratio

Building ID	Connection failure		Building collapse	
	$S_{MC}$	CMR	$S_{MC}$	CMR
3WE	0.070	0.259	0.072	0.266
3NS	0.050	0.213	0.062	0.268
6WE	0.052	0.385	0.054	0.399
6NS	0.021	0.182	0.027	0.233

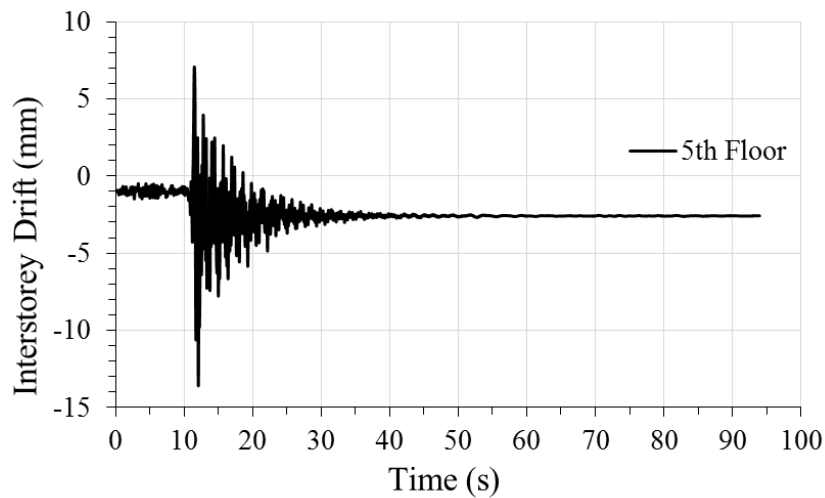
The collapse margin ratio (*CMR*) is the primary parameter used to characterize the collapse safety of the structure. For a ratio smaller than 1.0, the building strength should be increased (FEMA P695).

#### 4.3.5 Time-history seismic response of CBF structures

The seismic response of 6-storey chevron braced frame subjected to the Saguenay ground motion (S8EN1) which is given in Table 4.7 is presented below. The accelerogram is illustrated in Figure 4.20a, and the time-history interstorey drift recorded at the 5<sup>th</sup> floor is plotted in Figure 4.20b. The peak ground floor acceleration occurs at  $t = 11.7s$  and the maximum interstorey drift that occurred at the 5-th floor was reached at  $t = 11.8s$ .



(a)



(b)

Figure 4.20: The 6-st. (E-W) response under the record S8EN1: a) ground motion accelerogram; b) interstorey drift at the 5<sup>th</sup> floor

As resulted from the IDA curve plotted in Figure 4.17 and Figure 4.18 the CBF building designed in 1980 is not able to sustain the current seismic demand. However, to understand the seismic response, it was assumed that failure of connections occurs later on due to the buckling of gusset plate which is the second possible failure mode after the shearing of fillet welds (see Table 4.5b). The captured 2D picture of the deflected shape of the 6-storey

building (E-W) extracted from OpenSees is shown in Figure 4.21. Under the S8EN1 ground motion, the left side brace of the 5<sup>th</sup> floor buckles first at  $t = 4.6\text{s}$  because its compression strength is lower than that of its attached gusset plate. At  $t = 5.28\text{s}$ , the right side brace of the 4<sup>th</sup> floor reached buckling. Because of the reduced stiffness of the 5<sup>th</sup> floor, large forces were triggered in the top floor braces that subjected the top beam of the CBF to hinge at its mid-span and the failure of connections was encountered at  $t = 11.72\text{s}$  and  $11.92\text{s}$ , respectively. Then, due to large deformation, the column at the 5<sup>th</sup> floor was subjected to partial collapse ( $t = 11.97\text{s}$ ) due to the development of large axial forces and bending moment. As beam-column connection was modelled as shear tab connection that allows the transfer of bending moment equals to 20% of beam plastic moment resistance. This amount of moment effect was considered when checking the column buckling. Columns were considered to act in bending and compression. Step by step behaviour of the 6-storey CBF (E-W) under the S8EN1 record is given in Table 4.12. As resulted, after the peak ground acceleration was reached, the building was damaged. The spectral acceleration intensity was  $Sa(T_1) = 0.04g$  which was less than  $0.155g$  corresponding to 2%/50 yrs.

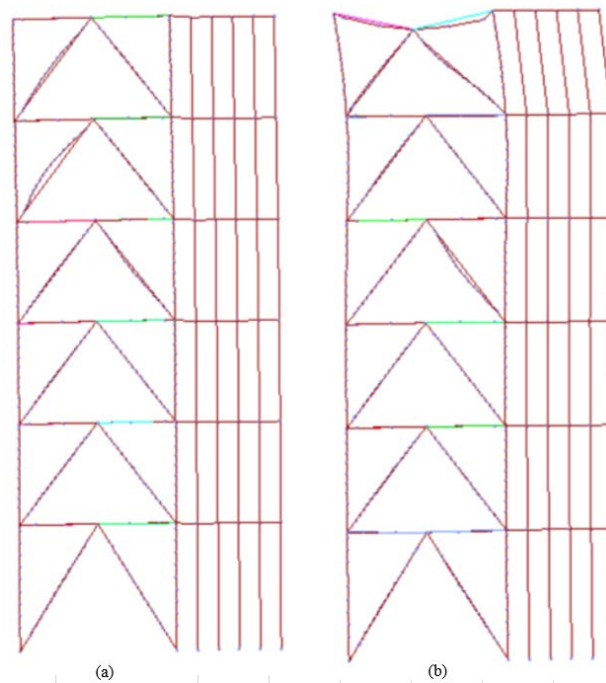


Figure 4.21: 2D view of deformed braced frame under S8EN1 record: a) first brace buckling ( $t = 4.6\text{s}$ ); b) first gusset plate failure because beam hinging ( $t = 11.72\text{s}$ )

Table 4.12: Step by step behaviour of the 6-storey CBF (E-W) under the S8EN1 record

Time (s)	Event	Location	Inter-storey Drift Ratio (IDR)					
			GF	2F	3F	4F	5F	6F
4.6	First Brace Buckling	5F-Left	0.01	0.01	0.02	0.02	0.03	0.03
5.28	Second Brace Buckling	4F-Right	0.00	0.01	0.02	0.02	0.03	0.02
11.475	First Beam Hinging	6F-Left	0.06	0.14	0.15	0.31	0.19	0.12
11.72	First GP failure	6F-top	0.08	0.08	0.14	0.18	0.29	0.26
11.92	Second GP failure	GF-bottom	0.17	0.12	0.02	0.11	0.10	1.57
11.975	Column Hinging (OMS)	5F-Right	0.27	0.02	0.06	0.03	0.06	1.82
11.975	Second Column Hinging	5F-Left	0.27	0.02	0.06	0.03	0.06	1.82

Figure 4.22 shows the hysteresis response of braces at each floor. It is noted that at the 5<sup>th</sup> floor, the brace cross-section is HSS 101.6x101.6x9.53 and the probable compression resistance is  $C_u = 1360$  kN. By considering the real length of brace, from OpenSees, the resulted probable compression resistance is 1133 kN.

Failure of beams and columns are defined based on the interaction of axial load and bending moment. As shown in Table 4.12, the columns at the fifth floor of the 6-storey CBF (E-W) reached buckling under the S8EN1 record. In order to better understand the seismic behaviour of the interested columns, the axial load and bending moment was recorded at each step of time and the boundary line that encloses the elasto-plastic zone corresponds to that proposed by Pillai (1974) and expressed in Equation (2.23). Hence, the axial load and bending moment of each column were picked up from the time-history analysis to calculate the interaction ratio. However, only the results from the 11s to 15 s are shown on Figure 4.23. For comparison, the pairs of  $M_f/M_{rx}$  and  $P_f/P_{ry}$  recorded at the ground floor column are also given in Figure 4.23.

Similar procedure can be applied to plot the axial force and bending moment developed in beams of CBFs. However, from this example, it can be seen that the development of partial failure of the upper two floors happened under the S8EN1 ground motion.

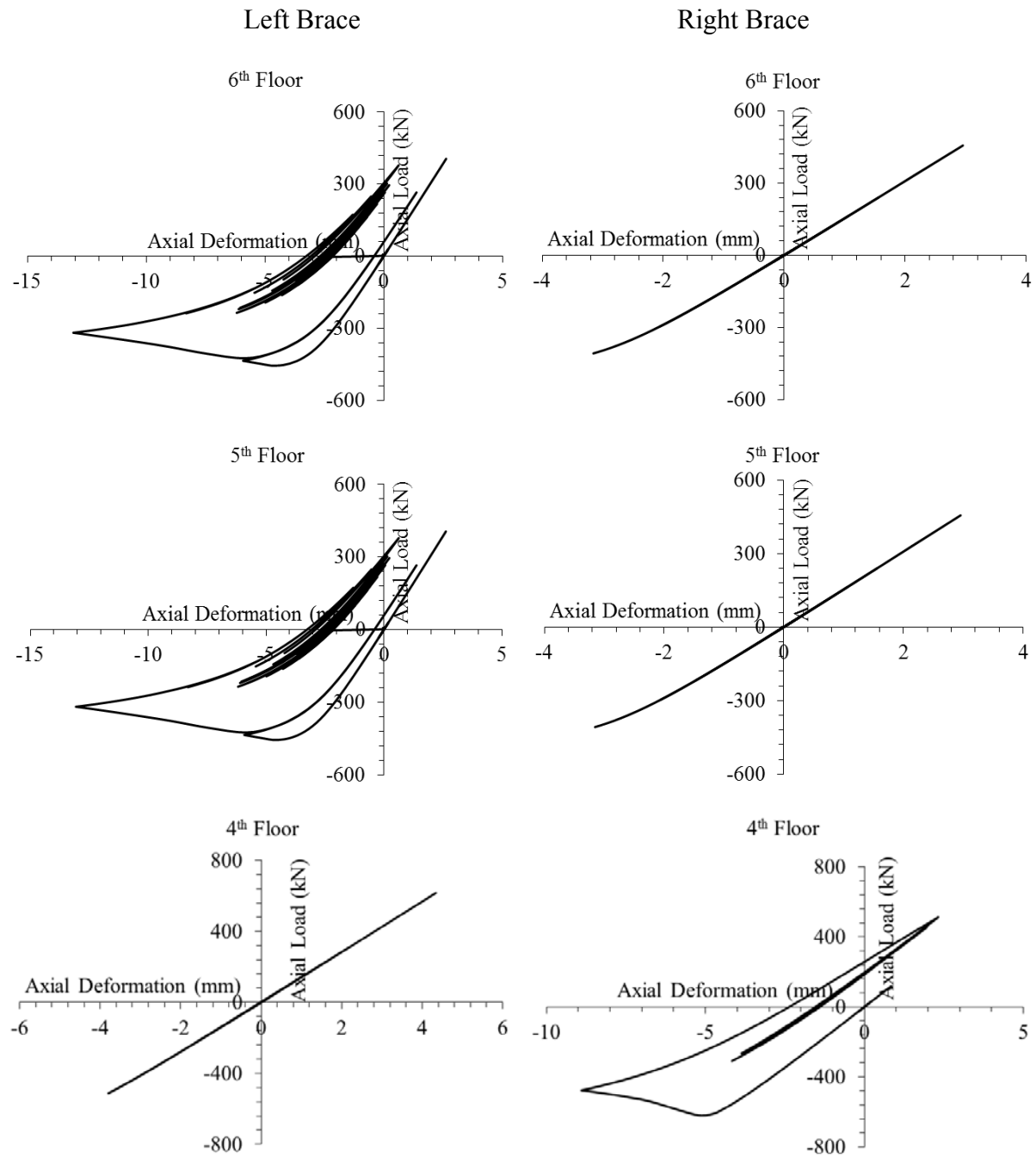


Figure 4.22a: Hysteresis loop of braces at each floor (4<sup>th</sup> Floor ~ 6<sup>th</sup> Floor)

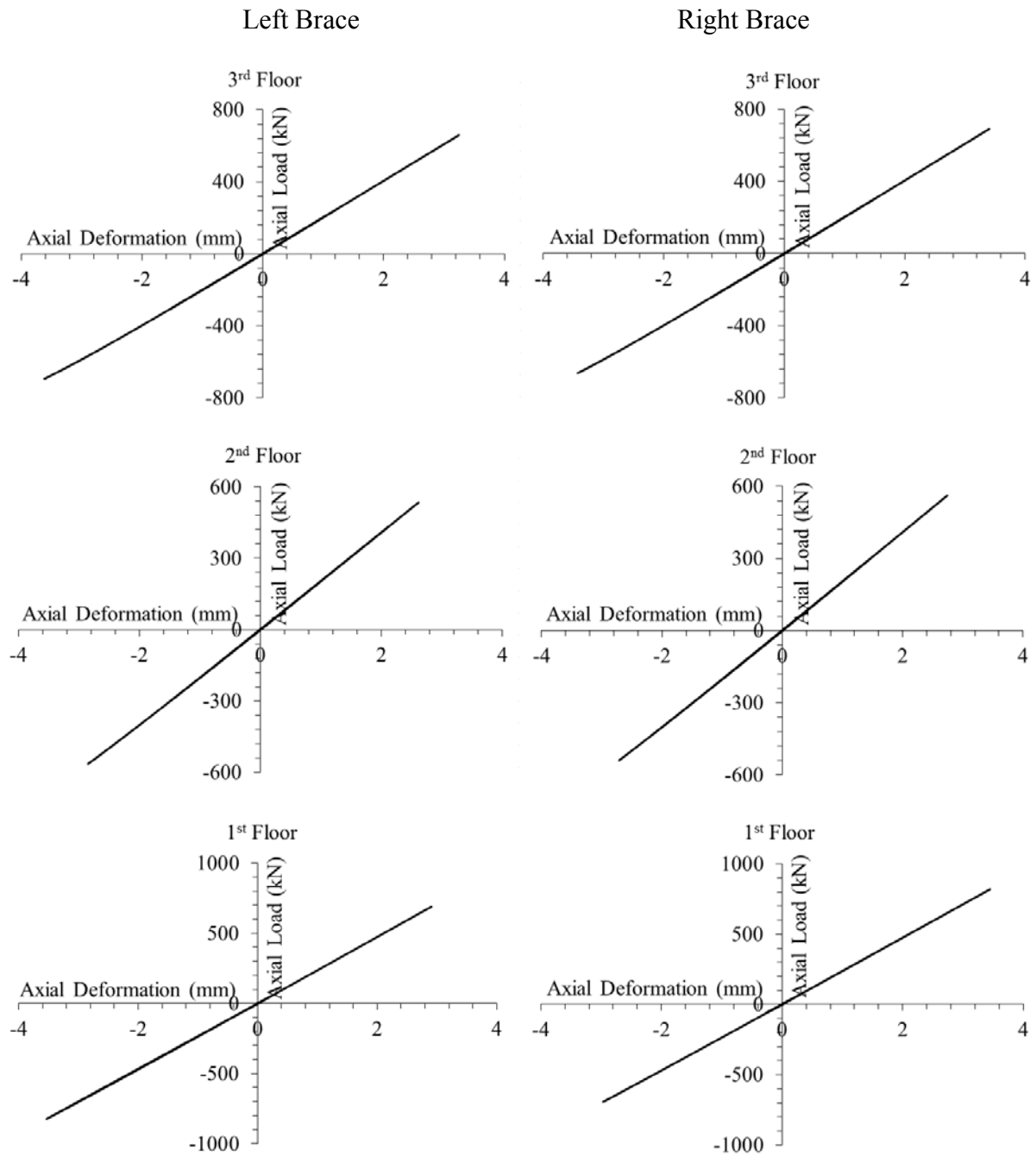


Figure 4.22b: Hysteresis loop of braces at each floor (1<sup>st</sup> Floor~3<sup>rd</sup> Floor)

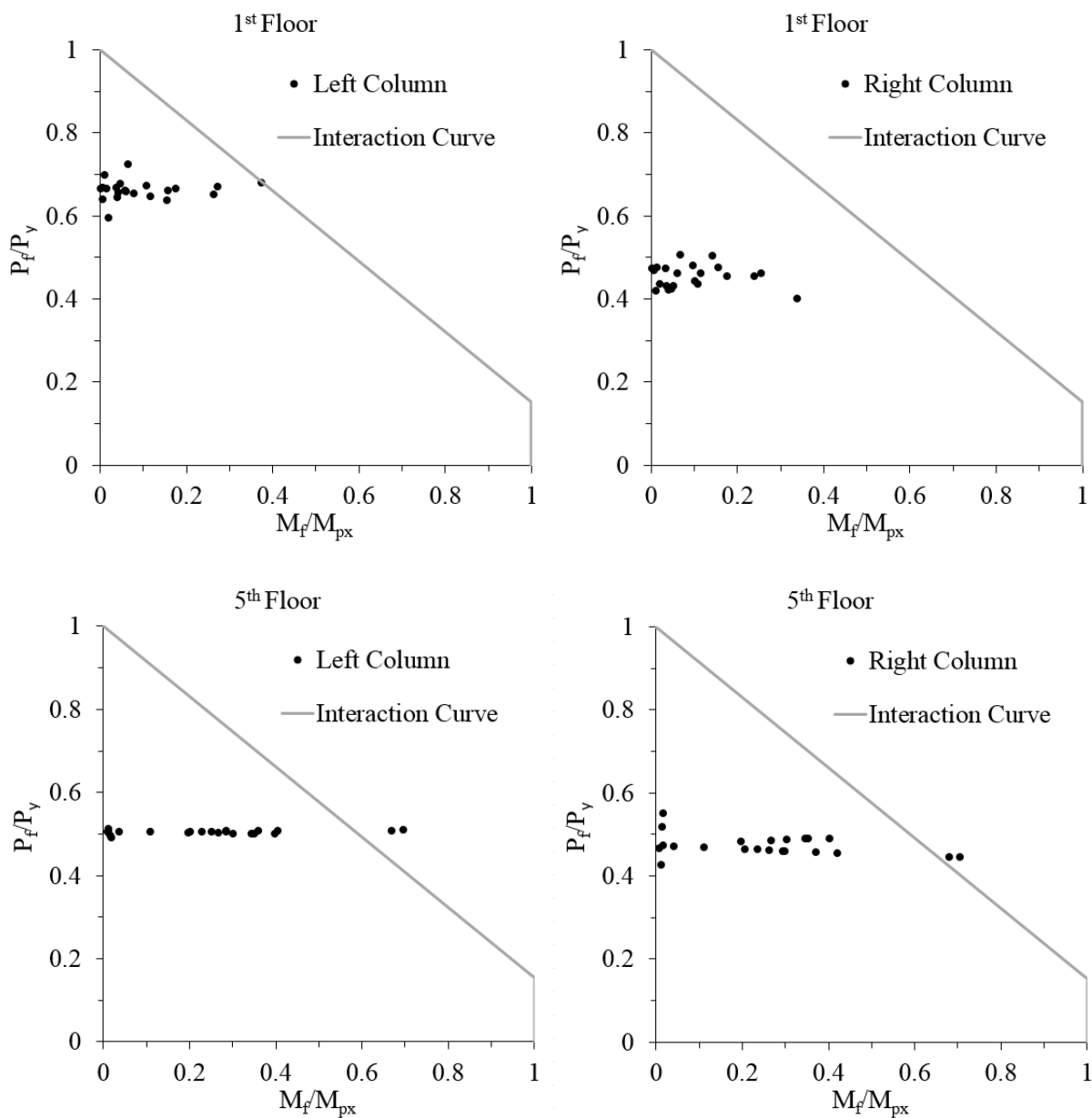


Figure 4.23: Axial load-bending moment interaction diagram of column of 6-st CBF (E-W) under the S8EN1 record

#### 4.4 Seismic Assessment Conclusion

As a result of the new seismic hazard map and revised equations for member design, the seismic design load and member forces have increased. From computation, all brace to frame

connections have insufficient strength and shown failure due to shearing of fillet welds before braces reach the probable compressive strength. As illustrated from IDA curves, all studied buildings experienced collapse when subjected to ground motion intensities in agreement with the current code demands and showed adequate strength when subjected to the seismic forces required by the 1980 code (50%/50 yrs. probability of exceedance).

## CHAPTER 5. FRAGILITY ASSESSMENT OF PRE- AND POST-RETROFIT BUILDING

### *5.1 Numerical Analysis of Post-Retrofit Buildings*

#### *5.1.1 Selection of Retrofit Scheme*

As shown in Chapter 4, the connections of brace to frame fail first and the beams of chevron CBF cannot sustain the forces transferred from braces in addition to bending moment resulted from the associated gravity component (*OMS*). In general, columns of chevron CBFs possess the required compression strength to carry the axial forces but the middle column of the 3- and 6-storey CBFs with tensile/ compressive diagonal braces (N-S) shows weakness in the compression strength. Therefore, the brace-to-frame connections have to be redesigned in order to carry the forces associated with the capacity of braces and re-detailed to allow the out-of-plan buckling of braces. Thus, in order to possess sufficient compression strength the size of the gusset plates has to increase, as well as the length of fillet welds. After these deficiencies were corrected the HSS brace was able to buckle and to dissipate the input energy. In the second step, beams were strengthened in order to carry the transferred forces from braces. In the 3<sup>rd</sup> step, the middle column of the 6-storey CBF (N-S) and the middle column of the 3-storey CBF (N-S) was strengthened, as well as other columns at the level of the critical floor.

To overcome these drawbacks a traditional retrofit technology consisting in adding steel cover plates to the flanges of W-section of the middle column and longitudinal steel plates at two sides of the web of W-shape beam cross section.

#### *5.1.2 Retrofitting of studied CBFs*

The re-detailed gusset plate with  $2tg$  clearance is showed in Figure 5.1 for corner brace connection and in Figure 5.2 for middle brace connection of chevron CBF.

The same verifications as those given in Chapter 4 were applied in order to re-design the brace-to-frame connections. First, the length of welds  $L_w$  was calculated such that the shear resistance of welding and tensile resistance of gusset plate to be larger than the probable tension

resistance of braces. In addition, it was verified that the failure mode of connection, if occurs, to be a ductile failure mode such as yielding of gusset or block shear. The length of welds,  $L_w$ , the  $D_w$  together with the thickness of gusset plate are given in Table 5.1 for the 3- and 6-storey CBF (E-W) and in Table 5.2 for the 3- and 6-storey CBF (N-S). Thus, for the same ground floor brace connection of the 6-storey CBF (E-W) the shear resistance of welds is:

$$V_r = 0.67\phi_w A_w X_u = \frac{0.67(0.67)(360)(0.707)(9.5)(490)}{1000} = 511 \text{ kN} > \left(\frac{1977}{4}\right) \text{ kN} \quad \text{OK.}$$

The tensile resistance of HSS brace due to block shear failure is checked according to the current code demand as per Equation (2.22) and the calculation is given below:

$$\begin{aligned} T_{rBS} &= \phi_u \left[ U_t A_n F_u + 0.6 A_{gv} \frac{(F_y + F_u)}{2} \right] \\ &= 0.75 \left[ (1.0)(0)(345) + (0.60)(13723) \frac{(345 + 448)}{2} \right] / 1000 = 2449 \text{ kN} \end{aligned}$$

The calculation of nominal capacity for tensile rupture in the net section of HSS brace with shear lag effect is conducted in the same way as in Chapter 4:

$$L_w = 380 \text{ mm} > 2b_{brace} = 2 \times 152.4 = 304.8 \text{ mm}$$

$$\text{So, the net area } A_{n2} = 4 \times 152.4 \times 9.53 = 5809 \text{ mm}^2$$

$$\text{The shear lag factor } U \text{ is calculated as } U = 1.1 - 0.105 = 0.995$$

Then the effective net area is modified as  $A_{ne} = A_{n2}U = 5809 \times 0.995 = 5780 \text{ mm}^2$  and nominal capacity for tensile rupture in the net section of HSS brace is:

$$T_u = 0.85\phi A_{ne} F_u = 0.85 \times 0.9 \times 5780 \times 448 / 1000 = 1982 \text{ kN}$$

$$> 1977 \text{ kN OK.}$$

Therefore, the tensile rupture with shear lag governs the tensile limit state.

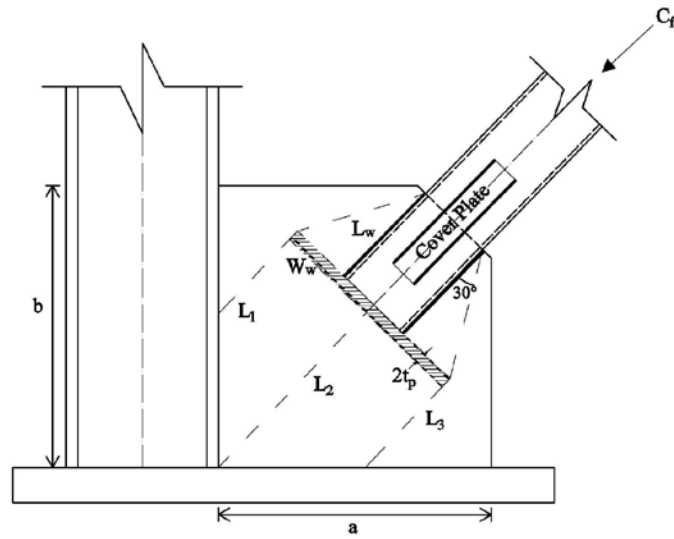


Figure 5.1: Detail of corner brace connection as per the current standard demand

For the middle brace connection, the vertical clearance equal to  $Nt_g$  was considered. Although the CSA/S16 – 09 standard required  $2t_g$  clearance, in this study, a value of  $N = 6$  that was recommended by Hsiao et al. (2012) was considered.

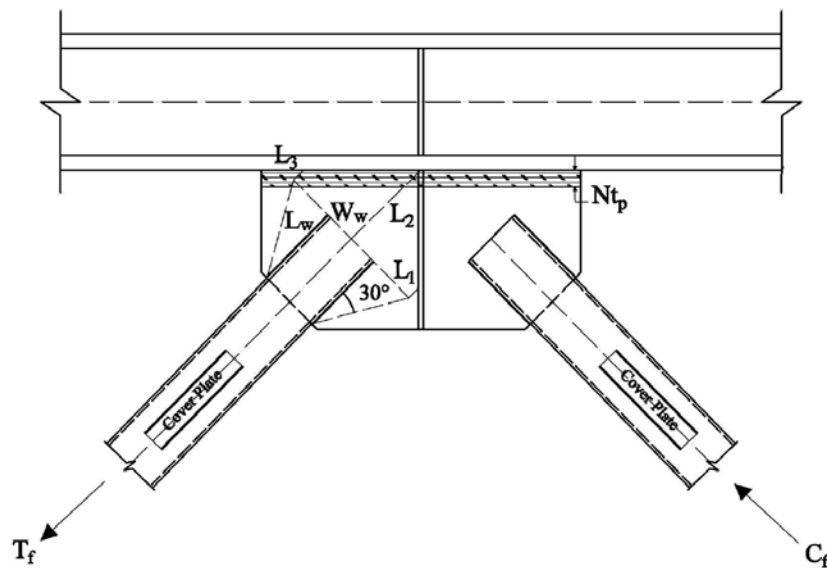


Figure 5.2: Detail of middle brace connection according to model recommended by Hsiao et al. (2012)

Table 5.1a: Re-designed brace connection (3-st, E-W), (unit: mm)

Storey	L <sub>w</sub>	D <sub>w</sub>	t <sub>gusset</sub>	W <sub>w</sub>	L1	L2	L3	a	b
3	260	8	12.7	416	125	325	158	451	469
2	250	9.5	12.7	405	121	316	153	438	456
1	320	8	12.7	511	279	586	92	916	763

Table 5.1b: Re-designed brace connection (6-st, E-W), (unit: mm)

Storey	L <sub>w</sub>	D <sub>w</sub>	t <sub>gusset</sub>	W <sub>w</sub>	L1	L2	L3	a	b
6	250	8	12.7	405	121	316	153	438	456
5	250	9.5	12.7	405	121	316	153	438	456
4	310	8	12.7	500	143	384	182	532	553
3	310	9.5	12.7	500	143	384	182	532	553
2	310	9.5	12.7	500	143	384	182	532	553
1	380	9.5	15.9	610	327	693	105	1082	901

Table 5.2a: Re-designed brace connection (3-st, N-S), (unit: mm)

Storey	L <sub>w</sub>	D <sub>w</sub>	t <sub>gusset</sub>	W <sub>w</sub>	L1	L2	L3	a	b
3	320	8	12.7	511	440	562	30	624	487
2	380	9.5	12.7	606	516	661	30	733	572
1	450	9.5	12.7	712	410	623	30	727	641

Table 5.2b: Re-designed brace connection (6-st, N-S), (unit: mm)

Storey	L <sub>w</sub>	D <sub>w</sub>	t <sub>gusset</sub>	W <sub>w</sub>	L1	L2	L3	a	b
6	320	8	12.7	511	440	562	30	624	487
5	380	8	12.7	606	516	661	30	733	572
4	440	9.5	12.7	701	592	760	30	843	658
3	510	9.5	15.9	785	659	848	30	940	734
2	560	9.5	15.9	843	706	908	30	1007	786
1	580	9.5	15.9	891	505	773	30	901	795

The results corresponding to the resistance of re-designed brace connections are shown in Table 5.3 and for the 3- and 6-storey chevron CBF (E-W) and in Table 5.4 for the 3- and 6-storey CBF (N-S). In all cases, the tensile rupture in the net section of HSS brace with the consideration of shear lag effect is the governing failure mode.

Table 5.3a: Resistance of brace connections (3-st, E-W), (unit: kN)

St	Shear Resistance of Welding			Tensile Resistance of Metal Base		Yielding of Gusset Plate		Buckling of Gusset Plate		Net Rupture and block shear of brace with shear lag		
	$V_r$	$C_u/V_r$	$T_u/V_r$	$T_{rMB}$	$T_u/T_{rMB}$	$T_{rGP}$	$T_u/T_{rGP}$	$C_{rGP}$	$C_u/C_{rGP}$	$T_{u-NR}$	$T_{r-BS}$	$T_u/\min(T_{u-NR}, T_{r-BS})$
3	1170	0.38	0.91	1646	0.65	1428	0.75	1297	0.35	1116	1362	0.96
2	1332	0.39	0.93	1577	0.79	1389	0.90	1270	0.41	1336	1564	0.93
1	1463	0.51	0.94	2057	0.67	1753	0.78	1318	0.57	1378	1702	1.00

Table 5.3b: Resistance of brace connections (6-st, E-W), (unit: kN)

St	Shear Resistance of Welding			Tensile Resistance of Metal Base		Yielding of Gusset Plate		Buckling of Gusset Plate		Net Rupture and block shear of brace with shear lag		
	$V_r$	$C_u/V_r$	$T_u/V_r$	$T_{rMB}$	$T_u/T_{rMB}$	$T_{rGP}$	$T_u/T_{rGP}$	$C_{rGP}$	$C_u/C_{rGP}$	$T_{u-NR}$	$T_{r-BS}$	$T_u/\min(T_{u-NR}, T_{r-BS})$
6	1121	0.40	0.95	1577	0.68	1389	0.77	1270	0.35	1112	1305	0.96
5	1332	0.39	0.93	1577	0.79	1389	0.90	1270	0.41	1336	1564	0.93
4	1414	0.47	0.79	1989	0.56	1713	0.66	1488	0.44	1373	1645	0.82
3	1679	0.56	0.96	1989	0.81	1713	0.94	1488	0.63	1649	1972	0.98
2	1679	0.57	0.96	1989	0.81	1713	0.94	1488	0.64	1649	1972	0.98
1	2084	0.67	0.95	3091	0.64	2617	0.76	2044	0.68	1982	2449	1.00

Table 5.4a: Resistance of brace connections (3-st, N-S), (unit: kN)

St	Shear Resistance of Welding			Tensile Resistance of Metal Base		Yielding of Gusset Plate		Buckling of Gusset Plate		Net Rupture and block shear of brace with shear lag		
	$V_r$	$C_u/V_r$	$T_u/V_r$	$T_{rMB}$	$T_u/T_{rMB}$	$T_{rGP}$	$T_u/T_{rGP}$	$C_{rGP}$	$C_u/C_{rGP}$	$T_{u-NR}$	$T_{r-BS}$	$T_u/\min(T_{u-NR}, T_{r-BS})$
3	1463	0.22	0.94	2057	0.67	1753	0.78	1252	0.26	1378	1702	1.00
2	2084	0.32	0.95	2469	0.80	2077	0.95	1305	0.51	1968	2449	1.00
1	2490	0.37	0.94	2949	0.80	2442	0.96	1707	0.55	2287	2925	1.03

Table 5.4b: Resistance of brace connections (6-st, N-S), (unit: kN)

St	Shear Resistance of Welding			Tensile Resistance of Metal Base		Yielding of Gusset Plate		Buckling of Gusset Plate		Net Rupture and block shear of brace with shear lag		
	$V_r$	$C_u/V_r$	$T_u/V_r$	$T_{rMB}$	$T_u/T_{rMB}$	$T_{rGP}$	$T_u/T_{rGP}$	$C_{rGP}$	$C_u/C_{rGP}$	$T_{u-NR}$	$T_{r-BS}$	$T_u/\min(T_{u-NR}, T_{r-BS})$
6	1463	0.23	0.94	2057	0.67	1753	0.78	1252	0.27	1378	1702	1.00
5	1755	0.33	0.96	2469	0.68	2077	0.81	1305	0.45	1639	2043	1.03
4	2432	0.45	0.96	2880	0.81	2402	0.98	1315	0.83	2281	2857	1.03
3	2837	0.45	0.95	4207	0.64	3370	0.80	2083	0.61	2725	3892	0.99
2	3126	0.47	0.97	4636	0.65	3618	0.84	2092	0.70	3139	4895	0.96
1	3242	0.49	0.96	4808	0.65	3826	0.82	2710	0.59	3099	4448	1.01

It can be seen that after connections were re-designed, braces may still experience net section rupture due to the reduction of cross section area for the gusset plate slot. Therefore, a cover plate was added to reinforce the net section, as shown in Figure 5.3. The design of the cover plate is summarized in Table 5.5 and Table 5.6. The steel material G40.21-300W was selected to for the cover plate fabrication, with  $F_y = 300 \text{ MPa}$ . The process of determining the cover plate thickness is iterative because the center of gravity ( $\bar{X}$ ), depends on the cover plate thickness. This process can be conducted by using a spreadsheet. The calculation conducted for the ground floor HSS 152.4x152.4x9.53 brace of the 6-storey chevron CBF (E-W) is given as example.

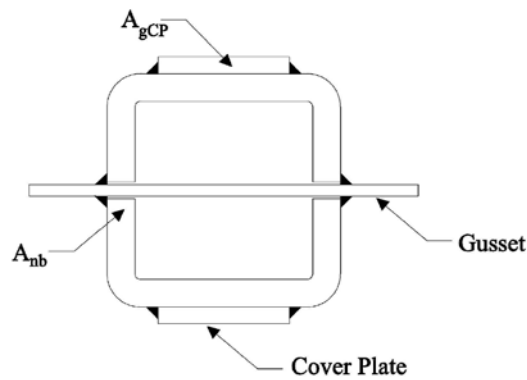


Figure 5.3: Cross-section view of HSS brace connection with added cover plates

After going through several iterations, a plate thickness of 8 mm and 100 mm width was chosen. The plate width of 100 mm allows enough room for the plate to be set on the flat part of the brace with additional space for the fillet welds on both sides.

The next step is to ensure that the capacity of the net section is greater than the ultimate tensile strength of the brace ( $T_u$ ). The equation proposed by Haddad and Tremblay (Haddad and Tremblay, 2006) was used for the connection resistance calculation with cover plates:

$$T_{rb} = U(\Phi_r R_t A_{nb} F_{u,b} + \Phi A_{gCP} F_{u,CP})$$

where  $A_{nb}$  is the cross-sectional area of the brace after the gusset plate slot has been made.  $A_{gCP}$  is the gross cross-sectional area of the added cover plate. A 1.5 mm cutting spacing between brace and gusset plate at the slot was considered.

$$A_{nb} = 5210 - 2(9.53)(15.9 + 2 * 1.5) = 4850 \text{ mm}^2$$

$$A_{gCP} = 2(8)(100) = 1600 \text{ mm}^2$$

The centre of gravity ( $\bar{X}$ ) was determined to be 53.2 mm, therefore the shear lag factor can be determined as follows:

$$U = 1.1 - \frac{\bar{X}'}{L_w} = 1.1 - \frac{52.3 - 15.9/2}{380} = 0.983$$

$$\begin{aligned} T_{rb} &= (0.983)[(0.75)(1.1)(4850)(448) + (1.0)(1600)(450)]/1000 \\ &= 2465 \text{ kN} > T_u = 1977 \text{ kN OK} \end{aligned}$$

The length of the net section was set at 400 mm, in order to match the brace splice length. Therefore an 8-mm x 100-mm x 400-mm net section cover plate is adequate to develop the expected tensile yield capacity of the brace.

The longitudinal fillet welds used to connect the net section reinforcing plates to the brace were designed conservatively so that they were able to develop the full plastic capacity of the plate. E490 electrodes were used and the required weld leg  $D_w$  is:

$$D_w = \frac{R_y F_y A_{g,CP}}{0.67 \Phi_w L_{w,GP} X_u} = \frac{1.1(300)(8)(100)}{0.67(0.67)(400)(480)(2)(0.707)} = 2.2 \text{ mm}$$

However, the minimum value of  $D_w$  is 5 mm. The design summary of each brace's cover plate is shown in Table 5.5 for the braces of CBF in the E-W direction and Table 5.6 for those in the N-S direction.

Table 5.5a: Design of braces cover plate (3-st E-W), (unit: mm; kN)

Storey	t <sub>CP</sub>	l <sub>CP</sub>	C.G.	x'/L <sub>w</sub>	U	T <sub>rb</sub>	T <sub>u</sub> /T <sub>rb</sub>
3	6	60	34	0.12	0.98	1244	0.86
2	6	60	33	0.11	0.99	1418	0.88
1	6	80	44	0.14	0.96	1613	0.85

Table 5.5b: Design of braces cover plate (6-st E-W), (unit: mm; kN)

Storey	t <sub>CP</sub>	l <sub>CP</sub>	C.G.	x'/L <sub>w</sub>	U	T <sub>rb</sub>	T <sub>u</sub> /T <sub>rb</sub>
6	8	60	35	0.13	0.97	1343	0.80
5	8	60	34	0.11	0.99	1520	0.82
4	8	80	46	0.17	0.93	1479	0.76
3	8	80	44	0.12	0.98	1989	0.81
2	8	80	44	0.12	0.98	1989	0.81
1	8	100	53	0.12	0.98	2465	0.80

Table 5.6a: Design of braces cover plate (3-st N-S), (unit: mm; kN)

Storey	t <sub>CP</sub>	l <sub>CP</sub>	C.G.	x'/L <sub>w</sub>	U	T <sub>rb</sub>	T <sub>u</sub> /T <sub>rb</sub>
3	6	80	44	0.14	0.96	1641	0.84
2	8	80	53	0.12	0.98	2372	0.83
1	8	100	64	0.13	0.97	2860	0.82

Table 5.6b; Design of braces cover plate (6-st N-S), (unit: mm; kN)

Storey	t <sub>CP</sub>	l <sub>CP</sub>	C.G.	x'/L <sub>w</sub>	U	T <sub>rb</sub>	T <sub>u</sub> /T <sub>rb</sub>
6	6	80	44	0.14	0.96	1641	0.84
5	6	100	54	0.14	0.96	2027	0.83
4	8	100	64	0.13	0.97	2852	0.82
3	8	100	62	0.11	0.99	3220	0.84
2	8	100	61	0.09	1.01	3450	0.88
1	8	100	71	0.11	0.99	3622	0.86

In this study, braces were maintained the same. However, by strengthening the brace connections it is expected that the level of CBF ductility to be increased.

For columns, as illustrated in Figure 4.7, although only the ground floor column of the 6-storey chevron braced frame (E-W direction) has a demand to capacity ratio larger than 1.0, it is also required that columns of the fifth floor to be slightly reinforced. Columns of the 3-storey chevron braced frame are not reinforced. However, all the middle columns of CBFs with tension/compression diagonal braces (N-S direction) have insufficient compression resistance and were retrofitted with the exception of the top floor column. Referring to side

columns of CBFs (N-S), only the ground floor and the 3<sup>rd</sup> floor columns of the 6-storey building were retrofitted by adding steel plates to the flanges of W-shape column cross-section, as shown in Figure 5.4. The  $T_{SP}$  and  $L_{SP}$  given in Figure 5.4 are the thickness and width of the steel cover plate, respectively. The retrofitted columns are summarized in Table 5.7 for E-W direction and Table 5.8 for N-S direction.

As previously stated in Chapter 4, columns were verified under the effect of axial compression force and bending moment developed due to lateral loading. Because the shear tab connection between beams and columns were assumed to carry 20% of the beam plastic bending capacity some bending moment was developed.

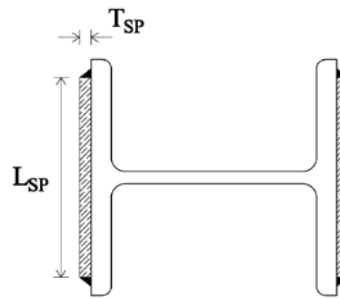


Figure 5.4: Retrofitted column cross-section

Table 5.7: Retrofitting of columns (6-st E-W), (unit: mm)

St	$T_{SP}$	$L_{SP}$	Section Class	$C_{r,after}/C_{r,before}$	$C_{f,10}/C_{r,after}$
6	-	-	1	1.00	0.21
5	5.0	160	1	1.45	0.33
4	-	-	1	1.00	0.45
3	-	-	1	1.00	0.69
2	-	-	1	1.00	0.71
1	9.5	260	1	1.38	0.61

Table 5.8a: Retrofitting of columns (3-st N-S), (unit: mm)

St	Middle Column				
	$T_{SP}$	$L_{SP}$	Section Class	$C_{r,after}/C_{r,before}$	$C_{f,10}/C_{r,after}$
3	-	-	1	1.00	0.63
2	6.4	160	1	1.41	0.66
1	15.9	160	1	1.85	0.78

Table 5.8b: Retrofitting of columns (6-st N-S), (unit: mm)

St	Side Column					Middle Column				
	$T_{SP}$	$L_{SP}$	Section Class	$C_{r,after}/C_{r,before}$	$C_{f,10}/C_{r,after}$	$T_{SP}$	$L_{SP}$	Section Class	$C_{r,after}/C_{r,before}$	$C_{f,10}/C_{r,after}$
6	-	-	1	1.00	0.39	-	-	1	1.00	0.62
5	-	-	1	1.00	0.74	9.5	130	1	1.66	0.76
4	-	-	1	1.00	0.51	9.5	160	1	1.48	0.70
3	6.4	160	1	1.30	0.62	22	160	1	2.12	0.68
2	-	-	1	1.00	0.65	12.7	270	1	1.58	0.65
1	6.4	220	1	1.24	0.77	22	270	1	2.03	0.68

Failure of beam is mainly due to the bending moment from gravity load in addition to the axial load transferred from braces. In order to maintain the centre of gravity of the W-shape cross-section, two longitudinal steel plates were added at each side of the web of W-shape beam cross-section, as shown in Figure 5.5.

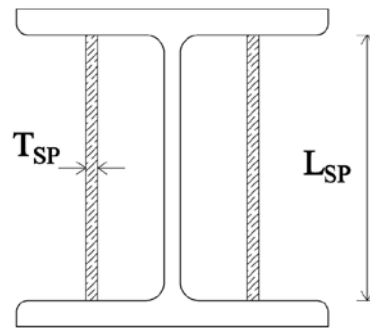


Figure 5.5: Retrofitted beam cross-section

From the demand to capacity ratios computed for beams (Figure 4.6), all beams of chevron braced frame (E-W direction) were retrofitted. The thickness of the retrofit plate  $T_{SP}$  and the ratio  $M_{r,after}/M_{r,before}$  are given in Table 5.9 for the 3- and 6-storey CBF (E-W) and in Table 5.10 for the 3- and 6-storey CBF (N-S).

Table 5.9a: Retrofitting of beams (3-st E-W), (unit: mm)

St	$T_{SP}$	Section Class	$M_{r,after}/M_{r,before}$	$M_{f,10}/M_{r,after}$
3	12.7	1	2.07	0.924
2	22	1	2.64	0.969
1	16	1	2.34	0.967

Table 5.9b: Retrofitting of beams (6-st E-W), (unit: mm)

St	T <sub>SP</sub>	Section Class	M <sub>r,after</sub> /M <sub>r,before</sub>	M <sub>f,10</sub> /M <sub>r,after</sub>
6	12.7	1	2.07	0.92
5	22	1	2.64	0.97
4	19	1	2.07	0.97
3	19	1	2.07	0.97
2	19	1	2.07	0.97
1	12.7	1	1.83	1.01

Table 5.10a: Retrofitting of beams (3-st N-S), (unit: mm)

St	T <sub>SP</sub>	Section Class	M <sub>r,after</sub> /M <sub>r,before</sub>	M <sub>f,10</sub> /M <sub>r,after</sub>
3	0	1	1.00	0.72
2	6.4	1	1.23	0.53
1	9.5	1	1.40	0.46

Table 5.10b: Retrofitting of beams (6-st N-S), (unit: mm)

St	T <sub>SP</sub>	Section Class	M <sub>r,after</sub> /M <sub>r,before</sub>	M <sub>f,10</sub> /M <sub>r,after</sub>
6	0	1	1.00	0.72
5	6.4	1	1.23	0.53
4	6.4	1	1.29	0.46
3	6.4	1	1.24	0.41
2	9.5	1	1.41	0.36
1	9.5	1	1.35	0.34

## 5.2 Seismic Assessment of Retrofitted Buildings

Incremental dynamic analysis (*IDA*) method was applied in order to compute fragility of post-retrofit buildings. Because some members of CBFs were retrofitted, the stiffness of the system was slightly increased and the fundamental period of both 3- and 6-storey buildings is given in Table 5.11. For comparison purpose, the fundamental period of the building before retrofit is also given. As resulted, the fundamental building period remained almost the same (about 0.1 s difference) and the increment of seismic intensity was around 10%.

Table 5.11: Dynamic properties of retrofitted buildings and pre-retrofit buildings

Building ID	Post-retrofit		Pre-retrofit	
	$T_1$ (s)	$S_a(T_1)$ (g)	$T_1$ (s)	$S_a(T_1)$ (g)
3St W-E	0.552	0.292	0.611	0.272
3St N-S	0.671	0.252	0.727	0.233
6St W-E	0.956	0.155	1.060	0.134
6St N-S	1.122	0.129	1.243	0.118

### 5.2.1 Incremental dynamic analysis of retrofitted buildings

Incremental dynamic analysis was performed for the post-retrofit buildings and the resulted IDA curves of the 3- and 6-storey CBF (E-W) are plotted in Figure 5.6 against the IDA curves of pre-retrofit buildings that were previously computed (Figure 4.17).

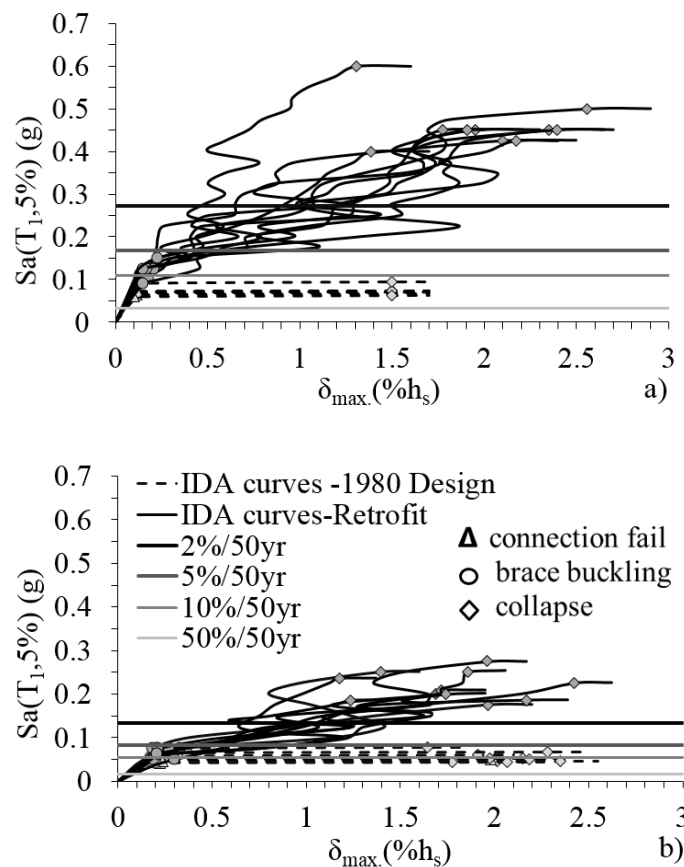


Figure 5.6: IDA curves of studied buildings: a) 3-st. (E-W); b) 6-st. (E-W)

The resulted IDA curves of the 3- and 6-storey CBF (N-S) are plotted in Figure 5.7 against the IDA curves of pre-retrofit buildings that were previously computed. As illustrated in Figure 5.6 and Figure 5.7, the post-retrofit buildings are able to withstand the earthquake loads computed for a probability of exceedance of 2%/50 yrs.

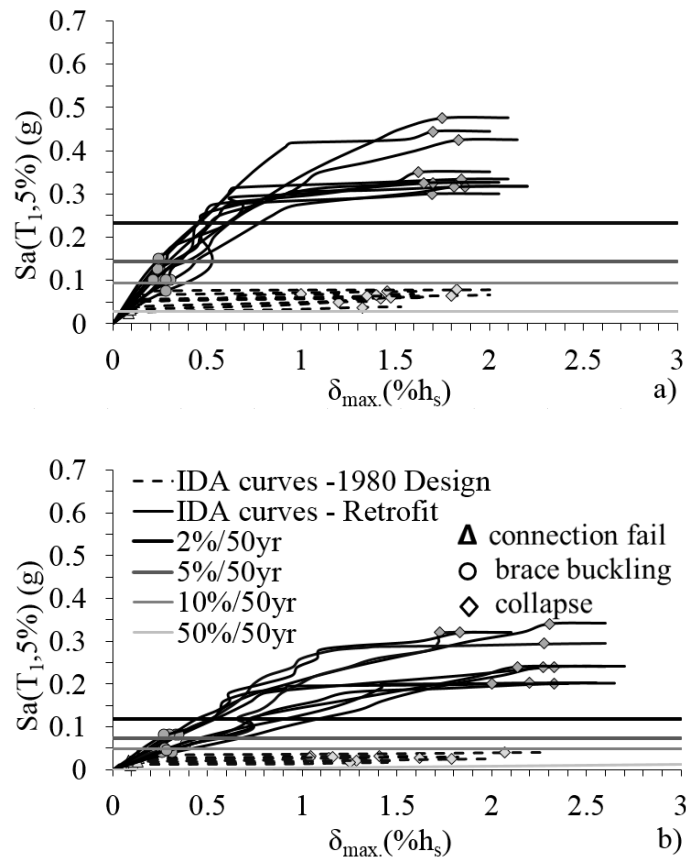


Figure 5.7: IDA curves of studied buildings: a) 3-st. (N-S); b) 6-st. (N-S)

Analysis results from the IDA curves are given in Table 5.12 for the 3- and 6-storey CBF (E-W) in term of the intensity measure parameter ( $Sa(T_1)$ ) recorded when the first brace reaches buckling, the first beam or column encountered hinging and at the collapse point where the IDA curve flattening (Near Collapse). The results obtained from the IDA curves of the CBF system in N-S direction are given in Table 5.13.

Table 5.12a: Summary of results from the IDA curves of post-retrofit 3-st CBF (E-W)

GM	First brace buckling		First Beam Buckling		Collapse of building	
	Sa(T <sub>1</sub> ) (g)	Floor	Sa(T <sub>1</sub> ) (g)	Floor	Sa(T <sub>1</sub> ) (g)	Floor
M6C1-10.7	0.100	F2	0.225	F1	0.450	F1
M6C1-12.8	0.125	F1	0.400	F1	0.425	F1
M6C1-16.6	0.112	F2	0.325	F2	0.450	F2
M7C1-20.1	0.100	F3	0.350	F2	0.450	F2
M7C1-25.2	0.125	F2	0.250	F2	0.450	F2
M7C1-25.8	0.125	F2	0.375	F2	0.450	F2
M7C2-41.6	0.091	F2	0.325	F1	0.425	F1
S8.EN1	0.125	F2	0.375	F2	0.400	F2
S9.EN1	0.125	F2	0.400	F2	0.500	F1
S10.EN2	0.150	F2	0.550	F1	0.600	F1

Table 5.12b: Summary of results from the IDA curves of post-retrofit 6-st CBF (E-W)

GM	First brace buckling		First column buckling		Collapse of the building	
	Sa(T <sub>1</sub> ) (g)	Floor	Sa(T <sub>1</sub> ) (g)	Floor	Sa(T <sub>1</sub> ) (g)	Floor
M6C1-10.7	0.061	F5	0.158	F5	0.209	F5
M6C1-12.8	0.075	F5	0.150	F5	0.175	F5
M6C1-16.6	0.050	F5;F6	0.200	F5	0.275	F5
M7C1-20.1	0.075	F5	0.125	F5	0.250	F3
M7C1-25.2	0.065	F5;F6	0.175	F5	0.200	F5
M7C1-25.8	0.050	F5	0.200	F2;F5	0.250	F2;F5
M7C2-41.6	0.075	F5	0.175	F3	0.186	F5
S8.EN1	0.075	F5;F6	0.138	F3	0.186	F3
S9.EN1	0.062	F5	0.200	F5	0.225	F5
S10.EN2	0.062	F5;F6	0.100	F3	0.236	F3

Table 5.13a: Summary of results from the IDA curves of post-retrofit 3-st CBF (N-S)

GM	First brace buckling		First Column Buckling		Collapse of the building	
	Sa(T <sub>1</sub> ) (g)	Floor	Sa(T <sub>1</sub> ) (g)	Floor	Sa(T <sub>1</sub> ) (g)	Floor
M6C1-10.7	0.100	F3	0.308	F1	0.316	F1
M6C1-12.8	0.125	F1	0.400	F1	0.425	F1
M6C1-16.6	0.150	F3	0.325	F2	0.334	F2
M7C1-20.1	0.075	F3	0.292	F1	0.300	F1
M7C1-25.2	0.100	F3	0.303	F1	0.317	F1
M7C1-25.8	0.125	F3	0.316	F1	0.325	F1
M7C2-41.6	0.125	F3	0.319	F1	0.325	F1
S8.EN1	0.125	F3	0.450	F3	0.475	F3
S9.EN1	0.100	F3	0.325	F1	0.350	F1
S10.EN2	0.150	F3	0.425	F1	0.444	F1

Table 5.13b: Summary of results from the IDA curves of post-retrofit 6-st CBF (N-S)

GM	First brace buckling		First Column Buckling		Collapse of the building	
	Sa(T <sub>1</sub> ) (g)	Floor	Sa(T <sub>1</sub> ) (g)	Floor	Sa(T <sub>1</sub> ) (g)	Floor
M6C1-10.7	0.060	F6	0.220	F5	0.340	F5;F6
M6C1-12.8	0.080	F5;F6	0.260	F5	0.294	F2
M6C1-16.6	0.080	F6	0.180	F1	0.240	F5;F6
M7C1-20.1	0.060	F6;F5	0.140	F5;F6	0.320	F5;F6
M7C1-25.2	0.080	F6	0.200	F1	0.320	F1;F5;F6
M7C1-25.8	0.040	F6	0.120	F5;F6	0.240	F5
M7C2-41.6	0.040	F6	0.120	F5	0.200	F5;F6
S8.EN1	0.048	F6	0.120	F5;F6	0.203	F5;F6
S9.EN1	0.080	F6	0.180	F5	0.200	F5;F6
S10.EN2	0.045	F6	0.160	F5	0.240	F5;F6

In this study, two quantities expressed in term of margin ratio were introduced: i) the elastic margin ratio, *EMR*, which reflects the level of ground motion intensity at the boundary elastic/ plastic limit (the first brace reaches the onset of buckling) versus the design acceleration spectrum and ii) the damage margin ratio, *DMR*, which reflects the level of ground motion intensity when dynamic instability starts versus the design acceleration spectrum. As summarized in Table 5.14, it can be seen that the first brace buckling of the post-retrofit 3-

storey building was initiated at a spectral acceleration of 0.12g and encountered beam/column hinging at a level of ground motion intensity larger than the current code demand ( $CMR > 1.0$ ). The reserve capacity of the 3-storey CBF (E-W) is 1.57 whereas for the 3-storey CBF in the N-S direction is 1.43. Referring to the 6-storey building, the first brace buckling occurs at 0.07g and beam/column hinging occurs for a  $CMR > 1.0$ . On the other hand, the  $CMR$  for the 6-storey CBF (E-W) is 1.41 while for the 6-storey CBF (N-S) is 2.02. This difference consists in the extended level of retrofit (e.g., columns of the 6-st CBF (N-S) were strengthened at a higher level than those of the chevron CBF (E-W)). It can be summarized that the retrofit action was efficient and the  $CMR$  is larger than 1.0. The selection of retrofit strategy depends on the level of expected building performance state. A higher performance limit state means extended retrofit actions. It is noted that CBF buildings are not prone to large interstorey drift as are the moment resisting frame systems.

Table 5.14: Collapse margin ratio of retrofitted building for various performance levels

Building ID	First brace buckling		First column/bream buckling		Collapse of building	
	$S_{MC}$	EMR	$S_{MC}$	DMR	$S_{MC}$	DMR
3WE	0.12g	0.40	0.36g	1.22	0.46g	1.57
3NS	0.12g	0.47	0.35g	1.37	0.36g	1.43
6WE	0.07g	0.22	0.16g	1.05	0.22g	1.41
6NS	0.06g	0.48	0.17g	1.32	0.26g	2.02

### 5.2.2 Detailed analysis example upon collapse of the retrofitted

After retrofit, the brace-to-frame connections of studied CBF buildings are able to sustain brace buckling and yielding. However, columns and beams were not strengthened to withstand an intensity level of ground motions larger than the code demand without hinging. For this reason, hinging in beams/columns occurs before braces exhibit fracture due to low-cycle fatigue.

A typical response of the post-retrofit 6-storey chevron CBF (E-W) under the simulated ground motion M6C1-16.6 is explained below. This structure has a fundamental building period of 0.956 s and the corresponded design spectral acceleration is  $(S_a(T_1)) = 0.155g$ , which can be read from Table 5.11. The computed IDA curve obtained for the 6-storey CBF (E-W) subjected to ground motion record M6C1-16.6 is depicted in Figure 5.8.

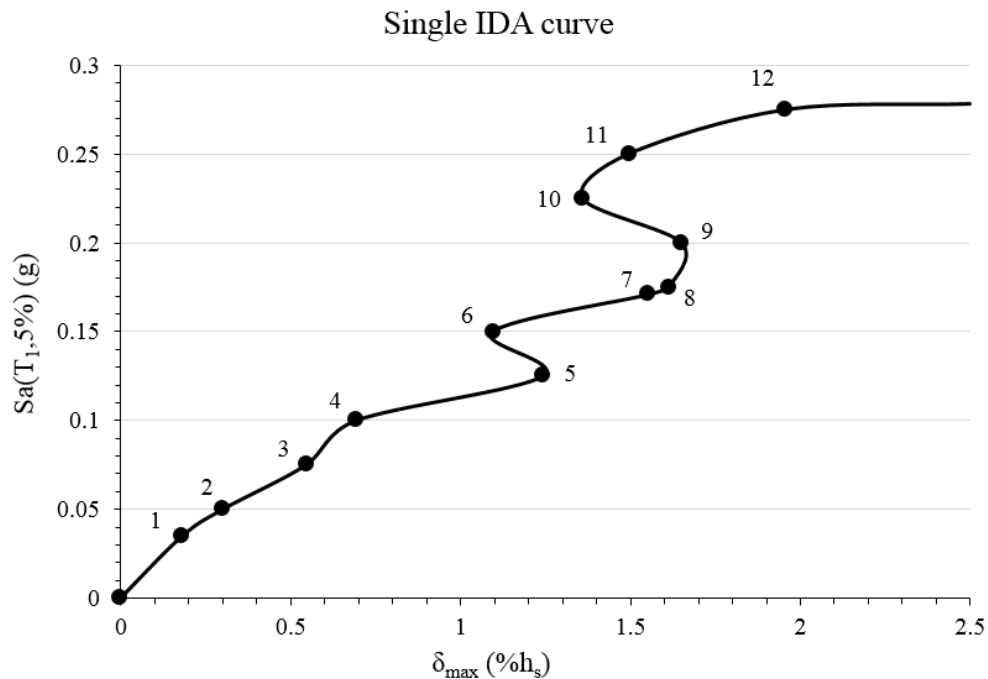


Figure 5.8: IDA curve of 6-storey CBF (E-W) subjected to ground motion M6C1-16.6

The average incremental step used to build this IDA curve is about 0.025g and each step that means one analysis is marked on the IDA curve. In this case, the IDA curve displays a wavy shape after point 2 which means that the waving segments are successive segments of “softening” and “hardening” whereas the local slope (stiffness) decreases and increases, respectively with higher spectral acceleration or intensity of ground motion (Vamvatsikos and Cornell, 2002). This behaviour indicates that buckling or yielding of some structural components happened and dynamic instability is locally reached. For example, the analysis results from OpenSees show that up to point 2 the structure performs elastically (linear segment) and at point 2 the first brace buckles, so the stiffness of structure is on a decreasing slope. A large increasing interstorey drift is shown between points 4 and 5 and between points 6 and 9. A detailed structural response at the critical points 5 and 9 is depicted in Figure 5.9 where a rapid increase of interstorey drift indicates that more and severer damage happen within that segment and the near collapse limit state follows immediately. After point 12, which corresponding to  $(Sa(T_1)) = 0.275$  g at the ground motion scaling factor of 2.38, which is larger than the code demand, the interstorey drift started to increase suddenly with a small amount of

incremented ground motion and the near collapse point is defined. However, this collapse point doesn't mean the collapse of the building but it can be said that is the "Near Collapse, (NC)" limit state. Detailed structural behaviour corresponding to NC is also illustrated in Figure 5.9.

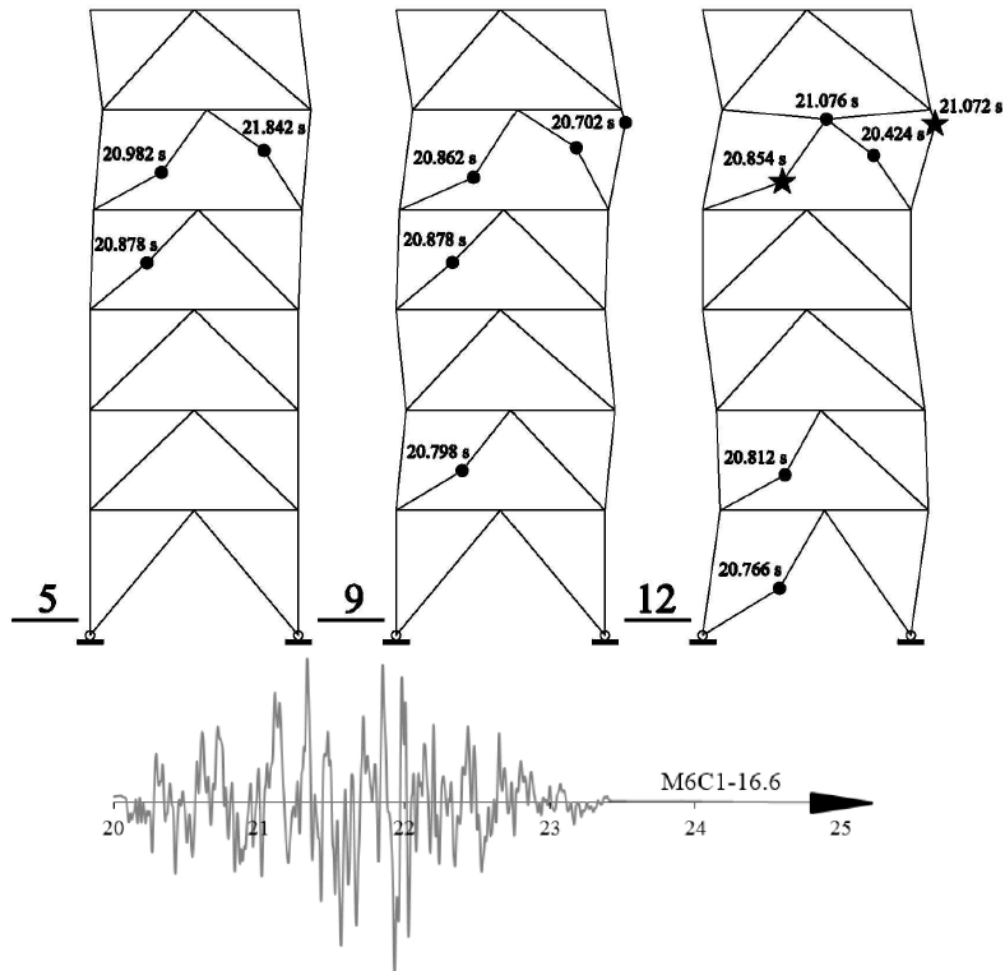


Figure 5.9: Seismic response of retrofitted 6-Storey chevron braced frame (E-W) under ground motion M6C1-16.6. (Point 5, Point 9 and Point 12 on the IDA curve; ● buckling of structural member, ★ failure of structural member)

From the accelerogram of M6C1-16.6 record it can be seen that the peak ground acceleration was reached at around 21.3s and from Figure 5.9 resulted that brace buckling and column hinging occurred around the same time step. Hysteresis loop of braces at the 5<sup>th</sup> floor at the near collapse point (point 12) are illustrated on Figure 5.10. As shown in Figure 5.11, major damage occurs within the fifth floor where the interstorey drift is about 70 mm (Figure

5.11a) and the maximum residual interstorey drift ( $\delta_{max.res.}$ ) is more than  $0.71\%hs$ . The interstorey drift at the second floor and the ground floor is almost the same as that at the fifth floor. It is noted that, the analysis cannot be conducted after point 12 because of convergence problems in OpenSees software. However, it is estimated that the complete building failure is anticipated to occur at the second floor. Thus the time history interstorey drift (Figure 5.11a) and the interstorey drift ratio (Figure 5.11b) developed at the second and ground floor are also illustrated. In order to assess the performance of non-structural components in further studies floor acceleration (Figure 5.11c) is also given.

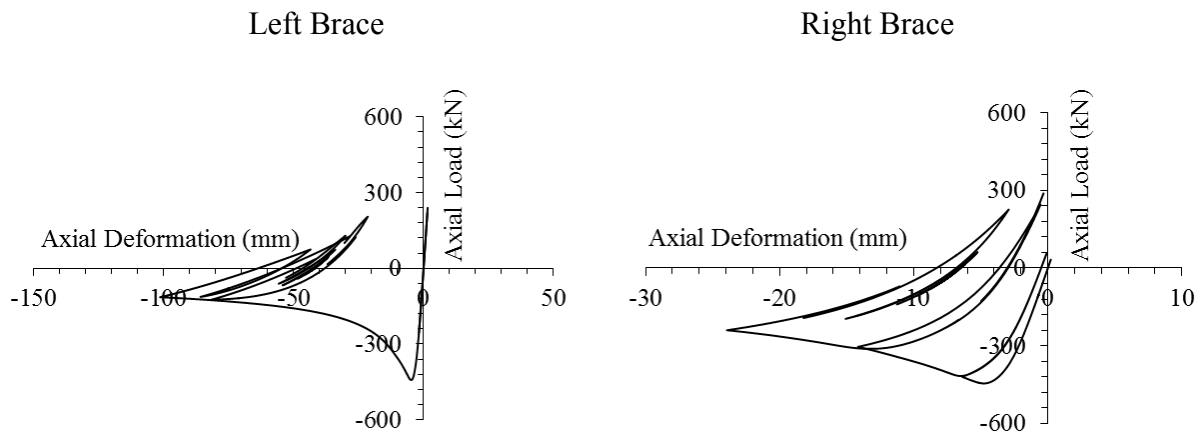


Figure 5.10: Hysteresis loop of braces located at 5th floor under the ground motion intensity corresponding to *Point 12* of Figure 5.9

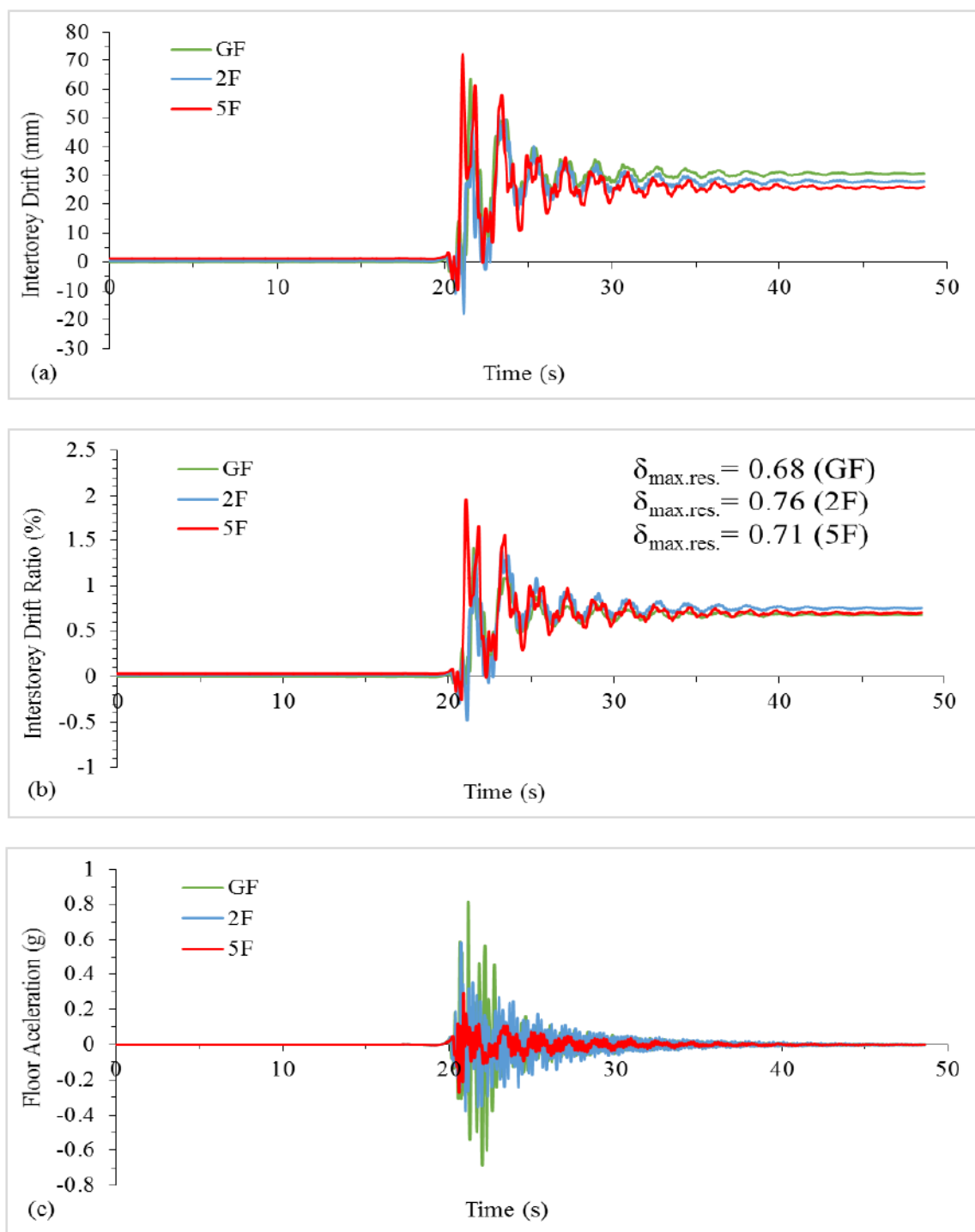


Figure 5.11: Time history response: (a) Interstorey Drift; (b) Interstorey Drift Ratio; (c) Floor acceleration

It can be concluded that the seismic performance of post-retrofit buildings has

significantly improved and due to brace buckling and yielding the remaining structural components are protected. The summary of CBF components subjected to retrofit is given in Table 5.15 and Table 5.15.

Table 5.15a: CBF components subjected to retrofit (3-st E-W)

Storey	Retrofit action			
	Connection	Brace	Beam	Column
3	Yes	NO	Yes	NO
2	Yes	NO	Yes	NO
1	Yes	NO	Yes	NO

Table 5.15b: CBF components subjected to retrofit (6-st E-W)

Storey	Retrofit action			
	Connection	Brace	Beam	Column
6	Yes	No	Yes	NO
5	Yes	No	Yes	Yes
4	Yes	No	Yes	NO
3	Yes	No	Yes	NO
2	Yes	No	Yes	NO
1	Yes	No	Yes	Yes

Table 5.16a: CBF components subjected to retrofit (3-st N-S)

Storey	Retrofit action				
	Connection	Brace	Beam	Middle Column	Side Column
3	Yes	No	Yes	NO	Yes
2	Yes	No	Yes	Yes	Yes
1	Yes	No	Yes	Yes	Yes

Table 5.16b: CBF components subjected to retrofit (6-st N-S)

Storey	Retrofit action				
	Connection	Brace	Beam	Middle Column	Side Column
6	Yes	No	Yes	NO	NO
5	Yes	No	Yes	Yes	Yes
4	Yes	No	Yes	Yes	Yes
3	Yes	No	Yes	Yes	Yes
2	Yes	No	Yes	Yes	Yes
1	Yes	No	Yes	Yes	Yes

### 5.3 Seismic Fragility Analysis

Fragility of components or systems defines the probability of reaching a given damage state as a function of a specified measure of earthquake ground motion intensity. To conduct a complete study within the resilience based design framework, the probability of exceedance of a damage state under the specified earthquake intensity level is required. By using these results, the probable expected losses can be estimated.

#### 5.3.1 Damage State and Performance Limit State

To manage the risk of existing building, proper retrofit strategy should be applied in accordance with the required rehabilitation objective classes which are defined as a combination of target building performance level and earthquake hazard level. According to ASCE/SEI 41-13, there are 3 rehabilitation objectives classes such as: i) Basic Safety Objective; ii) Enhanced Objectives; iii) Limited Objectives and 4 performance levels (*PL*): Operational (*O*), Immediate Occupancy (*IO*), Life Safety (*LS*) and Collapse Prevention (*CP*).

In terms of seismic hazard, the eastern Canada is prone to high and moderate risk, which can be seen on the seismic maps released in 1970, 1985 and 2005 NBCC editions. The first probabilistic seismic map was based on ground acceleration with a 50% probability of exceedance in 50 years (NBCC, 1970). However, the 1985 and 2005 maps were developed for 10% and 2%, respectively, probability of exceedance in 50 years (475 and 2500 years return period). Although seismic hazard has increased, the vulnerability of buildings has decreased

due to improvements incorporated in design regulations. The probabilistic earthquake hazard levels used in this study are summarized in Table 5.17.

Table 5.17: Seismic hazard considered in this study.

ID	Earthquake Having Probability of Exceedance	Mean Return Period (Years)
1	2%/50 year	2475
3	10%/50 year	475
4	50%/50 year	100

According to ASCE/SEI 41-13, the rehabilitation objective class for office buildings is the Basic Safety Objective which requires verifications on the following performance levels: i) Life Safety under the 10% in 50 year earthquake hazard level and ii) Collapse Prevention under the 2% in 50 year.

Damage states namely: *Very Light*, *Light*, *Moderate* and *Severe* vary as a continuous function of building deformation and are associated to the defined building performance levels. For example, the *Moderate* damage state extends from the threshold of *Moderate* damage to *Severe* damage. The damage state is a description of system damage during an earthquake event which includes the damage of structural and non-structural components. The damage of structural components is defined by a reduced capacity of resisting seismic forces. Damage of non-structural components is assessed based on the floor peak intersotey drift ( $\delta_{max}$ ), maximum residual interstorey drift ( $\delta_{max\_res}$ ) and floor acceleration ( $a_{max}$ ). In this study, the performance of non-structural components is not considered. When the structure accumulates a large value of floor peak interstorey drift materialized by a final softening segment it signalises the onset of dynamic instability. ASCE/SEI 41-13 provides suggested values for the maximum interstorey drift and maximum residual interstorey drift for each performance level, as given in Figure 5.12.

Performance Levels	<b>Operational</b>		<b>Immediate Occupancy</b>		<b>Life Safety</b>		<b>Collapse Prevention</b>	
Performance Ranges	No structural damage		Damage Control range		Limited Safety range		Collapse	
Degree of Damage	None	Very Light Damage	Light Damage		Moderate Damage		Complete Damage	
Damage Levels	<b>Very Light</b>		<b>Light</b>		<b>Moderate</b>		<b>Severe</b>	
Suggested $\delta_{max}$			0.5%hs		1.5%hs		2.0%hs	
Suggested $\delta_{max.res}$			-		0.5%hs		2.0%hs	

Figure 5.12: Mapping damage control against building performance levels according to ASCE/SEI 41. (Tirca et al., 2014)

Quantitative approaches were considered to define the performance levels by means of IDA curves. Thus, the displacement capacity point (last point) on the IDA curve associated to the *CP* performance level corresponds to storey mechanism and the point associated to the *IO* level corresponds to the first brace buckling. However, the *LS* performance level is difficult to determine (Wen et al., 2004). Based on qualitative approaches, the *LS* performance level can be defined when braces yield or buckle but do not fail, while the maximum residual interstorey drift is about 0.5%hs. It is assumed that both drift-sensitive and acceleration-sensitive nonstructural components are not interacting with the structure. According to the nonlinear time-history analysis performed by using OpenSees, the median of: maximum interstorey drift  $\delta_{max}$ , maximum residual interstorey drift  $\delta_{max.res}$  and the maximum floor acceleration  $a_{max}$  of retrofitted buildings are summarized in Table 5.18.

Table 5.18: Median peak interstorey drift, residual interstorey drift and floor acceleration of studied CBF buildings

Building ID (retrofitted)	<b>IO</b>			<b>LS</b>			<b>CP</b>		
	$\delta_{max}$ (%hs)	$\delta_{max.res}$ (%hs)	$a_{max}$ (g)	$\delta_{max}$ (%hs)	$\delta_{max.res}$ (%hs)	$a_{max}$ (g)	$\delta_{max}$ (%hs)	$\delta_{max.res}$ (%hs)	$a_{max}$ (g)
3-st E-W	0.44	0.15	0.34	1.1	0.49	0.42	2	1.04	0.49
3-st N-S	0.27	0.1	0.29	1.46	0.52	0.62	1.75	0.89	0.73
6-st E-W	0.41	0.11	0.33	1.33	0.49	0.61	1.8	0.58	0.63
6-st N-S	0.41	0.1	0.37	1.77	0.46	0.7	2.14	0.72	0.71

The 50 and 84 percentile peak interstorey drift, residual interstorey drift and floor

acceleration for each floor of post-retrofit buildings corresponding to each damage state are illustrated from Figure 5.13 to Figure 5.18. Floor acceleration of each floor is given in order to assess the damage of acceleration sensitive non-structural components in further studies. If the critical floor happen to be the bottom floor, the overall building failure is more likely to occur. If the roof floor became unstable, it may be only a floor failure or partial collapse of the building.

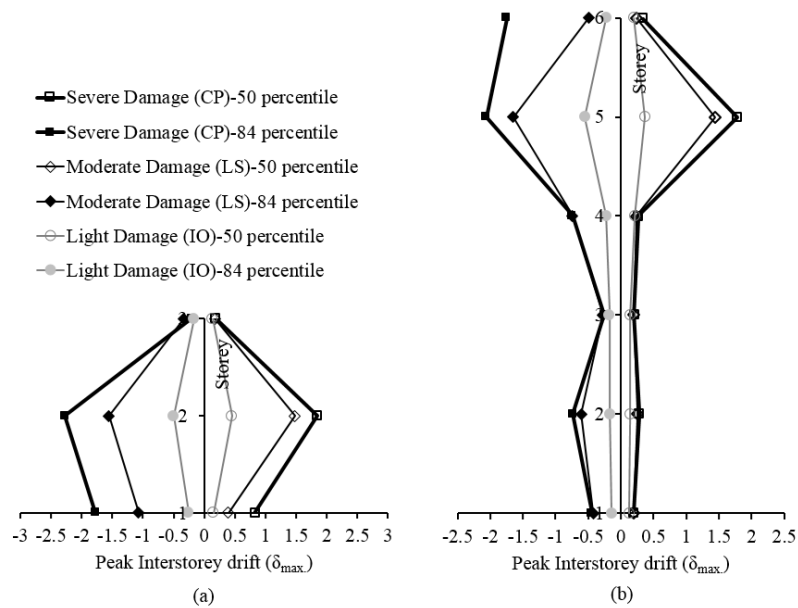


Figure 5.13: The 50 and 84 percentile peak interstorey drift of each floor: (a) 3-st CBF (E-W); (b) 6-st CBF (E-W)

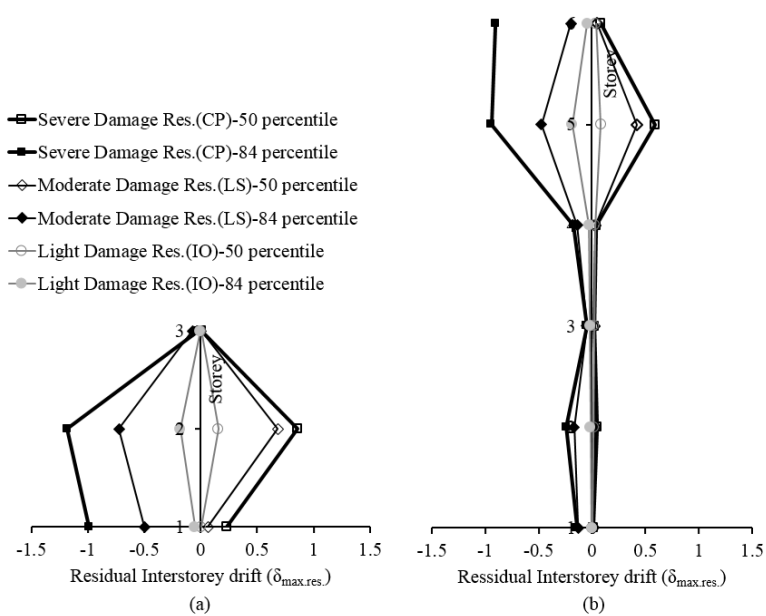


Figure 5.14: The 50 and 84 percentile residual interstorey drift of each floor: (a) 3-st CBF (E-W); (b) 6-st CBF (E-W)

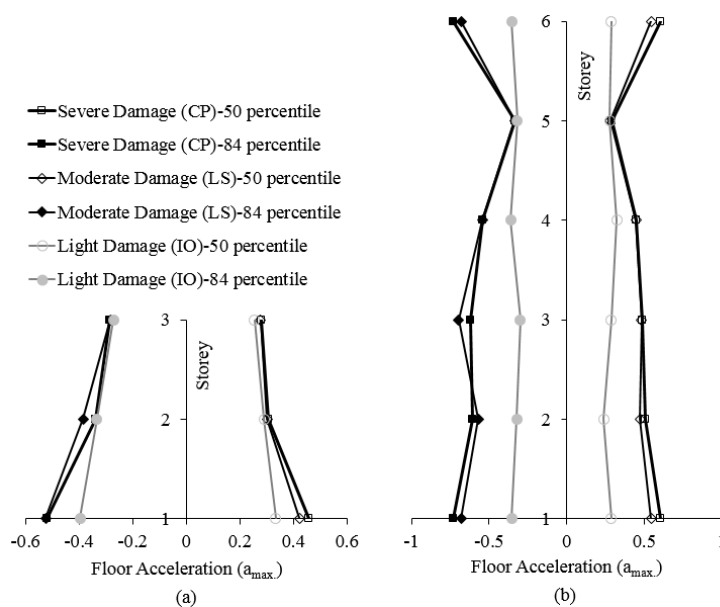


Figure 5.15: The 50 and 84 percentile floor acceleration of each floor: (a) 3-st CBF (E-W); (b) 6-st CBF (E-W)

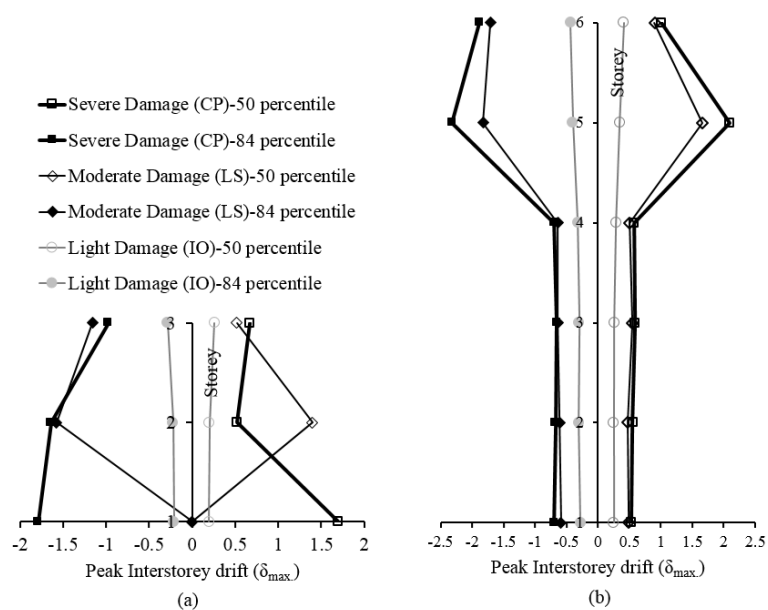


Figure 5.16: The 50 and 84 percentile peak interstorey drift of each floor: (a) 3-st CBF (N-S);  
(b) 6-st CBF (N-S)

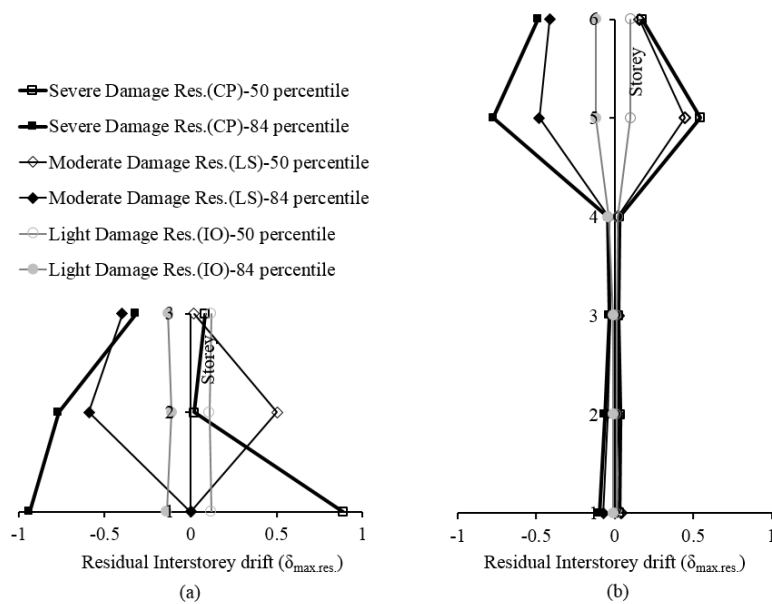


Figure 5.17: The 50 and 84 percentile residual interstorey drift of each floor: (a) 3-st CBF (N-S); (b) 6-st CBF (N-S)

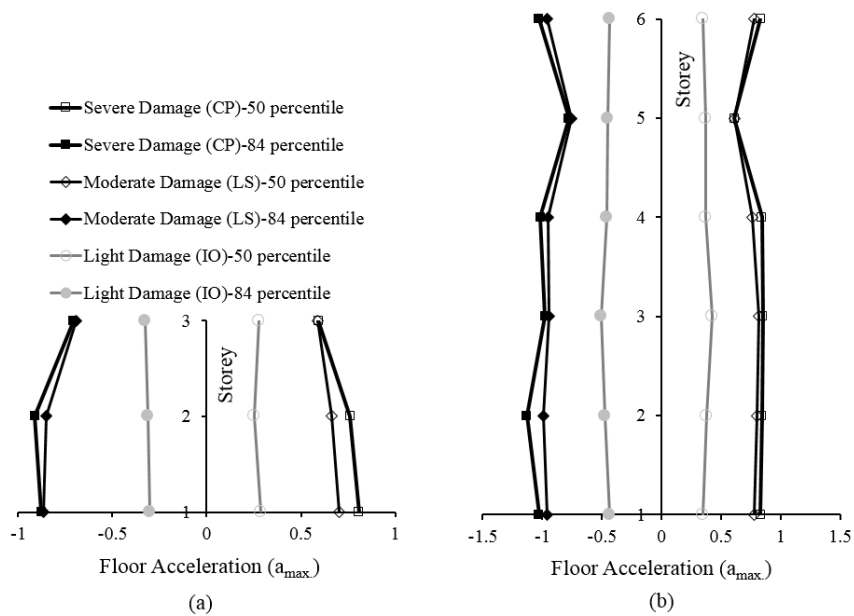


Figure 5.18: The 50 and 84 percentile floor acceleration of each floor: (a) 3-st CBF (N-S); (b) 6-st CBF (N-S)

### 5.3.2 Calculation of Fragility

Fragility of buildings can be clearly presented by means of a fragility curve which contains the probability of damage at a certain level. The summary of IDA curves is transposed into the fragility curves that emphasise the probability of collapse to the spectral intensity of considered ground motions. In this study, fragility functions were derived from parameters estimated using IDA curves. The fragility function proposed by Baker and Cornell (2005) is used as per Equation (2.35) where  $P(PL/IM = x)$  is the probability that a ground motion with  $IM = x$  will exceed a given performance level (e.g. *IO*, *LS*, *CP*),  $\Phi(\cdot)$  is the standard normal cumulative distribution function (CDF),  $m_R$  is the median of the fragility function (the  $IM$  level with 50% probability of exceeding the given  $PL$ ) and  $\beta_R$  is the logarithmic standard deviation. In this study, for the uncertainties, the same value as suggested by Elligwood et al. (2007) was assumed for  $\beta_C$  and  $\beta_{RU}$  i.e.:  $\beta_C = 0.25$  and  $\beta_{RU} = 0.20$ . Sources of uncertainties in structural steel material properties were not considered. To calculate the seismic demand uncertainty,  $\beta_{D|S_a}$ , the paired values  $\{(IM_i, \delta_i), i = 1, \dots, 10\}$  corresponding to the response obtained from

each one out of the 10 selected ground motions were generated for each of the defined performance levels (e.g. *IO*, *LS*, *CP*) that were identified from the IDA curves. In this study, to assess  $\beta_{D|Sa}$ , a nonlinear regression analysis of the power-law form given in Equation (2.39) was used, in which  $\theta_{max} = \delta_{max}$  and  $Sa = S_a(T_1)$ , where  $S_a(T_1)$  is the spectral acceleration at the fundamental period of the building corresponding to the associated performance limit. Thus, the seismic demand was examined using the 2%/50 years ground motion sets. The statistical analysis of data is summarized in Table 5.19. For the pre-retrofitted buildings, as the damage states were not gradually transited, seismic demand uncertainty was hard to be estimated and large uncertainty value could be predicted. In this light, according to FEMA P695, the total uncertainty that was assumed is 0.62. This value is the largest uncertainty value that is allowed to be used.

Table 5.19: Seismic demand statistics of investigated steel structures

3-WE	3-NS	6-WE	6-NS
$\delta_{max} = 4.40S_a^{1.19}$	$\delta_{max} = 7.02S_a^{1.46}$	$\delta_{max} = 15.90S_a^{1.36}$	$\delta_{max} = 8.91S_a^{1.14}$
$\beta_{D Sa} = 0.47$	$\beta_{D Sa} = 0.43$	$\beta_{D Sa} = 0.51$	$\beta_{D Sa} = 0.44$

For post-retrofit buildings, the seismic response at each performance level obtained under the selected 10 ground motions is illustrated on Figure 5.19. The difference in interstorey drift response for a single performance level obtained under different ground motion ensembles reflects the epistemic uncertainty in the ground motion modelling. This difference for the chevron braced frame (E-W) is larger than that that of CBF with tension/ compression diagonal braces (N-S), because the seismic demand uncertainty ( $\beta_{D|Sa}$ ) is larger.

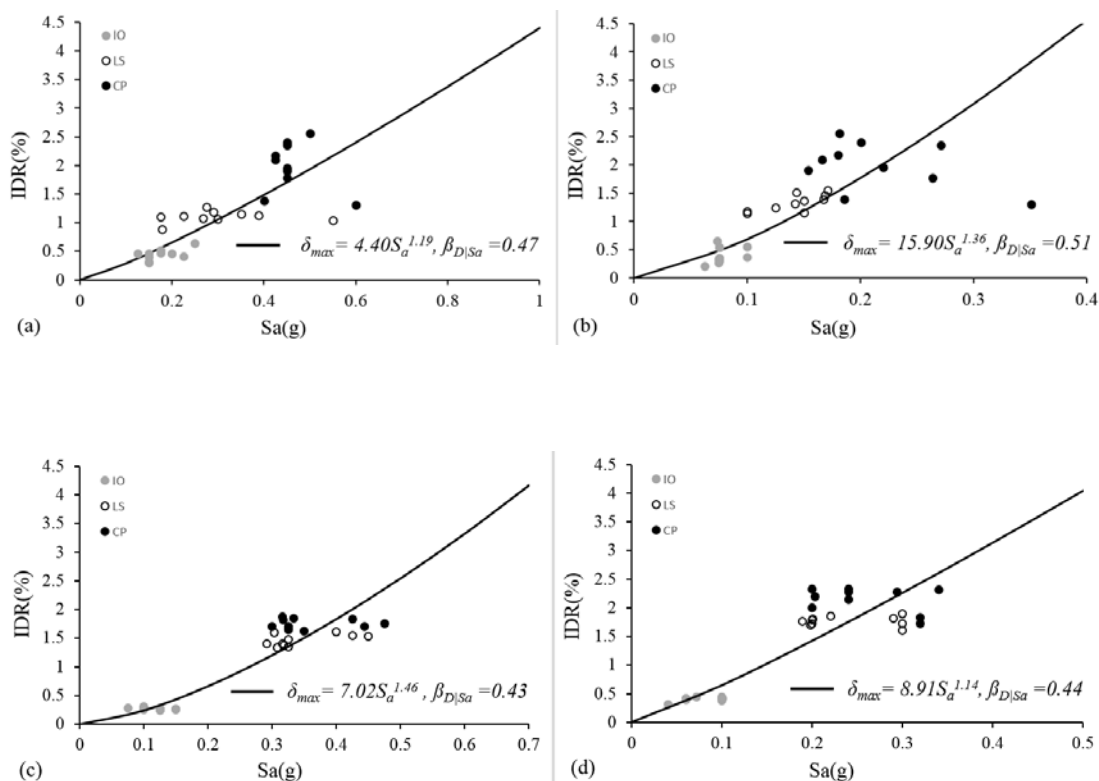


Figure 5.19: Seismic response of each performance level: (a) 3-st E-W; (b) 6-st E-W; (c) 3-st N-S; (d) 6-st N-S

Fragility curves with the consideration of uncertainties are illustrated in Figure 5.20, together with the fragility curves for the pre-retrofit buildings. The probability of severe damage of post-retrofit buildings is very low, less than 30%, when subjects to the 2%/50yr ground motion with a return period of 2500 years, which is the demand of NBCC 2010 for seismic design. The maximum probability of exceedance of light damage after retrofitting is about 90%, which means structural components, like braces, may buckle but not reach failure.

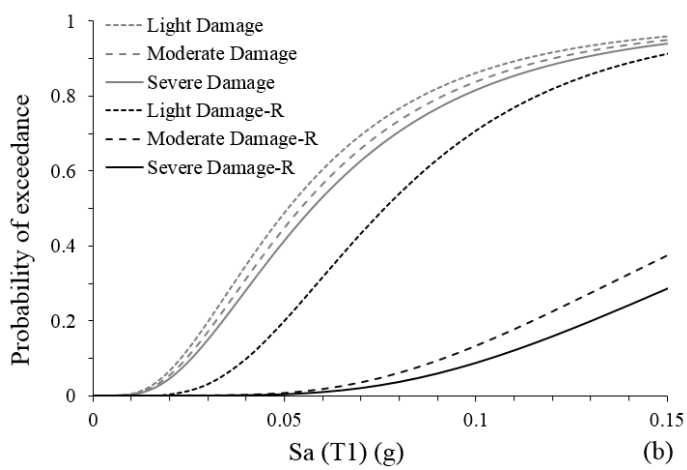
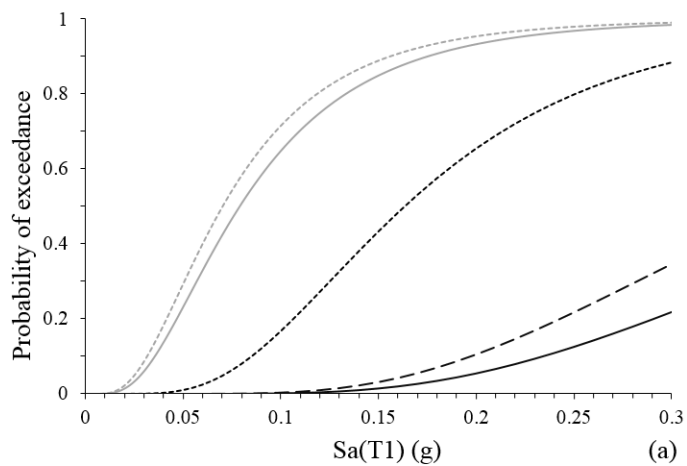


Figure 5.20a: Fragility curves of studied buildings: a) 3-st CBF (E-W); b) 6-st CBF (E-W)

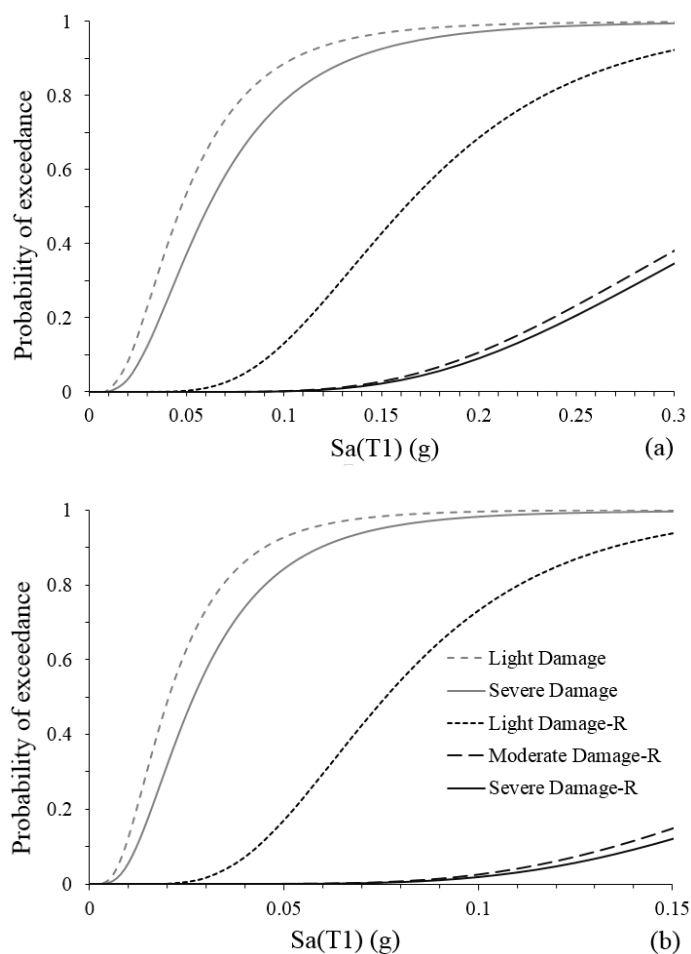


Figure 5.20b: Fragility curves of studied buildings: a) 3-st CBF (N-S); b) 6-st CBF (N-S)

For better understanding of the fragility of studied pre- and post-retrofit office building structures, the probabilities of exceeding or reaching a given damage state corresponding to spectral accelerations for hazard levels of 2%/50 years, 10%/50 years and 50%/50 years are listed in Table 5.20 for CBFs in E-W direction and Table 5.21 for CBFs in N-S direction.

Table 5.20: Fragility of studied buildings for different hazard level (E-W)

	2%/50yr			10%/50yr			50%/50yr		
	LD	MD	SD	LD	MD	SD	LD	MD	SD
3-st E-W	98.9%	-	98.2%	79.3%	-	73.9%	11.1%	-	7.9%
3-st R E-W	87.5%	31.9%	19.8%	25.0%	0.6%	0.2%	0.0%	0.0%	0.0%
6-st E-W	96.3%	95.5%	94.6%	63.3%	59.5%	55.7%	3.1%	2.3%	2.0%
6-st R E-W	92.0%	38.0%	30.0%	35.0%	2.0%	1.2%	0.2%	0.0%	0.0%

Table 5.21: Fragility of studied buildings for different hazard level (N-S)

	2%/50yr			10%/50yr			50%/50yr		
	LD	MD	SD	LD	MD	SD	LD	MD	SD
3-st N-S	99.6%	-	98.8%	88.6%	-	78.5%	23.0%	-	12.0%
3-st R N-S	85.0%	24.0%	21.0%	13.5%	0.2%	0.1%	0.0%	0.0%	0.0%
6-st N-S	99.8%	-	98.0%	93.5%	-	85.9%	23.5%	-	12.3%
6-st R N-S	88.6%	8.6%	6.7%	19.0%	0.9%	0.1%	0.0%	0.0%	0.0%

For pre-retrofit buildings, as brittle failure of brace-to-frame connections was developed due to shearing of welds, the damage state jumped from *light damage* to *severe damage*. The probability of *severe damage* exceeding in the view of current code demand is very high, around 98% for the 3-storey chevron braced frame building and 95% for that in 6-storey chevron braced frame building, and about 98% for the diagonal braced frame in both 3- and 6-storey building. For the post-retrofit buildings, the probabilities for light damage are relatively larger compared with those for *moderate* and *severe damage*. In addition, the probability for all retrofitted buildings (E-W) to sustain *severe damage* is 20% for the 3-storey and 30% for the 6-storey. A similar probability of *severe damage* was obtained for the CBF with diagonal braces located in the N-S direction.

## CHAPTER 6. CONCLUSIONS AND RECOMMENDATIONS

### *6.1 Conclusions*

In this study, fictitious 3- and 6-storey concentrically braced steel frame office buildings located on firm soil in Montreal and designed according to the NBCC 1980 and CSA/S16.1-M78 standard were assessed to identify their seismic fragility and the failure hierarchy. Seismic assessment of these buildings was conducted against the current code design provisions through nonlinear dynamic analysis. Retrofit schemes were proposed and fragility of pre- and post-retrofitted buildings was derived from the developed IDA curves.

Two seismic force resisting systems consisting of CBFs with chevron braces and CBFs with tension/ compression diagonal braces were studied. Critical seismic deficiencies were detected at the brace-to-frame connections consisting of a gusset plate welded to the slotted HSS brace. These pre-retrofit brace-to-frame connections are characterized by short length of fillet welds, they were not detailed based on the  $2t_g$  clearance and especially the connections at lower floors cannot sustain buckling of braces due to the lack of strength. The governing failure mode of these pre-retrofit brace-to-frame connections is the shearing of welds. On the other hand, beams do not have sufficient strength to carry in bending the tributary gravity load component in addition to the axial force developed due to the effect of braces and the governing failure mode is the overall member strength. Additionally, a lack of axial compression strength was encountered by the middle column of the two adjacent CBFs with tension/compression diagonal braces. These aforementioned deficiencies are common for CBF buildings designed in 1980s and earlier because the factored forces developed in members are used for members design instead of brace capacity. Moreover, when brace-to- frame connections fail at the same floor, the storey mechanism is formed due to the concentration of lateral deflection within that floor. When this mechanism occurs at the bottom floors it leads to building failure and if it happens at the upper floors it leads to partial failure.

Traditional retrofit techniques were applied in order to upgrade the seismic response of studied buildings. Thus, all the brace connections were re-designed to carry the probable tensile and compressive strength of braces and were replaced with thicker gusset plates detailed

to allow the  $2t_g$  clearance. Regarding the CBF beams, most of them were retrofitted by adding two longitudinal steel plates at each side of the W-shape web. Strength deficiency was observed for the middle columns of the two adjacent CBFs. To overpass this drawback, these CBF columns were strengthened with steel cover plates welded to the flanges of the W-shape column cross-section. This retrofit strategy was selected to respond to the Basic Safety Rehabilitation Objective Class that is required for office buildings, because it allows partial building functionality during the construction work. According to ASCE/SEI 41-13 standard, the target performance levels are Life Safety and Collapse Prevention that need to be achieved under the 10%/50 yrs. and 2%/50 yrs. earthquake hazard, respectively. Therefore, the performance base design approach was applied in order to assess the performance of post-retrofit buildings. From analysis it was found that all post-retrofit buildings were able to reach life safety when subjected to 10% in 50 years and collapse prevention when subjected to 2% in 50 years earthquake hazard level.

A numerical 3D model was built in OpenSees which is able to simulate the buckling and yielding of braces, fracture of brace, hinging of beams and buckling of CBF columns. The modelled CBFs were analysed under 10 ground motions by incremental dynamic analysis method. In the model, nonlinear force-based beam-column elements with distributed plasticity and fiber cross-section formulation were assigned to braces, beams and columns. A fatigue model calibrated based on experimental test results was assigned to braces in order to capture the fracture of braces due to low-cycle fatigue. Brace-to-frame connections properties were modeled as rotational springs inserted in Zero-length elements. However, the 1980 building was not designed based on the ductility principle and hinging of beams and buckling of columns occurred before the fracture of braces.

After seismic assessment was completed fragility of each performance level was calculated through lognormal cumulative distribution function. The analytical fragility curves were derived from the computed IDA curves on which the performance levels were defined such as: Immediate Occupancy at the end of the elastic segment when the first brace experienced buckling, Life Safety when the maximum residual interstorey drift reached  $0.5\%h_s$  and Collapse Prevention when the slope of the IDA curve approaches zero (flattening

effect). Three damage levels were associated to each performance level such as: light, moderate and severe damage. In the calculation of fragility curves both epistemic and aleatoric uncertainties were considered.

For pre-retrofit buildings, as brittle failure of brace-to-frame connections was developed due to shearing of welds, the damage state jumped from *light damage* to *severe damage*. The probability of exceeding the *severe damage* state according to the current code demand is very high, around 98% for the chevron braced frame of the 3-storey building and 95% for the 6-storey building. Similarly, there is a probability of exceedance of 98% for the diagonal braced frame in both 3- and 6-storey buildings. For the post-retrofit buildings, the probabilities for light damage are relatively larger compared with those for *moderate* and *severe damage*. In addition, the probability for all retrofitted buildings (E-W) to sustain *severe damage* is 20% for the 3-storey and 30% for the 6-storey. A similar probability of *severe damage* was obtained for the CBF with diagonal braces located in the N-S direction.

## **6.2 Recommendations for Future Studies**

- Existing CBFs with other braces configuration (split-X, X- braces at each floor), various storey height and building height, as well as different buildings locations should be investigated in order to assess their seismic fragility.
- Study the seismic fragility of the pre-1980 steel building stock, as well as the pre-1970 steel building stock in order to assess their deficiency. The proposed methodology can be used.
- Further experimental tests are required to investigate the behaviour of existing brace-to-frame connections in order and to validate the failure hierarchy and to better calibrate the computer model. As the failure mode of connection may vary with different loading protocols, these should be developed to comply to lateral deflection demand of studied CBF buildings.
- When incremental dynamic analysis is applied, a smaller incremental step is recommended in order to capture more accurately the system seismic response. “Softening” and

“hardening” are very common behaviour of structure due to changing of global stiffness, detecting of structural member yielding or buckling. In this case, the cost of computations will be substantially increased.

- Regarding to the OpenSees modelling, the convergence problems that appear when failure of structural member occurs doesn't necessary mean the collapse of the whole structure. Unfortunately, the OpenSees analysis will stop when calculation cannot converge, so the whole picture of post-local failure cannot be obtained. Extensive research should be conducted to solve this problem in OpenSees and a more flexible and intelligent model should be built.
- Seismic resilience analysis is recommended to be performed by using data from fragility curves and by developing a model of losses where both structural and non-structural components are considered and business interruption, reallocation, and building contents are included. Resilience can be computed as a function of hazard level, estimated losses, and demanded recovery time that is correlated to the selected retrofit strategy. Calculation of building resilience allows a better understanding of building functionally (resilience) in the aftermath of an earthquake event.

## REFERENCE

- Aguero, A., Izvernari, C., Tremblay, R., (2006) “Modelling of the Seismic Response of Concentrically Braced Steel Frames using the OpenSees Analysis Environment,” *International journal of Advanced Steel Construction*, 2(3), 242-274.
- American Society of Civil Engineers (ASCE). (2013). “Seismic Rehabilitation of Existing Buildings.” *ASCE/SEI 41-13*, Reston, VA, in press.
- Atkinson, G. (2009). “Earthquake Time Histories Compatible with the 2005 National Building Code of Canada Uniform Hazard Spectrum.” *Can. Journal of Civil Eng.*, 36(6), 991-1000.
- Baker, J.W., Cornell, C.A. (2005a) “A Vector Valued Ground Motion Intensity Measure Consisting of Spectral Acceleration and Epsilon”, *Earthquake Engineering & Structural Dynamic*, 34(10), 1193-1217.
- Bankoff, G., Frerks, G., Hilhorst, D., eds., (2004) “Mapping Vulnerability: Disasters, Development and People.” Earthscan, London, UK.
- Bertero, VV., (1977) “Strength and Deformation Capacities of Buildings under Extreme Environments”, In *Structural Engineering and Structural Mechanics*, Pister KS (ed.). Prentice Hall: Englewood Cliffs, NJ; 211–215.
- Castonguay, P.X., (2009) “Seismic Performance of Concentrically Braced Steel Frames of the Conventional Construction Category”, Master’s Thesis, École Polytechnique de Montréal, Qc.
- Canadian Standards Association (CSA), (1978) “Limit States Design of Steel Structures”, *S16.1-M78 Standard*, CSA, Toronto, ON.
- Canadian Standards Association (CSA). (2009) “Design of Steel Structures”, *S16.1-09 Standard*, CSA, Toronto, ON.
- Canadian Standards Association (CSA). (2014) “Design of Steel Structures”, *S16.1-14 Standard*, CSA, Mississauga, ON.

- Coburn, A., Spencer, R., (2002) "Earthquake protection", Second edition, J. Wiley & Sons Ltd, ISBN: 0-471-49614-6, Chichester, UK.
- Constantinou, M.C., Soong, T. T., Dargush, G.F., (1998) "Passive Energy Dissipation Systems for Structural Design and Retrofit", Multidisciplinary Center for Earthquake Engineering Research (MCEER): Buffalo, NY.
- Ellingwood, B., Celik, O.C., Kinali, K., (2007) "Fragility Assessment of Building Structural Systems in Mid-America", *Earthquake Engng. And Structural Dynamics*, 26:1935-1952.
- Federal Emergency Management Agency (FEMA), (2000) "Recommended Seismic Design Criteria for New Steel Moment-Frame Buildings", *FEMA 350*, prepared by the SAC Joint Venture, Washington DC.
- Federal Emergency Management Agency (FEMA), (2003a) "Incremental Seismic Rehabilitation of Office Buildings: Providing Protection to People and Buildings." *FEMA 397*, Washington.
- Federal Emergency Management Agency (FEMA). (2003b), Multi-Hazard Loss Estimation Methodology, earthquake model, *HAZUS-MR4*, technical manual, developed by the Department of Homeland Security, Emergency Preparedness and Response Directorate, FEMA, Mitigation Division, Washington, D.C., under a contract with the National Institute of Building Sciences.
- Gunnarsson, I.R., (2004) "Numerical Performance Evaluation of Braced Frame Systems," a thesis submitted in partial fulfillment of the MSCE, University Washington, Seattle.
- Haddad, M., Tremblay, R., (2006) "Influence of Connection Design of the Inelastic Seismic Response of HSS Steel Bracing Members", *WELDING IN THE WORLD-LONDON*, 50(I):574
- Heidebrecht, A., (2003) "Overview of Seismic Provisions of the Proposed 2005 Edition of the National Building Code of Canada", *Canadian Journal of Civil Eng.*, Vol. 30, No.2, pp241-254.

- Hsiao, P.C., Lehman, D.E., Roeder, C.W., (2013) "A Model to Simulate Special Concentrically Braced Frames beyond Brace Fracture", *Journal of Earthquake Engineering & Structural Dynamics*, 42:183-200.
- Ikeda, K., Mahin, S.A., (1986) "Cyclic Response of Steel Braces", *Journal of Structural Engineering*, ASCE, 112(2), 342-361.
- Kennedy, D.J.L., Kriviak, G.J., (1985) "The Strength of Fillet Welds under Longitudinal and Transverse Shear: a Paradox", *Canadian Journal of Civil Engineering*, 12(1), 226-231
- Jiang, Y., Balazadeh-Minouei, Y., Tremblay, R., Koboevic, S., Tirca, L. (2012) "Seismic Assessment of Existing Steel Braced Frames Designed in Accordance with the 1980 Canadian Code Provisions", *Proceedings of Stessa Conf.* Santiago, Chile, 531-537.
- Kafali, C., Grigoriu, M., (2005) "Rehabilitation Decision Analysis" In: ICOSAR'05, *Proceedings of the 9<sup>th</sup> international conference on structural safety and reliability*, 19-23 June, Rome, Italy.
- Kennedy, R.P, Ravindra, M.K., (1984) "Seismic Fragility for Nuclear Power Plant Risk Studies", *Nuclear Engineering and Design*, 79(1), 47-68.
- Lamarche, C.P., and Tremblay, R., (2008) "Accounting for Residual Stresses in the Seismic Stability of Nonlinear Beam-Column Elements with Cross-Section Fiber Discretization", *2008 Annual Stability Conference*, P. 59-78.
- Lignos, D., Karamanci, E., (2013) "Predictive Equations for Modelling Cyclic Buckling and Fracture of Steel Braces," *The 10<sup>th</sup> International Conference on Urban Earthquake Engineering*, Tokyo.
- Liu, J., Astaneh-Asl, A., (2004) "Moment-Rotation Parameters for Composite Shear Tab Connections", *Journal of structural engineering*, ASCE, 130(9)
- Martinez-Saucedo, G. and Packer, J.A., (2009) "Static Design Recommendations for Slotted End HSS Connections in Tension", *Journal of Structural Engineering*, ASCE, 135(7), 797-805.
- Matsagar, V.A., Jangid, R.S., (2008) "Base Isolation for Seismic Retrofitting of Structures",

- Practice Periodical on Structural Design and Construction*, 13(4), 175-185
- Mazzoni, S., McKenna, F., Scott, M., Fenves, G.L. et al., (2009) "OpenSees User Manual", Pacific Earthquake Engineering Research Center (PEER), University of California, Berkeley.
- Mokha, A., Amin N., Constantinou, M., and Zayas, V., (1996) "Seismic Isolation Retrofit of Large Historic Building". *Journal of Structural Engineering*, 122(3), 298-308
- Morales Ramirez, J.D., and Tirca, L., (2012) "Numerical Simulation and Design of Friction-Damped Steel Frame Structures", *15 WCEE*.
- National Research Council of Canada (NRCC). (1970) (1980) and (2010), "National Building Code of Canada-Part 4", NRCC, Ottawa, ON.
- Pall, A.S., Marsh, C., (1982) "Response of Friction Damped Braced Frames", *Journal of Structural Division*, ASCE, 1208(ST6), 1313-1323.
- Pillai, S., (1974) "Beam-Columns of Hollow Structure Sections", *Canadian Journal of Civil Engineering*, 1(2), 194-198.
- Plumier, A., Thanopoulos, P., Castiglioni, C.A., Vayas, L., Calado, L., (2005) "Behaviour of Seismic Resistant Braced Frame with Innovative Dissipative Connections", *EUROSteel 2005-4<sup>th</sup> European Conference on Steel and Composite Structures*, Maastricht, the Netherlands.
- Sarno, L.D., Elnashai, A.S., (2002) "Seismic Retrofitting of Steel and Composite Building Structures", Mid-America Earthquake Center Report, University of Illinois at Urbana-Champaign, USA.
- Schwinger, C., (2007) "Building Retrofit: Breathing New Life into Existing Building Structures", *North American Steel Construction Conference (NASCC)*, AISC.
- Shinozuka, M., Feng, M.Q., Lee, J., Naganuma, T., (2000) "Statistical Analysis of Fragility Curves", *Journal of Engineering Mechanics*, ASCE, 126(12), 1224-1231.
- Soroushian, P., Alawa, M.S., (1988) "Efficient Formulation of Physical Theory Brace Models," *Journal of Structural Engineering*, ASCE, 114(11), 2457-2473.

- Tabeshpour, M.R., Ebrahimian, H., (2010) "Seismic Retrofit of Existing Structures using Friction Dampers", *Asian Journal of Civil Engineering*, 11(4), 509-520.
- Tirca, L., Capraelli, C., and Danila, N., (2012) "Seismic Simulation and Design of Low-Rise CBF Buildings with and without Dissipative Connections using OpenSees", *Proc. Of the 7<sup>th</sup> Int. Cong. On: Behaviour of Steel Structures in Seismic Areas, Santiago, Chile*, 365-371
- Tirca, L., Serban, O., Lin, L., Wang, M.Z., Lin, N.H., (2014), "Improving the Seismic Resilience of Existing Braced Frame Office Buildings", Submitted to *Journal of Structural Engineering (ASCE)*, under review.
- Tirca, L., Serban, O., Wang, M.Z., Di, Modica D., (2013). "Incremental Dynamic Analysis of Existing Steel Braced Frame Buildings in Moderate Seismic Zones." *Proc., Structures Congress, ASCE, Reston, A*, 2298-2309.
- Tirca, L., Tremblay, R., (2009) "Incremental Dynamic Analysis of Multi-Storey Concentrically Braced Steel Frames", *Behaviour of Steel Structures In Seismic Areas, STESSA*, editor: Mazzolali F.M., Sause R., Ricles J.M., CRC Press.
- Tirca, L., Chen, L., (2014) "Numerical Simulation of Inelastic Cyclic Response of HSS Braces upon Fracture", *Int. Journal of Advanced Steel Construction*, 10(4), in print.
- Tirca, L., Chen, L., (2013) "Simulating the Seismic Response of Concentrically Braced Frames Using Physical Theory Brace Models", *Open Journal of Civil Engineering*, 3(2), 69-81
- Tirca, L., Serban, O., Wang, M.Z., Di Modica, D., (2012) "Methodology for Seismic Assessment of Existing Braced Frame Buildings", Report-NSERC Engage grant
- Tremblay, R., (2011) "Evolution of the Canadian Seismic Design Provisions for Steel Structures since 1989", *Proc. CSCE Annual Conf.*, Ottawa, ON.
- Tremblay, R., Bruneau, M., Driver, R., Metten, A., Montgomery, C.J., and Rogers, C., (2010) "Seismic Design of Steel Structures in accordance with CSA-S16-09", *Proc. 9<sup>th</sup> US National and 10<sup>th</sup> Canadian Conference on Earthquake Engineering*, Toronto, ON.,

Paper No. 1768.

- Uriz, P., Filippou, FC and Mahin, SA, (2008) “Model for Cyclic Inelastic Buckling of Steel Braces,” *J. Struct. Eng.*, ASCE, 134(4), 619-628.
- Uriz, P., Mahin, S.A., (2004) “Seismic Vulnerability Assessment of Concentrically Braced Steel Frames”, *International Journal of Steel Structures*, 4(4):239-248.
- Uriz, P., Mahin, S.A., (2008) “Toward Earthquake-Resistant Design of Concentrically Brace steel-Frame Structures”, Pacific Earthquake Engineering Research Center (PEER) report, University of California, Berkeley.
- Vamvatsikos, D, Cornell, CA. (2002) “Incremental Dynamic Analysis”. *Earthquake Engineering and Structural Dynamics*, 31(3), 491-514.
- Vansant, A.M., and Jangid, R.S., (2008) “Base Isolation for Seismic Retrofitting of Structures”, *Practice Periodical on Structural Design and Construction*, 13(4), 175
- Wen, Y.K., Ellingwood, B., Bracci, J., (2004) “Vulnerability Function Framework for Consequence-based Engineering”. *MAE Center Project DS-4 Report*